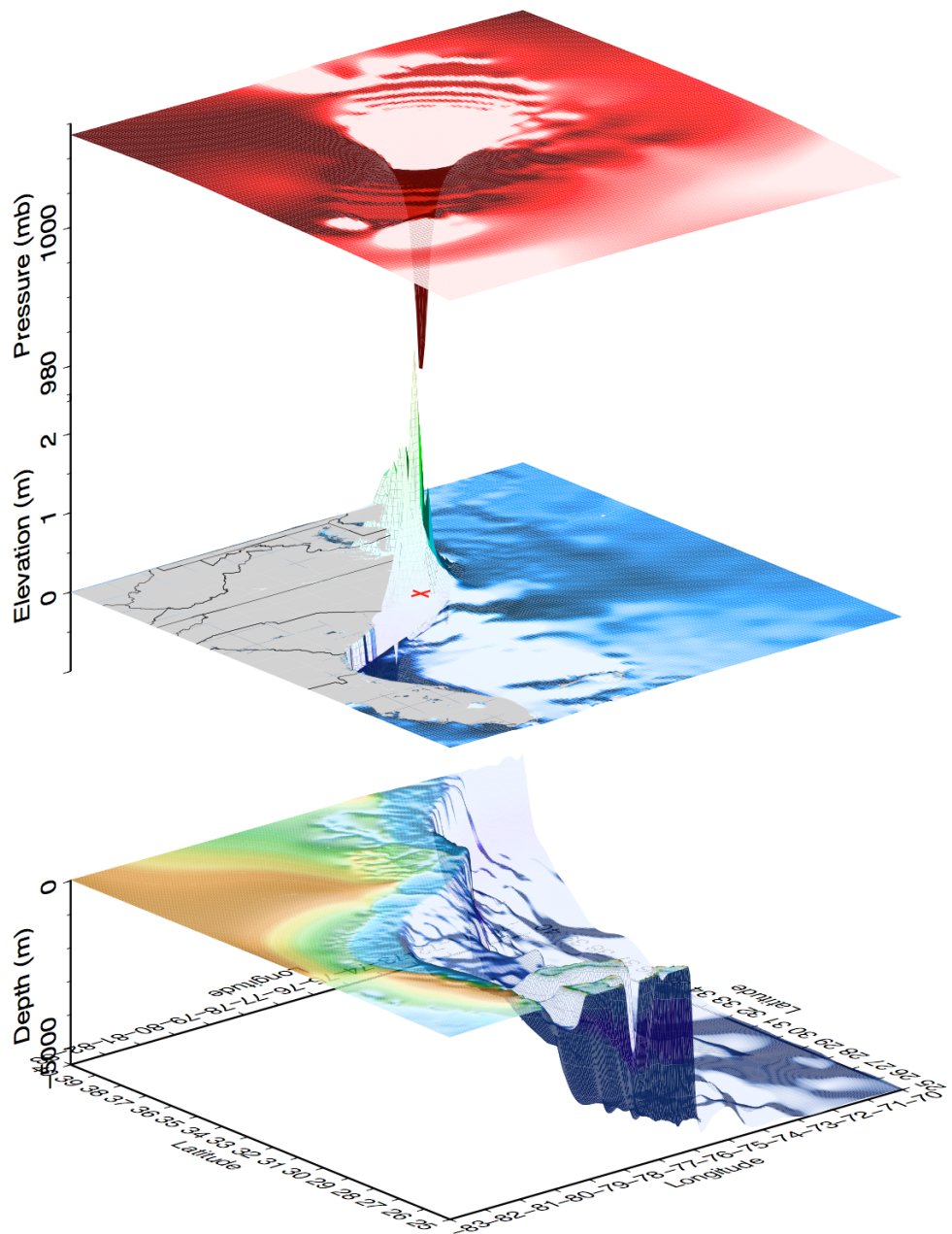


# Design and Implementation of a Real-Time Storm Surge and Flood Forecasting Capability for the State of North Carolina

CRAIG MATTOCKS, CRISTINA FORBES AND LIMEI RAN

*Carolina Environmental Program, University of North Carolina, Chapel Hill, North Carolina*



## Table of Contents

1. Abstract .....	3
2. Introduction .....	4
3. Technical Achievements .....	8
3.1 ADCIRC Wind Forcing .....	8
3.2 The North Carolina Forecast System Operational Workflow .....	18
3.2.1 Background Mode: Tides-only runs .....	20
3.2.2 Event Nowcast Mode .....	20
3.2.3 Event Forecast Mode .....	20
3.3 Operational Storm Surge Predictions .....	22
3.4 Additions to the ADCIRC Model to Increase its Accuracy .....	43
3.4.1 Generation of a Node Point Shapefile for ArcGIS .....	43
3.4.2 Computation of LIDAR Elevation for ADCIRC Nodes .....	44
3.4.3 Calculation of Directional Surface Roughness Length Values and Manning Roughness Coefficients .....	47
3.5 Improved Storm Surge Simulation Results .....	60
3.6 ADCIRC Performance Benchmarks .....	80
3.7 WRF-ARW Model Implementation .....	81
3.7.1 Modifications for Operational Use .....	81
3.7.2 Initialization .....	86
3.7.3 Operational Workflow .....	87
3.7.4 Scientific Visualization .....	87
3.7.5 Additional Tasks in Progress .....	87
4. Summary .....	92
5. References .....	93
6. List of Deliverables .....	95
7. List of Tables .....	99
8. List of Figures .....	99

# **Design and Implementation of a Real-Time Storm Surge and Flood Forecasting Capability for the State of North Carolina**

CRAIG MATTOCKS, CRISTINA FORBES AND LIMEI RAN

*Carolina Environmental Program, University of North Carolina, Chapel Hill, North Carolina*

## **ABSTRACT**

A new real-time storm surge prediction system has been created for the State of North Carolina to assist emergency managers, policy-makers and other government officials with evacuation planning, decision-making and resource deployment during tropical storm landfall and flood inundation events. The North Carolina Forecast System (NCFS) is built from high-resolution versions of the ADCIRC (Advanced Circulation) coastal ocean model and the Weather Research & Forecasting (WRF) numerical weather prediction model. A “rapid response” assessment of hurricane threat is accomplished by driving the storm surge model with winds from a synthetic asymmetric gradient wind vortex generated from the National Hurricane Center (NHC) forecast advisories the moment they are inserted into the real-time weather data stream. Preliminary comparisons of the model results against actual sea surface elevations measured by NOAA tide gauges along the NC coast indicate that this new system produces remarkably realistic predictions of storm surge. In addition, the real-time WRF weather forecasts provide estimates of surface temperature, winds, soil moisture, accumulated precipitation and runoff at unprecedented horizontal resolution. These digital output products can be used in hydrometeorological model coupling algorithms for the prediction of dynamic streamflow, flash floods and inundation depth.

Working in collaboration with the Renaissance Computing Institute (RENCI), scientists in the Carolina Environmental Program (CEP) and the Institute of Marine Sciences (IMS) at UNC designed and built this system at a rapid pace and at a low cost for the state, in only 6 months and below the budget originally allocated for this project. However, even though the numerical models are now running operationally at RENCI, the NCFS should still be considered an experimental prototype. Further scientific enhancements, such as improving the wind forcing, extending the embedded high-resolution portion of the ADCIRC model grid more inland/southward to encompass the entire NC coastline and incorporating topographic data from the NC Floodplain Mapping Program’s new 6-meter resolution LIDAR database, and verification/calibration of the system’s performance are required before it can be used as a mission-critical tactical decision aid (TDA) by state and county emergency management agencies. With the continued implementation of improvements such as these and critical evaluation by the coastal research community, this new forecast system offers the promise of minimizing the loss of life and structural damage that occurs in North Carolina during natural disasters.

## 2. Introduction

Hurricanes cause many casualties, structural destruction and significant economic losses in the United States. According to Table 10 in Blake et al. (2006), there were 46 direct hits on North Carolina from 1851-2005, of which 12 were major hurricanes (intensity breakdown: Cat 1 = 21, Cat 2 = 13, Cat 3 = 11, Cat 4 = 1, Cat 5 = 0). The highest death totals were primarily a result of a rise in the ocean surface elevation (storm surge) of 10 feet or greater associated with many of these major hurricanes. A large portion of the damage in four of the fifteen costliest tropical cyclones (Table 3a, Blake et al., 2006) resulted from coastal/sound-side/inland flooding caused by storm surge and torrential rain.

In addition, North Carolina faces a difficult evacuation challenge (see Table 1 below) due to the large numbers of tourists who flock to the Outer Banks during the summer and the narrow, two-lane roads that lead out of these areas.

**TABLE 1.** Estimates of the peak tourist population and the time required to evacuate the coast for a list of counties in North Carolina (WRAL News, 2006).

Time Needed to Evacuate the NC Coast		
County	Peak Tourist Population	Hours Needed to Evacuate
Currituck	20,000	12
Dare	160,000	18
Hyde	5,200	28
Carteret	200,000	12
Onslow	180,840	13
Pender	35,000	9
New Hanover	147,761	10
Brunswick	190,000	12

**Note: Parts of the Outer Banks can take longer to evacuate, in some cases up to 33 hours.**

NC county emergency managers insist that the evacuation times listed in Table 1 are grossly underestimated because they are based on an extrapolated Year 2000 census. For example, Brunswick County now estimates a peak tourist population near 350,000, given their recent growth and the large numbers of visitors from South Carolina who vacation in the county each summer. Evacuation is not a linear process, it slows down dramatically with moderate increases in population, while the number of vehicles fleeing coastal communities jumps by 50 percent when the intensity of a storm increases from category 1-2 to 3-5 strength. The original studies

crudely assumed that one county would evacuate at a time, not multiple counties jamming I-40, Highway 421, Highway 70 and Highway 64. Also no allowance was made for flooding ahead of a storm, which often inundates access roads leading to the main traffic arteries. Some estimates set the required evacuation times for Brunswick and New Hanover counties to well over 30 hours. Ideally, emergency managers would like a lead time of 36 hours to evacuate the barrier islands.

In the wake of Hurricane Floyd in 1999, the North Carolina Department of Transportation (NCDOT) developed a traffic reversal plan (<http://www.ncdot.org/traffictravel/emergencyinfo/>) for Interstate-40:

#### THREAT CRITERION

The decision process to reverse the flow of traffic in the eastbound lanes of I-40 begins when a strong Category II hurricane (sustained winds of 103 mph or higher) is forecast to reach Category III strength, and it is forecast to make landfall within 50 miles north or within 100 miles south of Wilmington, NC. This area includes the counties of Brunswick, Pender, New Hanover, and Horry County, SC.

However, to date, this plan has never been put into action. A traffic analysis and modeling study conducted at NCSU (Williams et al., 2005) showed how difficult it would be to actually implement this strategy. Long queues at primary bottlenecks and the transitions between normal and contraflow patterns are the major concerns.

Another threat from tropical storms is coastal erosion along North Carolina's fragile barrier islands. Besides damage to homes and buildings, the loss of sand costs the federal and state governments millions of dollars each year for beach renourishment (<http://www.csc.noaa.gov/opis/html/bchleg.htm>) and re-opening ship navigation channels. The NC Coastal Resources Commission uses erosion rates calculated every five years to set strict limits on the "setback" distance allowed for new development along the oceanfront.

To address these challenges, the North Carolina Forecast System (NCFS) was created to assist emergency managers, policy-makers and government officials in evacuation planning, decision-making and resource deployment during tropical storm landfall and flood inundation events. The prediction of storm surge in coastal North Carolina due to hurricane activity is the primary focus of the system. The NCFS utilizes computationally optimized and parallelized versions of the ADCIRC coastal circulation and storm surge model and the Advanced Research WRF (ARW) numerical weather prediction model.

ADCIRC is an unstructured grid finite element hydrodynamic model used to simulate storm surge, tides and riverine flow. The two dimensional, depth-integrated version employed in this project, ADCIRC-2DDI, model solves a vertically-integrated continuity equation for water surface elevation. Spurious oscillations associated with a primitive Galerkin finite element formulation of this equation are prevented by utilizing the Generalized Wave Continuity Equation (GWCE), wherein the vertically-integrated momentum equations are substituted into the continuity equation to conserve mass and momentum. The GWCE is solved to determine the new free surface elevation, while the vertically-integrated momentum equations are solved to determine the depth-averaged ocean current velocity. The NCFS model grid domain (Fig. 1),

which extends from  $97.85^{\circ}$  to  $60.04^{\circ}$  W and from  $7.90^{\circ}$  to  $45.83^{\circ}$  N, encompasses the Western Atlantic, the Gulf of Mexico and the Caribbean Sea.

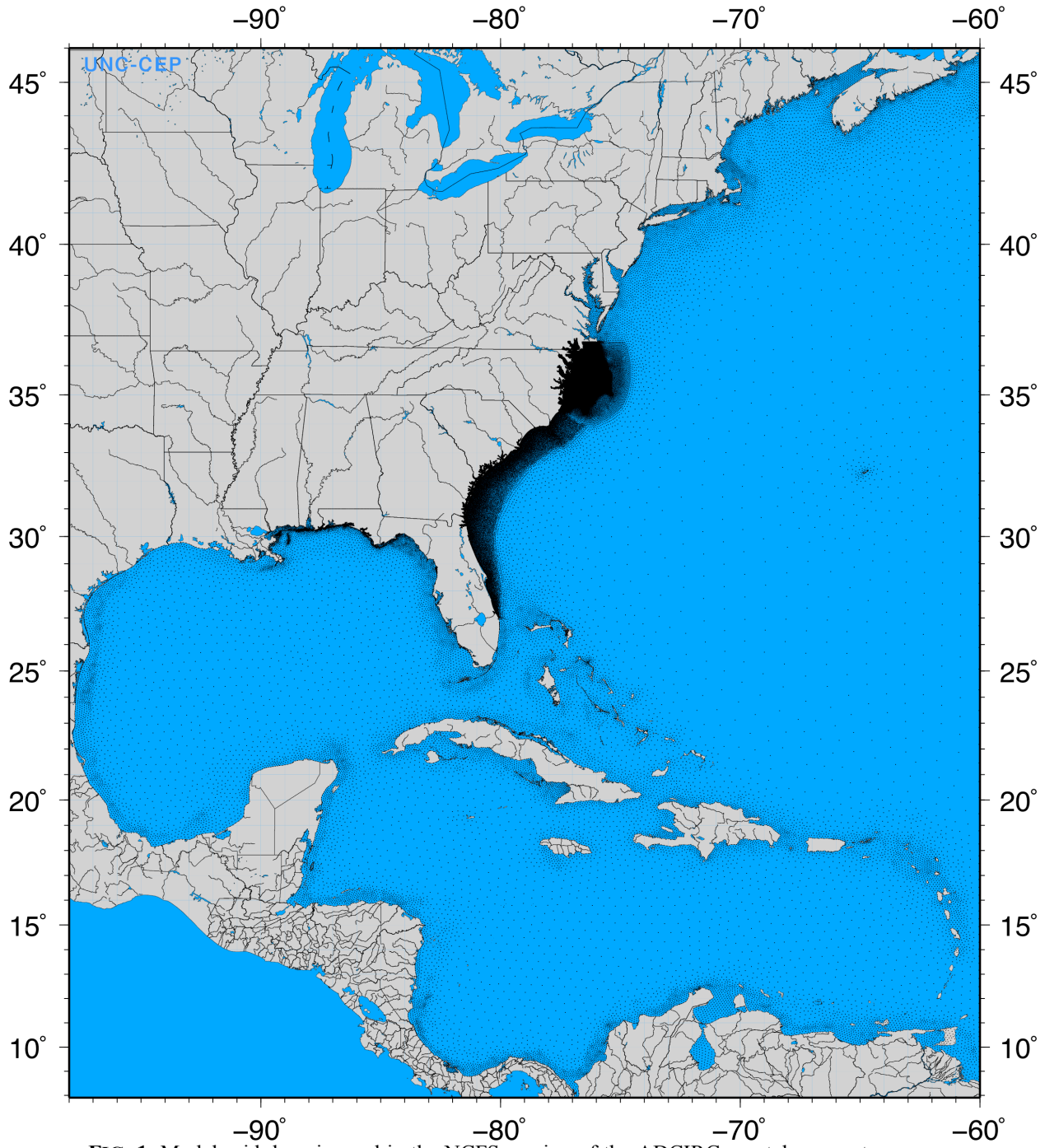


**FIG. 1.** Model grid domain used in the NCFS version of the ADCIRC coastal ocean storm surge prediction model.

ADCIRC's unstructured computational mesh, which consists of 227,240 nodes and 440,904 elements in the NCFS configuration, allows higher resolution in areas where it is needed, from tens of kilometers offshore to tens of meters through channels and inlets. The model is well documented, both in the published scientific literature and on the ADCIRC web site

(<http://adcirc.org/>). It has been used extensively for tidal prediction (Westerink, 1993; Westerink et al., 1993; Blain and Rogers, 1998), hurricane storm surge prediction (Blain et al., 1994; Dietsche, 2006) and in operational forecast systems (Luettich et al., 1996; Blain and McManus, 1998; Lynch et al., 1994; Graber et al., 2006).

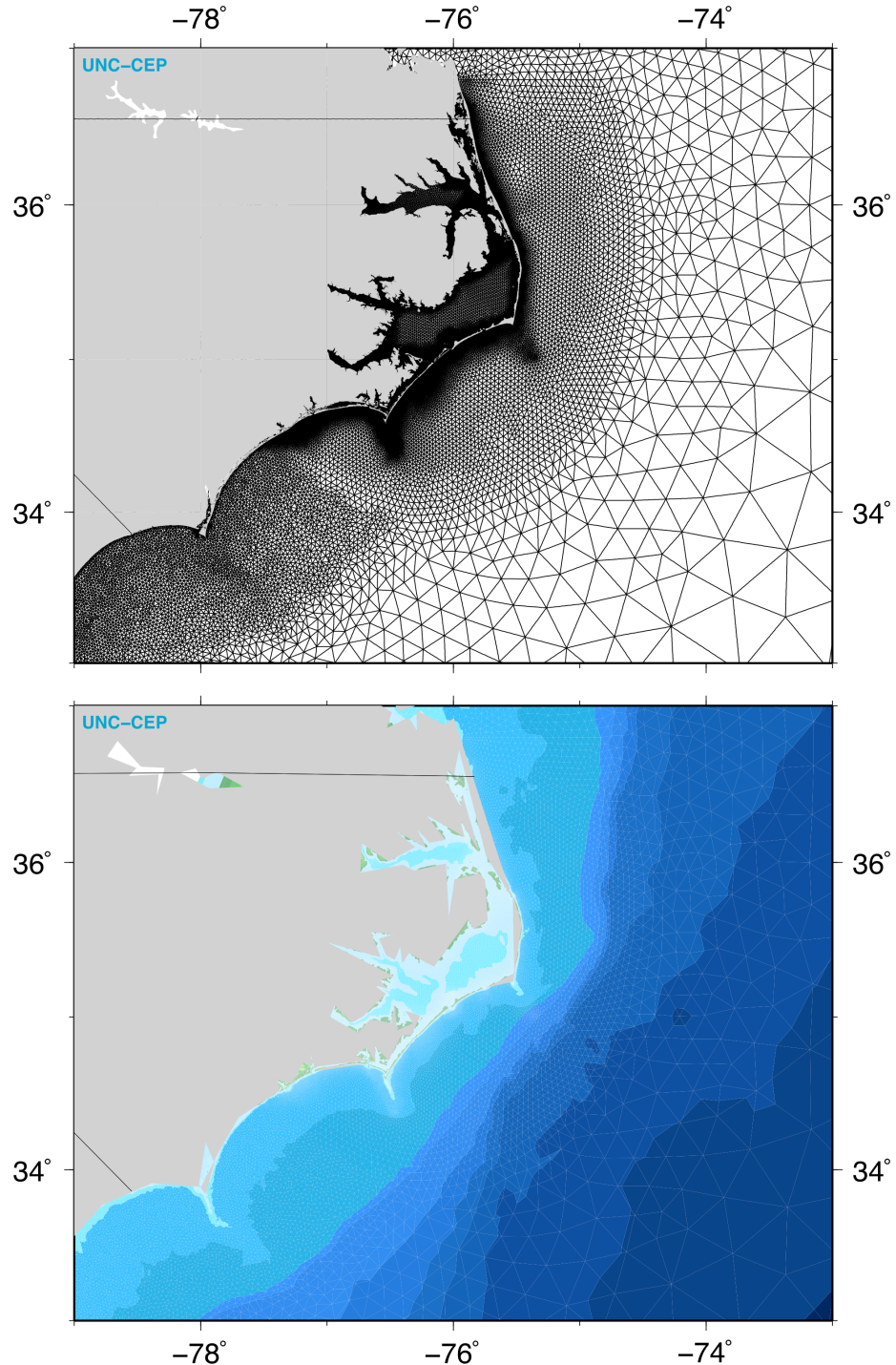


**FIG. 2a.** High-resolution grid and topography used in the NCFS version of the ADCIRC coastal ocean storm surge prediction model.

ADCIRC interpolates elevation and velocity data from ADCIRC nodes to user-specified NOAA tide station locations or any other locations of interest. Fig. 2b shows the stations selected for the NCFS analysis.

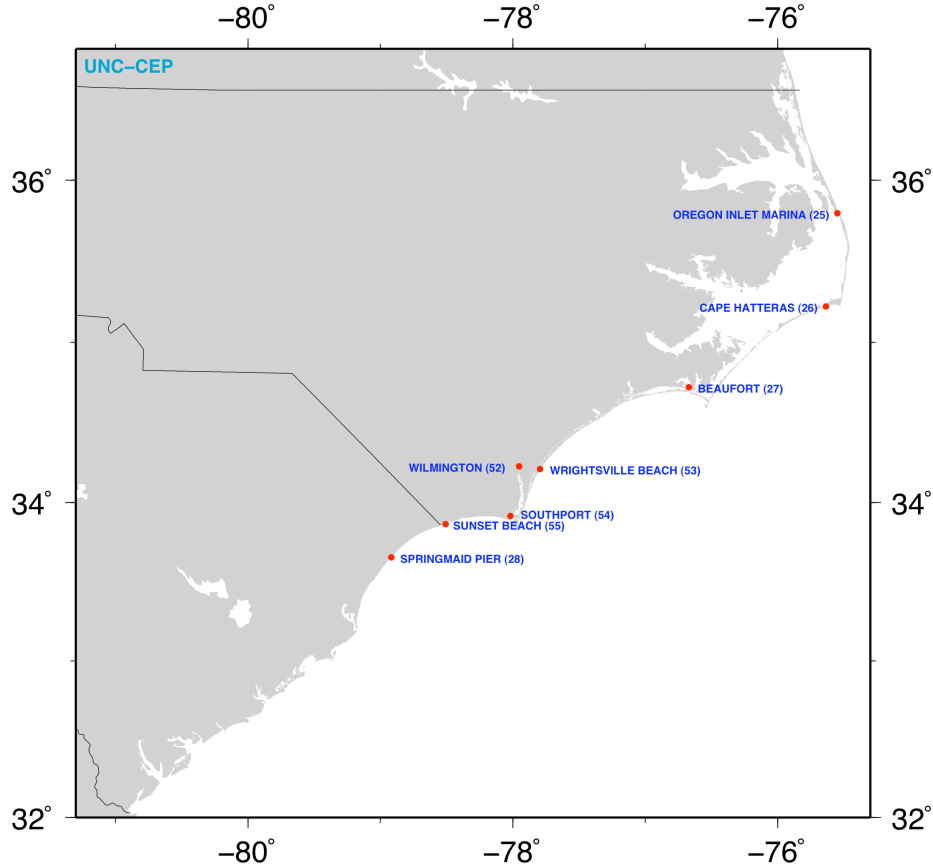


**FIG. 2b.** ADCIRC elevation recording stations used in the NCFS.

Developed and maintained by the Mesoscale and Microscale Meteorology (MMM) Division at the National Center for Atmospheric Research (NCAR) in Boulder, Colorado, the ARW/Eulerian mass core version of WRF (Skamarock et al., 2005) is a fully compressible, nonhydrostatic numerical weather prediction model that uses a terrain-following vertical coordinate with the top of the model set at a constant pressure surface. It employs Arakawa-C grid staggering in both the horizontal and vertical directions, a 3<sup>rd</sup>-order Runge-Kutta time integration scheme, and 2<sup>nd</sup> to 6<sup>th</sup> order spatial discretization operators. The model is conservative for all scalar variables. It supports one-way, two-way and moving nest options and runs on single-processor, shared- and distributed-memory machines. More information is available on the WRF web site (<http://www.wrf-model.org/index.php>).

### 3. Technical Achievements

#### 3.1 ADCIRC Wind Forcing

One of the first tasks undertaken by scientists at UNC-CEP was to research real-time sources of

wind data available through the Local Data Management (LDM) server at RENCI and NHC's anonymous ftp server for initializing and running the ADCIRC storm surge model. Extensive conversations were held with the Hurricane Specialists at NHC to obtain detailed information about NHC's forecast products, their generation, timing and accuracy. The decision was made to develop a synthetic asymmetric Holland (1980) gradient wind model (written in object-oriented Fortran 90) that could be used to construct a tropical storm vortex from the NHC forecast advisories that enter the LDM Family of Services (FOS) stream.

This approach has several important operational advantages. First, it allows a forecast simulation to be launched as soon as a NHC forecast advisory is issued, sometimes 10 minutes before the official release time, instead of waiting 1-6 hours for the National Center for Environmental Prediction (NCEP) North American Mesoscale (NAM) model winds to become available, plus an additional 1-2 hours for downloading and pre-processing the surface wind and pressure data. Second, the synthetic asymmetric vortex winds can be generated "on the fly" from the gradient wind formula, so they can be directly coupled to the ocean model at every time step in the model simulation. Since these winds are available at "perfect" analytical resolution and "true" intensity, they can be calculated exactly at each location of the ADCIRC model nodal points. In contrast, the NCEP NAM winds have a comparatively coarse horizontal resolution of 12-36 km and must be interpolated to model nodes in both space and time. This introduces error and often produces an artificial weakening of the storm and its attendant wind stress, especially in fast-moving storms (Westerink et al., 2006). An ADCIRC simulation initialized with synthetic asymmetric vortex winds provides a "quick-look, rapid-response" storm surge forecast that can serve as the first member of an ensemble of simulations. In the "near field", when a hurricane approaches the shoreline and the storm's circulation dominates over the background synoptic flow, this formulation provides a remarkably realistic representation of the wind field.

The original formulation of the asymmetric wind vortex is based on Xie et al. (2006):

$$P(r, \theta) = P_c + (P_n - P_c) \exp^{-[R_{max}(\theta)/r]^B} \quad (1)$$

where the surface pressure  $P$  varies as a function of the radial distance  $r$  from the hurricane center and the azimuthal angle  $\theta$  around the storm,  $P_c$  is the central surface pressure of the storm,  $P_n$  is the ambient undisturbed synoptic background surface pressure, and  $R_{max}$  is the radius of maximum wind, which varies azimuthally around the storm.

The tangential velocity  $V_{asym}$  is derived from the pressure field, assuming the winds are in gradient wind balance. In this case, when the tangential acceleration vanishes and the flow is parallel to the isobars, the equation that describes a three-way balance between the pressure gradient, centrifugal and Coriolis forces can be inverted and solved to obtain the tangential wind velocity:

$$V_{asym} = \sqrt{\frac{B}{\rho_a} \left( \frac{R_{max}(\theta)}{r} \right)^B (P_n - P_c) \exp^{-[R_{max}(\theta)/r]^B} + \left( \frac{rf}{2} \right)^2 - \left( \frac{rf}{2} \right)} \quad (2)$$

where  $\rho_a$  is the density of air,  $f$  is the horizontally varying Coriolis force,  $f = 2 \Omega \sin(\text{latitude})$  and  $\Omega$  is the rotational frequency of the earth.

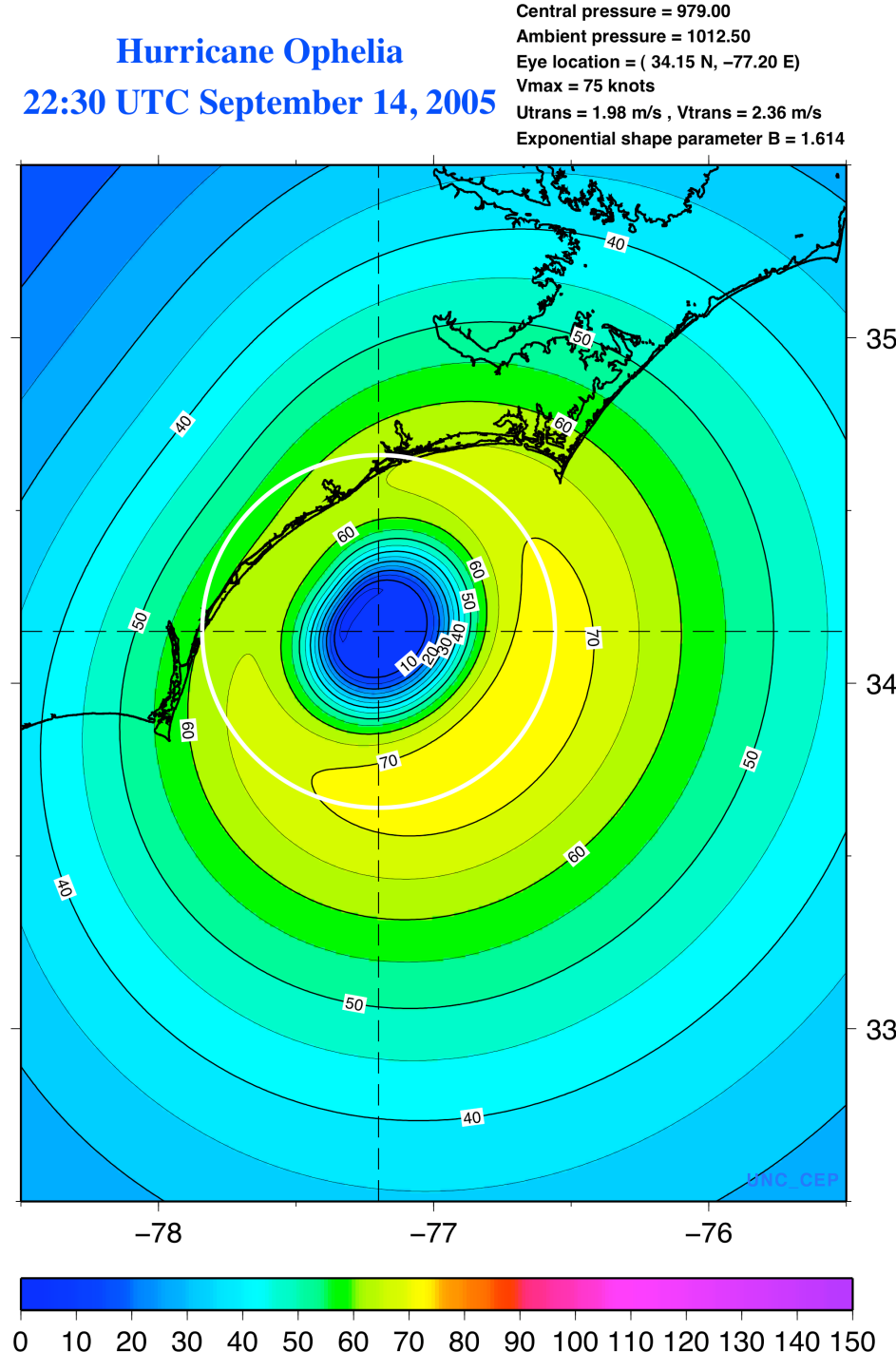


**FIG. 3.** Wind speeds produced by the synthetic asymmetric Holland gradient wind vortex algorithm for Hurricane Ophelia, valid at 22:30 UTC on September 14, 2005. The white circle indicates the approximate radius of maximum winds that would have been computed using a purely symmetric Holland wind formulation.

The hurricane shape parameter  $B$ , which controls the eye diameter and steepness of the tangential velocity gradient, is computed from Eq. (2) using data from the NHC guidance at the radius of maximum winds:

$$B = \frac{[(V_{\max} - V_T)/WR]^2 \rho_a e}{P_n - P_c} \quad (3)$$

where  $V_{\max}$  is the maximum sustained (1-minute) wind speed in the hurricane,  $V_T$  is the storm's forward motion, a translational storm velocity computed from successive NHC eye fixes that gradually ramps down to zero far from the storm's center, and  $WR$  is a wind reduction factor, defined at the gradient wind flow level above the influence of the planetary boundary layer, used to adjust the wind speeds down to the surface.  $B$  is restricted to values between 1 and 2.5 to limit the allowed shape and size of the vortex (Fig. 4).

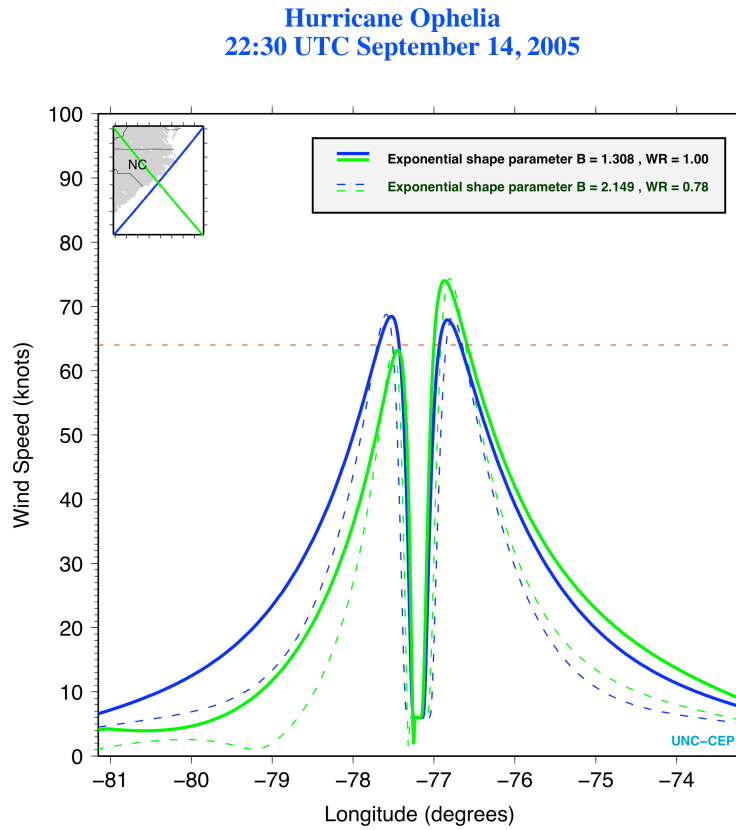


**FIG. 4.** Radial wind profiles from the asymmetric wind vortex in Fig. 3 along the NE-SW and NW-SE transects without (solid) and with (dashed) boundary layer adjustment using the Powell et al., (2003) wind reduction factor. Note how the wind adjustment increases the hurricane shape parameter  $B$ , which broadens the eye of the storm and enhances the tangential velocity gradient.

This formulation was enhanced with a more precise radius of maximum winds root-finding algorithm based on Brent's method, and a cross-isobar frictional inflow angle of approximately  $25^\circ$  that decreases towards the center of the storm, as described in the Queensland Government's Ocean Hazards Assessment (2001):

$$\alpha_F = \begin{cases} 10 \frac{r}{R_{\max}}, & 0 \leq r < R_{\max} \\ 10 + 75 \left( \frac{r}{R_{\max}} - 1 \right), & R_{\max} \leq r < 1.2 R_{\max} \\ 25, & r > 1.2 R_{\max} \end{cases} \quad (4)$$

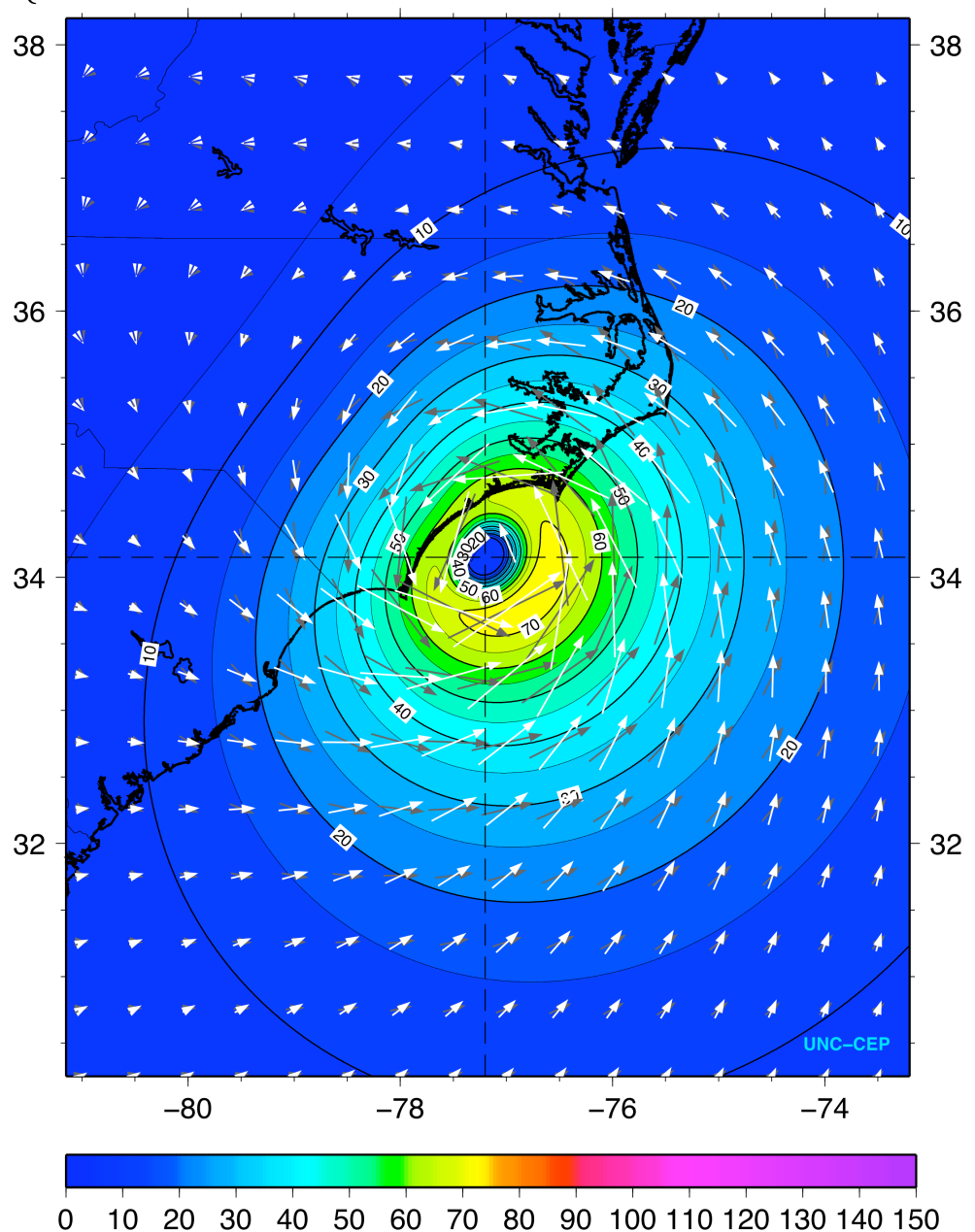


**FIG. 5.** Effect of including the radially dependent frictional inflow angle formulation in the asymmetric gradient wind vortex model. Note how the frictionally enhanced wind vectors (white) turn toward the center of the storm in a cross-isobaric manner.

The effect of this parameterized inward surface frictional deflection can be seen in Fig. 5.

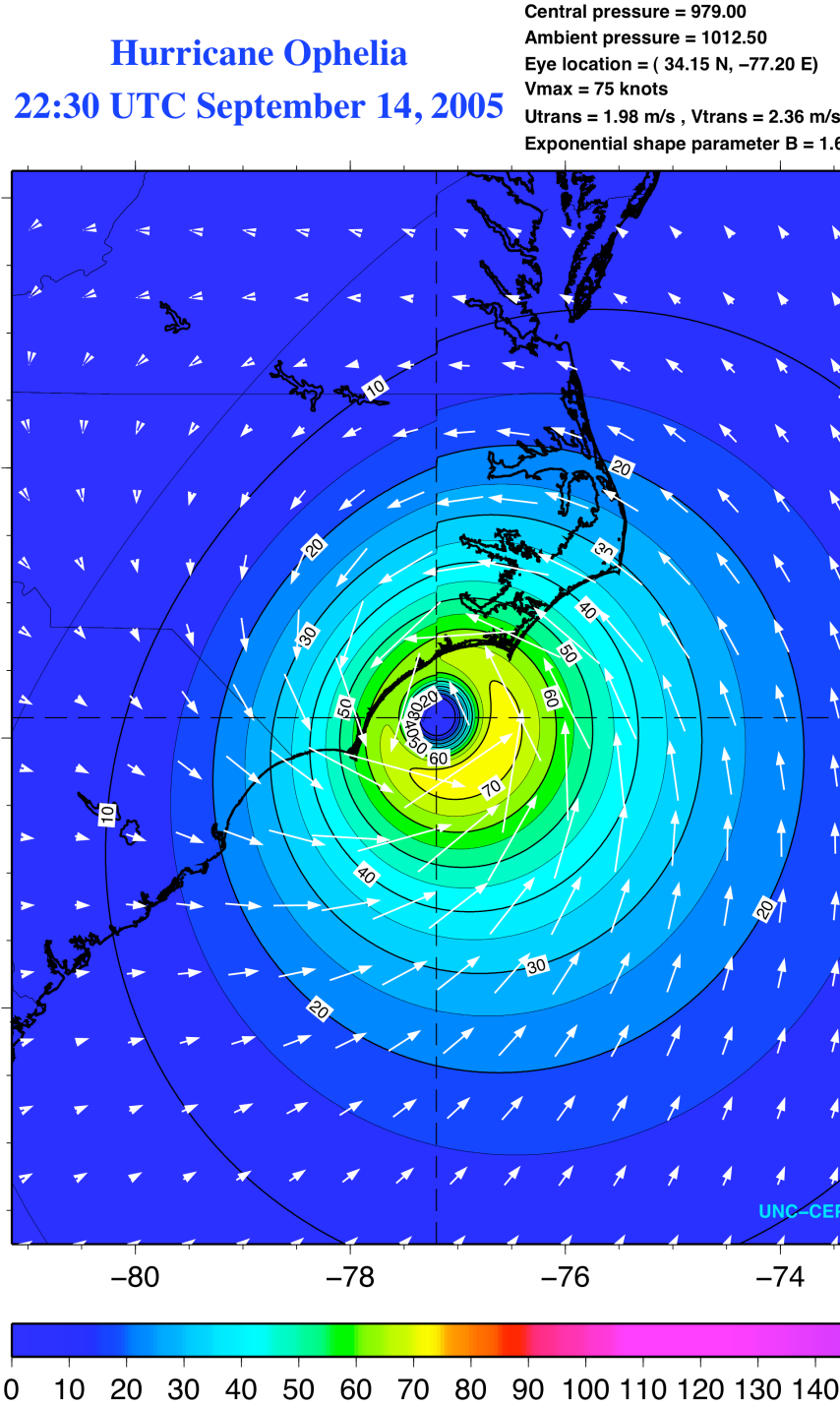


**FIG. 6.** Numerical discontinuity in the wind speed at  $\theta = 0, 360$  degrees due to the use of a 4<sup>th</sup>-order polynomial curve fit to obtain a relationship between the radius of maximum winds and the azimuth angle. This artifact, caused by the accumulation of error at the endpoints of the curve, was eliminated by switching to a cubic splines under tension curve fit. An added benefit of the new approach was an enhancement in the asymmetry of the vortex, making its shape more consistent with the observed/forecast wind radii reported by the National Hurricane Center.

In addition, the 4<sup>th</sup>-order polynomial curve fit for the radius of maximum winds vs. azimuth angle relationship used by Xie et al. (2006) was replaced with a cubic splines under tension fit because the former introduced a numerical discontinuity at 0 and 360 degrees due to the accumulation of error at the endpoints of the curve (Fig. 6), a well-known artifact of least-squares polynomial curve fits. The  $R_{\max}(\theta)$  relationship is computed from the wind radii reported in the NHC forecast advisory at the highest closed isotach available.

Because the gradient wind relationship is strictly valid only at the top of the surface boundary layer, where the atmospheric flow decouples from surface friction (Powell et al., 2003), the winds are linearly extrapolated to the top of the mean boundary layer (MBL) by dividing by the aforementioned wind reduction factor, after subtracting the translational velocity from the NHC advisory data. Once the shape parameter is calculated and the asymmetric  $R_{\max}$  vs.  $\theta$  curve fit is performed, the tangential velocity  $V_{\text{asym}}$  can be computed from Eq. (2). The winds are calculated at ADCIRC model nodal points, reduced back down to the surface, a 1-minute to 10-minute wind averaging operator is applied, the translational velocity components are restored, and the wind direction is altered by adding in the frictional inflow angle. This technique provides an analytical representation of a fully developed asymmetric tropical storm based on the following time-varying input parameters:

- (1) Surface pressure (mb) at the center of the storm:  $P_c$ ,
- (2) Ambient undisturbed synoptic background surface pressure (mb):  $P_n$ ,
- (3) Latitude (degrees N) and longitude (degrees E) of storm center: cLat, cLon,
- (4) Maximum sustained wind speed (knots) in the hurricane:  $V_{\max}$ ,
- (5) Wind radii (nm) in four (NE, SE, SW, NW) quadrants of the storm at either 34, 50, 64, or 100 knots:  $r(1), r(2), r(3), r(4)$ ,
- (6) Wind speed (knots) at which the above wind radii are measured or forecast:  $V_r$ ,
- (7) Date and time of the storm fix – used in computing the translational velocity (forward motion): year (yyyy), month (mm), day (dd), hour (hh), hourFcst (ff).

These parameters are highlighted in red in the sample NHC forecast advisory below:

```

ZCZC MIATCMAT1 ALL
TTAA00 KNHC DDHHMM
HURRICANE OPHELIA FORECAST/ADVISORY NUMBER 32
NWS TPC/NATIONAL HURRICANE CENTER MIAMI FL AL162005
0300Z WED SEP 14 2005

A HURRICANE WARNING REMAINS IN EFFECT FROM THE SOUTH SANTEE RIVER
SOUTH CAROLINA TO OREGON INLET NORTH CAROLINA...INCLUDING PAMLICO
SOUND.

... [more descriptive text by NHC Hurricane Specialist] ...

HURRICANE CENTER LOCATED NEAR 32.6N 78.0W AT 14/0300Z
POSITION ACCURATE WITHIN 10 NM

PRESENT MOVEMENT IS STATIONARY

ESTIMATED MINIMUM CENTRAL PRESSURE 982 MB

```

EYE DIAMETER 40 NM  
MAX SUSTAINED WINDS 65 KT WITH GUSTS TO 80 KT.  
64 KT..... 30NE 30SE 45SW 30NW.  
50 KT..... 60NE 60SE 60SW 45NW.  
34 KT..... 120NE 120SE 100SW 70NW.  
12 FT SEAS.. 200NE 250SE 225SW 80NW.  
WINDS AND SEAS VARY GREATLY IN EACH QUADRANT. RADII IN NAUTICAL MILES ARE THE LARGEST RADII EXPECTED ANYWHERE IN THAT QUADRANT.

REPEAT... CENTER LOCATED NEAR 32.6N 78.0W AT 14/0300Z  
AT 14/0000Z CENTER WAS LOCATED NEAR 32.6N 78.1W

FORECAST VALID 14/1200Z 33.4N 77.8W  
MAX WIND 70 KT... GUSTS 85 KT.  
64 KT... 30NE 30SE 30SW 30NW.  
50 KT... 60NE 60SE 60SW 45NW.  
34 KT... 120NE 120SE 100SW 70NW.

... [more forecast data] ...

Winds generated using the asymmetric gradient wind vortex algorithm from both operational NHC forecast advisories and the Automated Tropical Cyclone Forecasting (ATCF) system corrected “best track” data for several historical storms were compared with the National Oceanic and Atmospheric Administration (NOAA) Atlantic Oceanographic and Meteorological Laboratory (AOML) Hurricane Research Division’s H\*Wind surface wind analysis. Originally developed for input to DHS-FEMA’s HAZUS model, H\*Wind analyses are generally considered to be the best wind estimates available. Measurements from a multitude of observational platforms are assimilated by the system, including NHC advisories, Automated Surface Observing System (ASOS) weather stations, NOAA buoy, Coastal Marine Automated Network (C-MAN) towers, ship reports, surface-reduced flight track measurements and GPS dropwindsondes from the NOAA P3, G4 and US Air Force C-130 reconnaissance aircraft, remotely sensed winds from the polar orbiting SSM/I and ERS, the QuikScat platform and TRMM microwave imager satellites, and GOES cloud drift winds derived from tracking low-level near-infrared cloud imagery in the geostationary satellite imagery. Not only are these winds corrected for the influence of land/water and surrounding flow obstacles when the site exposure is known (Powell et al., 2004), but an exponential inland decay model (Kaplan and DeMaria, 1995) is applied to the landfall wind field projected along the official NHC forecast track.

These synthetic vortex vs. H\*Wind comparisons (Fig. 7) were used to calibrate the storm shape parameter B, the translational velocity damping coefficient, the frictional inflow angles, and the surface layer wind reduction and temporal wind averaging factors to obtain the most accurate storm surge forecasts possible. It is unlikely that the synthetic asymmetric vortex winds, constructed from a minimum of data (provided at the storm center and at 4 points in the surrounding quadrants), will ever be able to match the level of detail contained in the H\*Wind analyses due to the plethora of surface wind measurements used in the latter. Particularly noticeable is the lack of an exponential inland wind speed decay algorithm in the synthetic asymmetric vortex wind field, evident by the breaks in the isotachs over land in the H\*Wind product. This capability should be included in future versions of the software.

## Hurricane Ophelia 2230 UTC 14 SEP 2005

Max 1-min sustained surface winds (kt) for marine exposure  
Valid for marine exposure over water, open terrain exposure over land

Analysis based on ASOS\_LD\_TO from 1708 – 2147 z; SFMR43 from 1700 – 2130 z;  
CMAN\_LD\_TO from 1700 – 2105 z; GPSSONDE\_WL150 from 1726 – 2059 z;  
CMAN from 1700 – 2130 z; SHIP from 1815 – 1919 z; MOORED\_BUOY from 1700 – 2115 z;  
GOES from 1902 – 1902 z;

2230 z position extrapolated from 2005 z Vortex wind center using 40 deg @ 6 kts; mslp = 979.0 mb

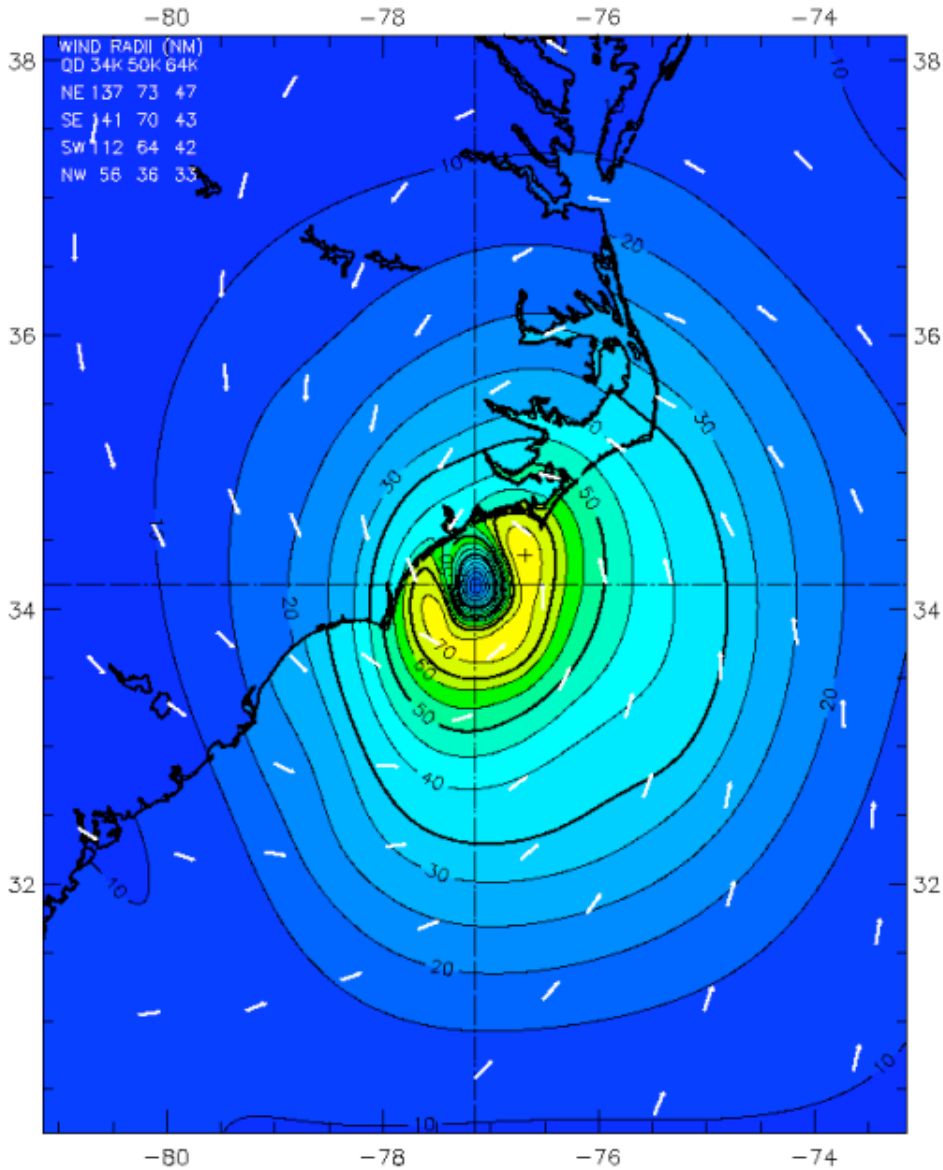


**FIG. 7a.** H\*Wind analysis for Hurricane Ophelia, valid at 22:30 UTC on September 14, 2005.

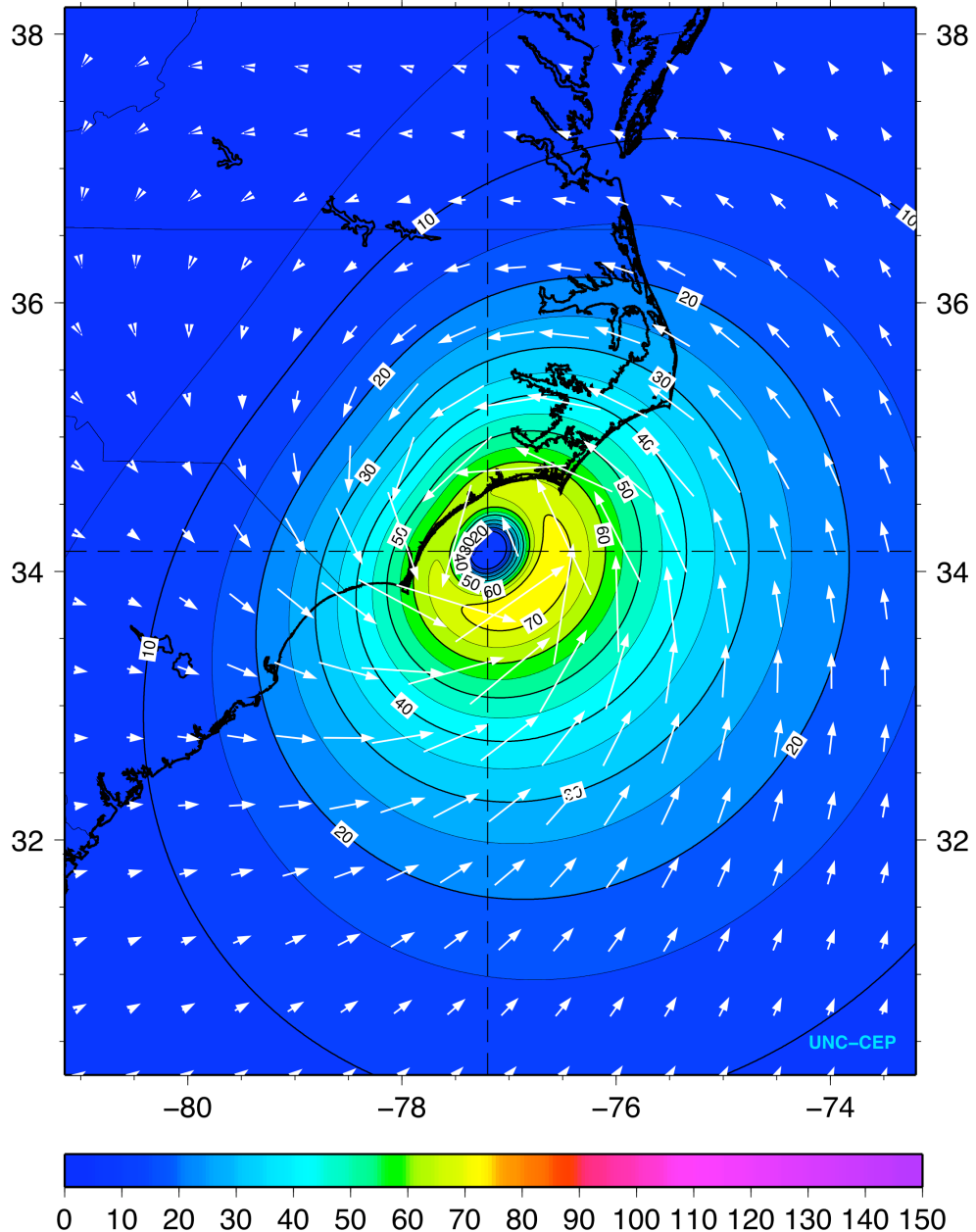


**FIG. 7b.** Asymmetric gradient wind vortex for Hurricane Ophelia, valid at 22:30 UTC on September 14, 2005. The quality of the parametric rendition is quite remarkable, given that the asymmetric vortex was constructed from very little observed meteorological data. The greatest difference between the two wind representations is due to the use of an exponential inland wind speed decay algorithm in the H\*Wind product.

Nevertheless, the aforementioned advantages of the analytical formulation and the timeliness in which the winds can be produced give the synthetic vortex approach an operational edge for the rapid prediction of storm surge.

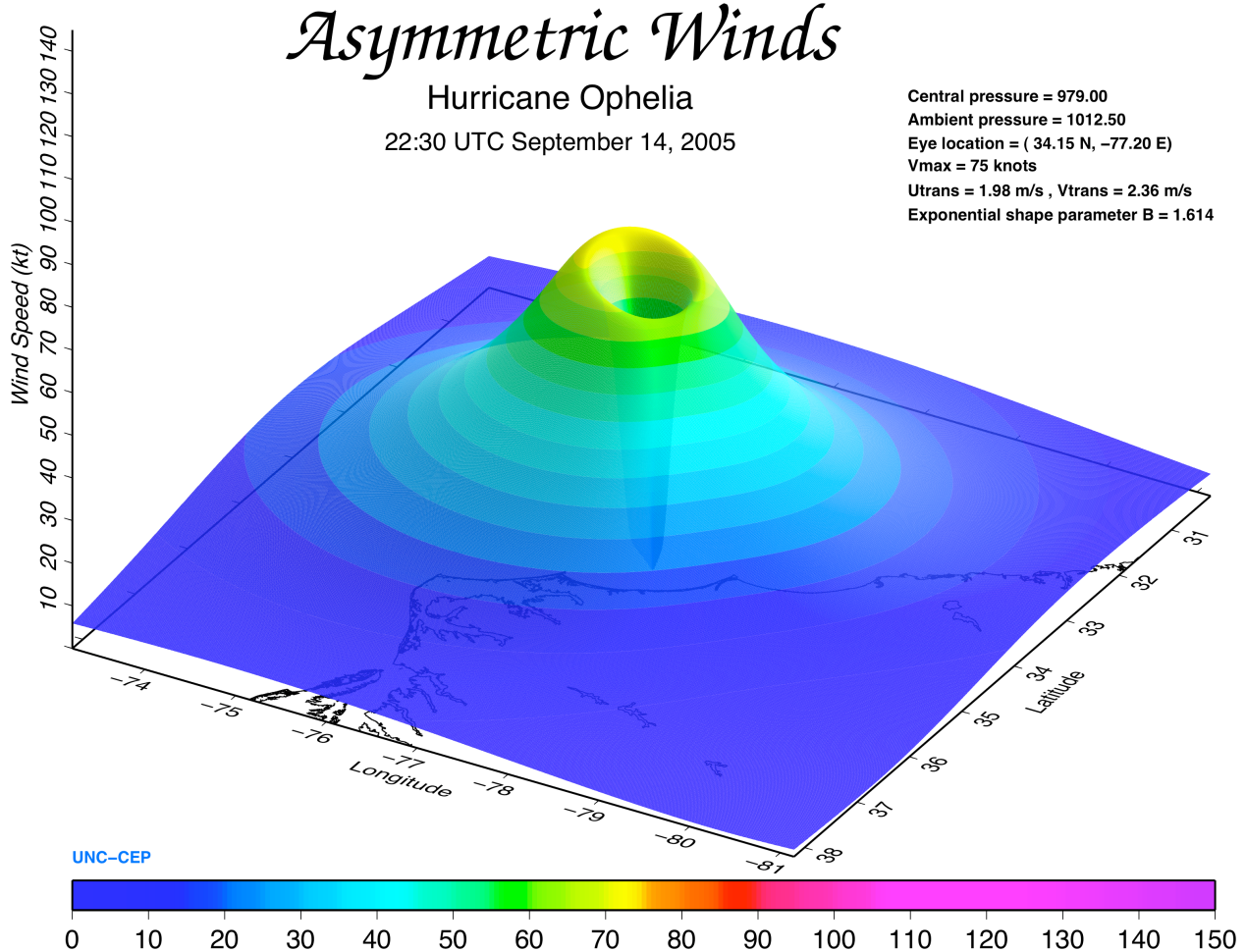


**FIG. 8.** A three dimensional perspective of the wind speeds generated using the asymmetric Holland gradient wind model for Hurricane Ophelia at 22:30 UTC on September 14, 2005. The view is from the northwest, looking offshore as the storm approached the NC coast.

### 3.2 The North Carolina Forecast System Operational Workflow

A schematic depiction of the NCFS operational workflow set up at RENCI is shown in Fig. 9.

The system runs in three different modes: background (tides only), event nowcast and event forecast.

## NORTH CAROLINA FORECAST SYSTEM Operational Workflow

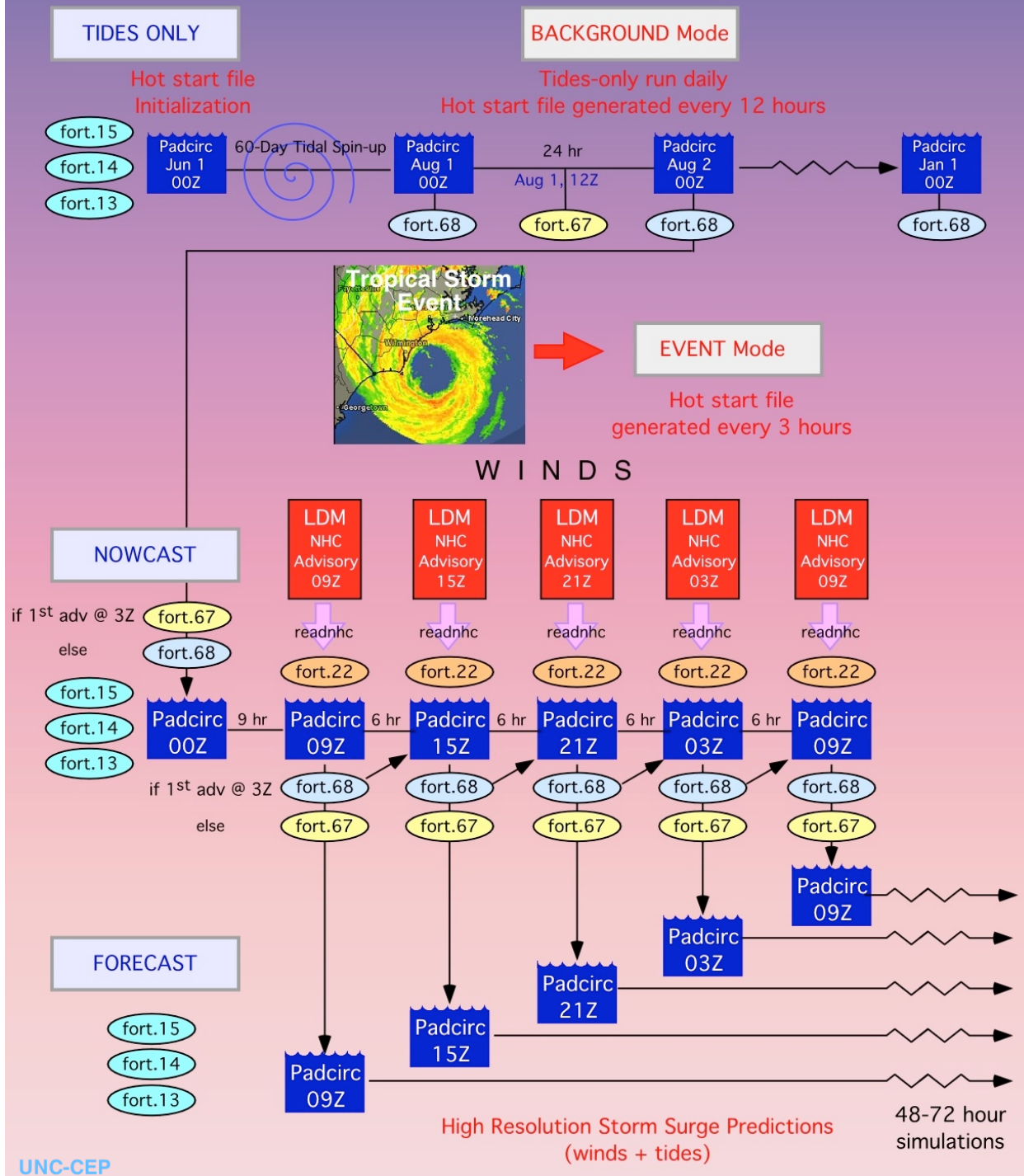


**FIG. 9.** Schematic depiction of the NCFS operational workflow set up at RENCI for the 2006 hurricane season, showing its three different modes of operation.

### **3.2.1 Background Mode: Tides-only runs**

Although the total tide is composed of approximately 399 known tidal constituents (Doodson, 1992), most have very small amplitudes so only the largest eight are required to capture over 90% of the tidal signal for ocean modeling applications. The eight primary lunar and solar tidal harmonic constituents (M2, S2, K2, N2, K1, O1, P1, Q1) were prescribed at the open water boundaries of the ocean model. Two steps are needed to incorporate the tides into ADCIRC. The first is the extraction of tidal data from a tidal database. The second step is to convert the data into ADCIRC format so it can be included in the input file (fort.15). The open-water lateral boundary conditions and tidal potential terms for the high-resolution NC ADCIRC model were generated from the Oregon State University's TOX0.62 Topex/Poseidon global model of ocean tides (<http://www.oce.orst.edu/research/po/research/tide/global.html>).

The start date for the initialization of the operational system was 00 UTC June 1, 2006. We allowed the tides-only run to reach equilibrium in 2 months and included tides in all operational ADCIRC model simulations to obtain more accurate forecasts of storm surge along the NC coastline. Once the tidal spin-up hotstart system was in place, the NCFS was ready for storm surge prediction. The hotstart (fort.67 and fort.68) files are kept up-to-calendar-date ("dragged along") by running simulations every 24 hours (at night) on RENCI's Linux cluster. The hotstart files are saved every 12 hours.

### **3.2.2 Event Nowcast Mode**

The storm nowcast simulation starts with the most recent tides-only hotstart file. The nowcast run brings the initial conditions up-to-date. The results are saved to initialize the nowcast phase of the next storm advisory run.

### **3.2.3 Event Forecast Mode**

Once a tropical storm enters the ADCIRC model domain (west of 60° W and north of 7.9° N), far in advance of an event that would threaten the NC coastline, forecast mode is automatically "switched on". This triggers a second model run initialized with NHC forecast advisories (or other wind datasets) that generates a series of 48-72 hour storm surge forecasts. We use the new asymmetric hurricane wind vortex code that produces wind fields on-the-fly at every time step from NHC forecast advisories.

The NHC forecast advisory data comes directly through the LDM to RENCI in real-time. These forecast advisories are fed to the LDM within 1-2 minutes after the Hurricane Specialists at NHC/TPC "hit the button" that submits the forecast to the National Weather Service (NWS) telecommunications gateway. Sent through AWIPS, then placed on the NOAA PORT, they are transmitted through the high-bandwidth Family of Services (FOS) Domestic Data Plus stream to subscribed LDMs. In order to capture this data, a line containing a regular expression was inserted into the LDM's pqact configuration-file (pqact.conf\_ddplus) to detect the AWIPS headers (MIATCMAT1-5) and the World Meteorological Organization (WMO) headers (WTNT21-25 KNHC) that identify these products:

```

ZCZC MIATCMAT5 ALL
000
WTNT25 KNHC 292045
TCMAT5
TROPICAL STORM ERNESTO FORECAST/ADVISORY NUMBER 21
NWS TPC/NATIONAL HURRICANE CENTER MIAMI FL AL052006
2100 UTC TUE AUG 29 2006

```

as soon as they enter the data stream, then the LDM PIPE command is used to automatically start up a unix shell script (invokeStormSurge.sh) that preprocesses this data and initiates the model run:

```

DDPLUS ^WTNT2([1-5]) KNHC PIPE -close -strip -flush
/home/.../ncfs/scoop/version2/scoop_ms/common/executables/linux-ncfs-
stormsurge/invokeStormSurge.sh

```

UNC-CEP scientists developed a NHC forecast advisory parser/decoding Fortran program (readnhc.F) to extract the current and forecast hurricane winds and radii information, then rewrite this data in compact “best track” format to very small output files (fort.22, Fortran logical unit 22). Below is an example of a fort.22 winds input file extracted from Tropical Storm Ernesto forecast advisory #21, issued at 21Z on August 29, 2006:

```

AL, 05, 2006082921, , ASYM, 0, 243N, 802W, 40, 1005, TS, 34, NEQ, 90, 90, 90, 40,
1013, 0, 0, 50, 0, L, 0, , 320, 11, ERNESTO, X
AL, 05, 2006083006, , ASYM, 9, 256N, 809W, 55, 1005, IN, 50, NEQ, 50, 50, 20, 30,
1013, 0, 0, 65, 0, L, 0, , 320, 11, ERNESTO, X
AL, 05, 2006083006, , ASYM, 9, 256N, 809W, 55, 1005, IN, 34, NEQ, 100, 100, 40, 75,
1013, 0, 0, 65, 0, L, 0, , 320, 11, ERNESTO, X
AL, 05, 2006083018, , ASYM, 21, 275N, 811W, 50, 1005, IN, 50, NEQ, 30, 30, 30, 30,
1013, 0, 0, 60, 0, L, 0, , 320, 11, ERNESTO, X
AL, 05, 2006083018, , ASYM, 21, 275N, 811W, 50, 1005, IN, 34, NEQ, 100, 100, 40, 60,
1013, 0, 0, 60, 0, L, 0, , 320, 11, ERNESTO, X
AL, 05, 2006083106, , ASYM, 33, 299N, 806W, 55, 1005, IN, 50, NEQ, 40, 40, 30, 50,
1013, 0, 0, 65, 0, L, 0, , 320, 11, ERNESTO, X
AL, 05, 2006083106, , ASYM, 33, 299N, 806W, 55, 1005, IN, 34, NEQ, 120, 120, 60, 100,
1013, 0, 0, 65, 0, L, 0, , 320, 11, ERNESTO, X
AL, 05, 2006083118, , ASYM, 45, 325N, 797W, 60, 1005, IN, 50, NEQ, 40, 40, 30, 50,
1013, 0, 0, 75, 0, L, 0, , 320, 11, ERNESTO, X
AL, 05, 2006083118, , ASYM, 45, 325N, 797W, 60, 1005, IN, 34, NEQ, 120, 120, 60, 100,
1013, 0, 0, 75, 0, L, 0, , 320, 11, ERNESTO, X

```

A new acronym (ASYM) for the objective technique designator was created to tag the records produced in this manner. These files are used to construct the synthetic asymmetric wind vortex that drives the ADCIRC model during the nowcast and forecast simulations.

NHC forecast advisories are issued at odd hours: 3Z, 9Z, 15Z, and 21Z. In event mode, the fort.67 file is used for a 3Z initialization and the simulation will always produce a fort.68 file at termination, while the fort.68 file is used to initialize simulations from the 9Z, 15Z and 21Z advisories and the simulation will always produce a fort.67 at its end. This ensures that the model spin-up time for the first advisory is at least 9 hours in duration, which allows any spurious transient waves generated by initialization shock to dissipate.

From the first advisory on, successive advisories arrive 6 hours apart. Hotstart files are saved at quadruple frequency, every 3 hours. All the nowcasts will then start with the fort.67 file (except in the 3Z case, which will start with the fort.68 file).

UNC-CEP scientists coded this operational workflow logic into initial and revised versions of the ADCIRC run scripts and provided them to RENCI IT personnel for operational deployment.

### 3.3 Operational Storm Surge Predictions

During the 2006 hurricane season, storm surge predictions were produced in real-time for three tropical storms (Beryl, Chris and Ernesto). We will focus our discussion on Tropical Storm Ernesto since it had the most impact on North Carolina.

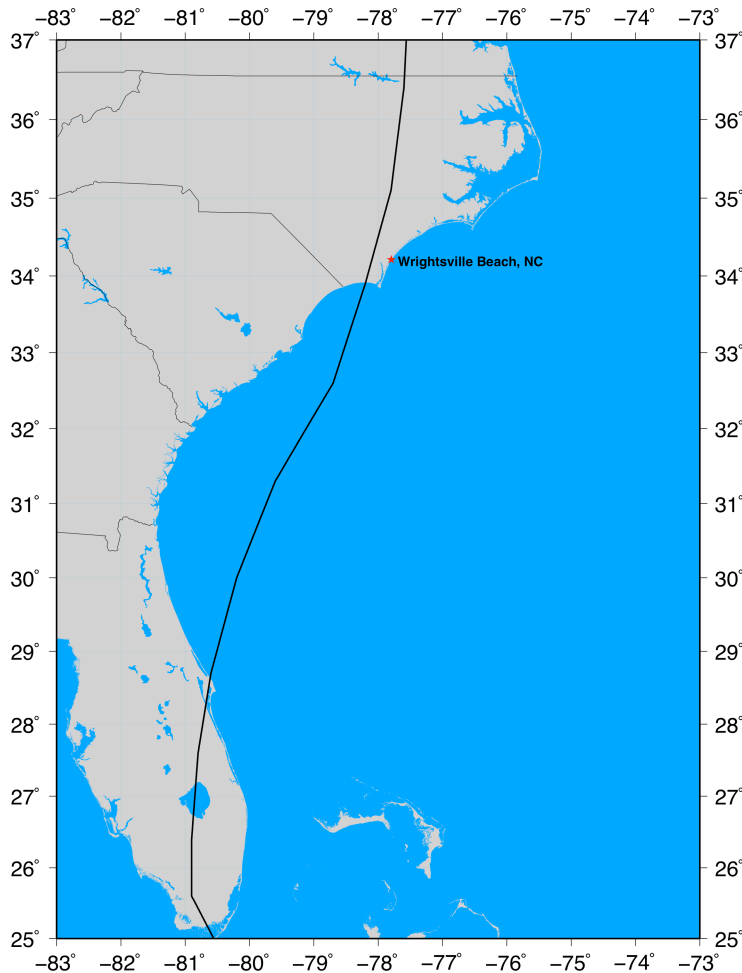


**FIG. 10.** Ernesto's track from Florida to North Carolina.

Tropical Storm (TS) Ernesto developed in a dry, sheared environment from a tropical wave moving through the windward islands on August 24, 2006. Originally forecast to track through the Caribbean and into the Gulf of Mexico, it turned northward instead, survived being ripped apart by the mountainous terrain in eastern Cuba, then crossed through the heart of the Florida

peninsula from the south. A tenacious little storm, it re-emerged over the Atlantic Ocean near Cape Canaveral late in the day on August 30. NCEP's NAM model persistently forecast Ernesto to be absorbed by a frontal system in South Carolina and dissipate but it remained offshore, intensified and just missed becoming a category 1 hurricane, with its peak winds nearing 75 mph, prior to making landfall at Long Beach, NC in Brunswick County around 11:40 P.M. Thursday, August 31, 2006 (3:40 UTC, September 1, 2006). TS Ernesto's path from Florida to NC is shown in Fig. 10.

The storm caused extensive flooding, with 14.61 inches (371 mm) of rain falling at Palmele Isle, in Wrightsville Beach in 24 hours. More than 100 people were forced out of their homes. Standing water and waves shut down major roads throughout the Outer Banks, and a 12-mile stretch of I-40 was briefly closed early September 1 due to flooding. Crop damage in North Carolina surpassed \$76 million. Ernesto's winds and rain caused power outages from North Carolina to Connecticut, with over 600,000 utility customers left in the dark. FEMA eventually declared 19 counties in Virginia disaster areas.

The NOAA/NOS/CO-OPs sea surface elevation record for the station at Wrightsville Beach is displayed in Fig. 11. It shows that TS Ernesto created a maximum surface elevation of 1.22 meters at 3:42 Z and a surge above tides of 0.982 meters.

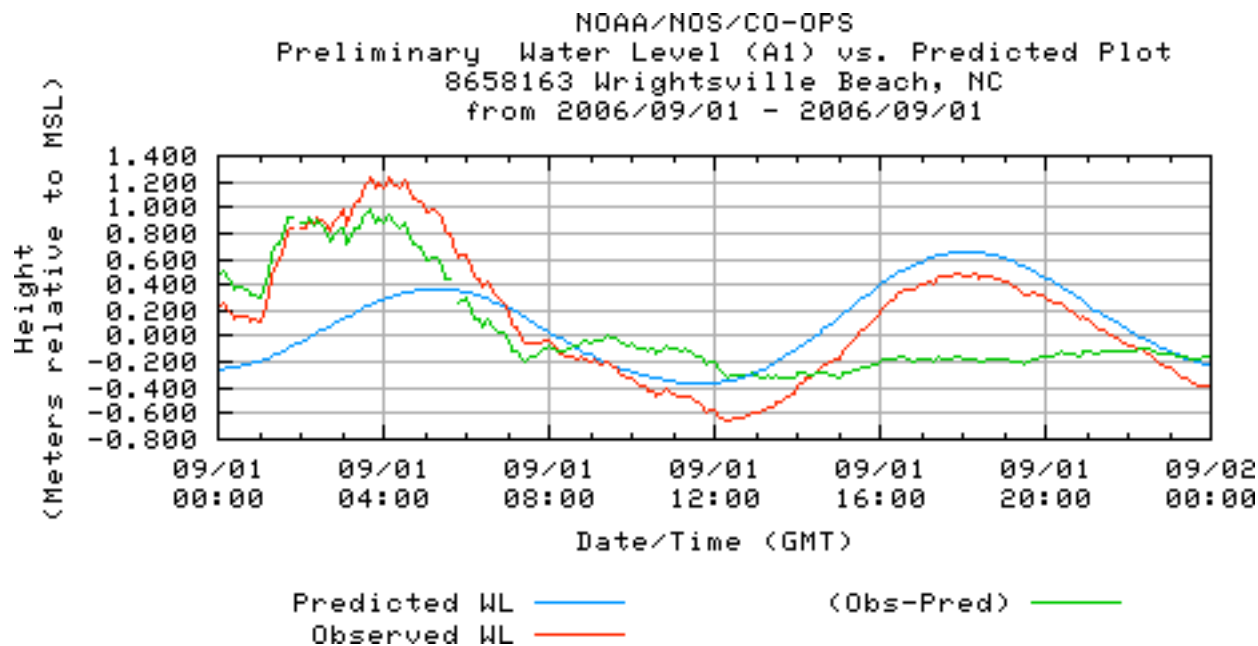


**FIG. 11.** The NOAA/NOS/CO-Ops sea surface elevation record for the station at Wrightsville Beach.

Tides were calculated starting June 1, 2006. ADCIRC was run daily in tides-only mode and, on August 28, 2006 when it was expected that TS Ernesto might impact the NC coast, the operational forecast system was triggered at 88 days into the simulations. The model was updated ("dragged along") every time a NHC forecast advisory was issued by running the simulation from the time of the previous advisory to the time of the current advisory (in nowcast mode) from August 28 through September 1, 2006 ("run days" 88 to 92.375). After each model

update, a storm surge prediction was run, starting from the current advisory time until the end of the forecast data (in forecast mode). This was done for all advisories issued by NHC.

An example of a 12-hour and a 6-hour forecast simulation follows.

### *Event Forecast Mode*

Fig. 12 shows the actual track (red) of TS Ernesto superimposed with NHC's operational 6-hour forecast track (brown) and 12-hour forecast track (green).

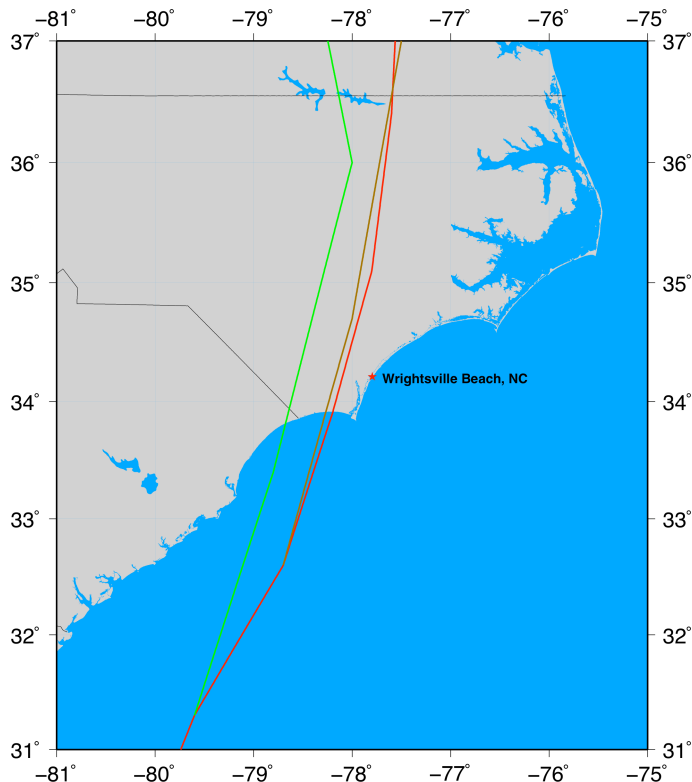


**FIG. 12.** Official National Hurricane Center “best track” (red) of Tropical Storm Ernesto superimposed with the operational 12-hour (green) and 6-hour (brown) forecast tracks. Note the abrupt shift eastward in the predicted landfall location over 12 hours.

The predicted landfall location shifted eastward by approximately 100 miles in 12 hours, from the Myrtle Beach area in South Carolina to the Holden Beach-Southport area along the southern coast of North Carolina. This error in the 12-hour forecast track is well beyond 40.1 nautical miles, the value used to define the radius in NHC's cone of uncertainty ([http://www.nhc.noaa.gov/verification/pdfs/OFCL\\_10-yr\\_averages.pdf](http://www.nhc.noaa.gov/verification/pdfs/OFCL_10-yr_averages.pdf)). Sudden changes like these in the predicted landfall location of tropical cyclones are good tests of an operational forecast system and justify the choices made in the design of the NCFS. If the TS Ernesto storm surge predictions had been delayed 3-6 hours while waiting to download and process the NCEP NAM model wind and pressure fields, they would have had very few hours of forecast utility remaining.

## 12-hour Operational Forecast

As soon as NHC forecast advisory #28 was issued at 15Z on August 31, the ADCIRC storm surge model was updated by running a 6-hour simulation from 9Z to 15Z. Then a forecast was initiated using the date and time of the forecast, location of the storm and surface pressure at its center, the maximum sustained winds, and radii information with the wind speed at the radii, extracted at all forecast times from the advisory.

The 10-minute averaged synthetic asymmetric vortex winds generated from NHC's 12-hour forecast advisory, valid at 3Z on September 1, 2006, are shown in Fig. 13. Note that the predicted center of TS Ernesto was located in South Carolina very close to the SC-NC border. Winds of 51.78 knots were predicted in the Wilmington area.

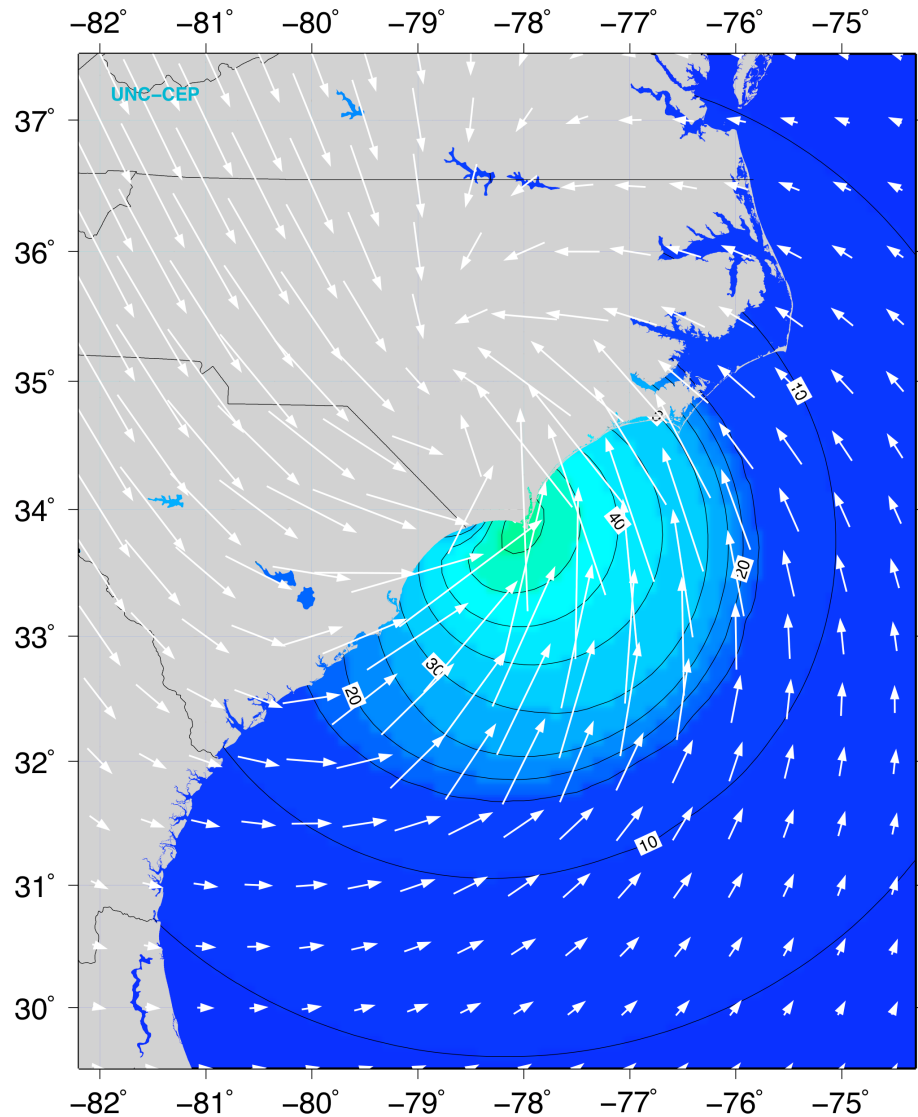


**FIG. 13.** The 10-minute averaged synthetic winds (kts) generated from the NHC's 12-hour forecast advisory valid at 3Z on September 1, 2006.

The predicted sea surface height and currents for the 12-hour forecast run are displayed in Fig. 14. A maximum surge of 1.595 meters is predicted up the Cape Fear River. The currents flow primarily northeastward, parallel to the NC coastline north of the SC-NC border, while there is a strong offshore component southwest of the hurricane.

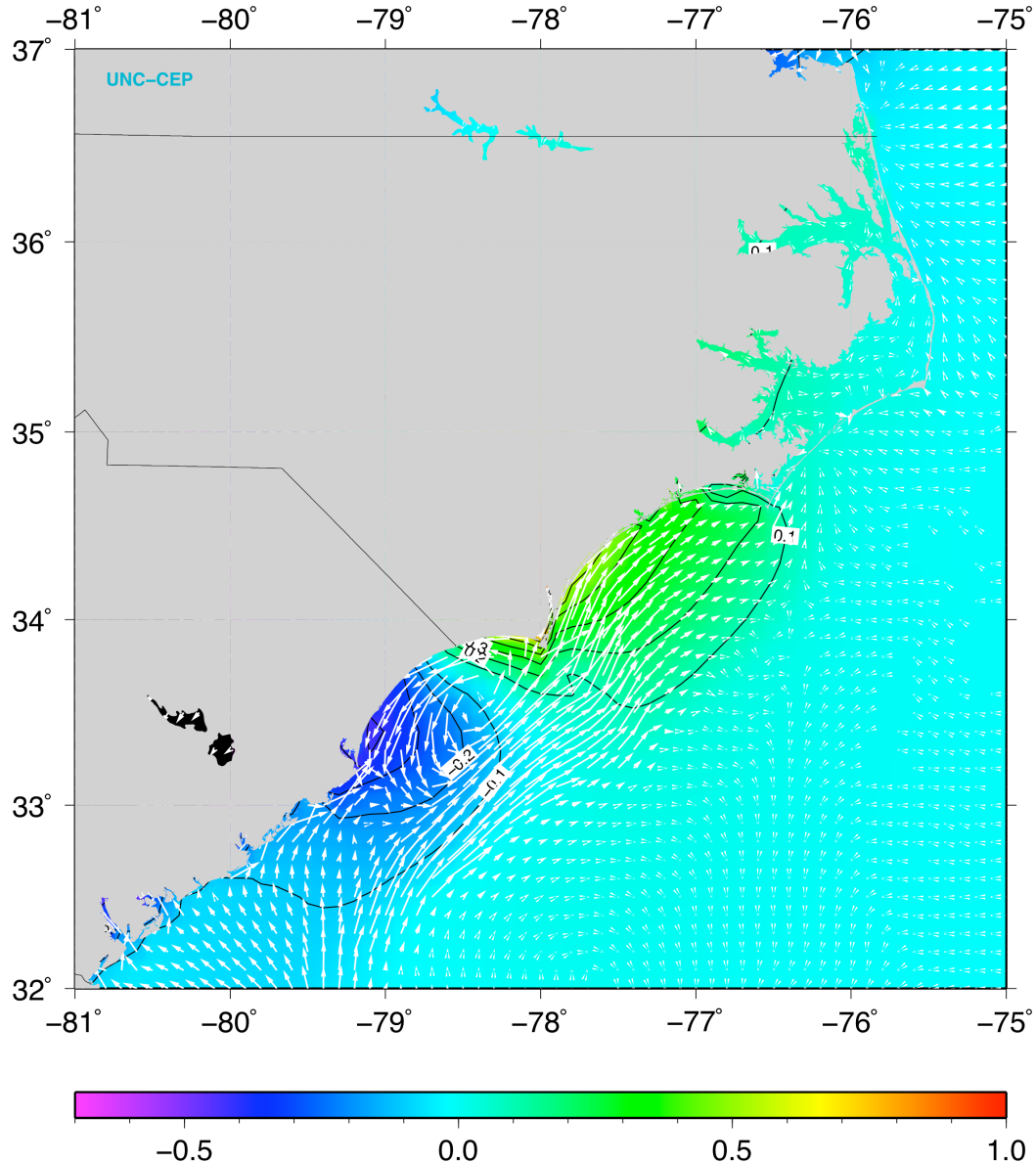


**FIG. 14.** Predicted sea surface elevation (m) and currents (m/s) from a 12-hour forecast of TS Ernesto, valid at 3Z on September 1, 2006.

The storm surge above tides, calculated by removing the model-predicted tides from the simulated sea surface elevation, is displayed in Fig. 15. A maximum surge above tides of 1.72 meters was predicted in the Cape Fear River.

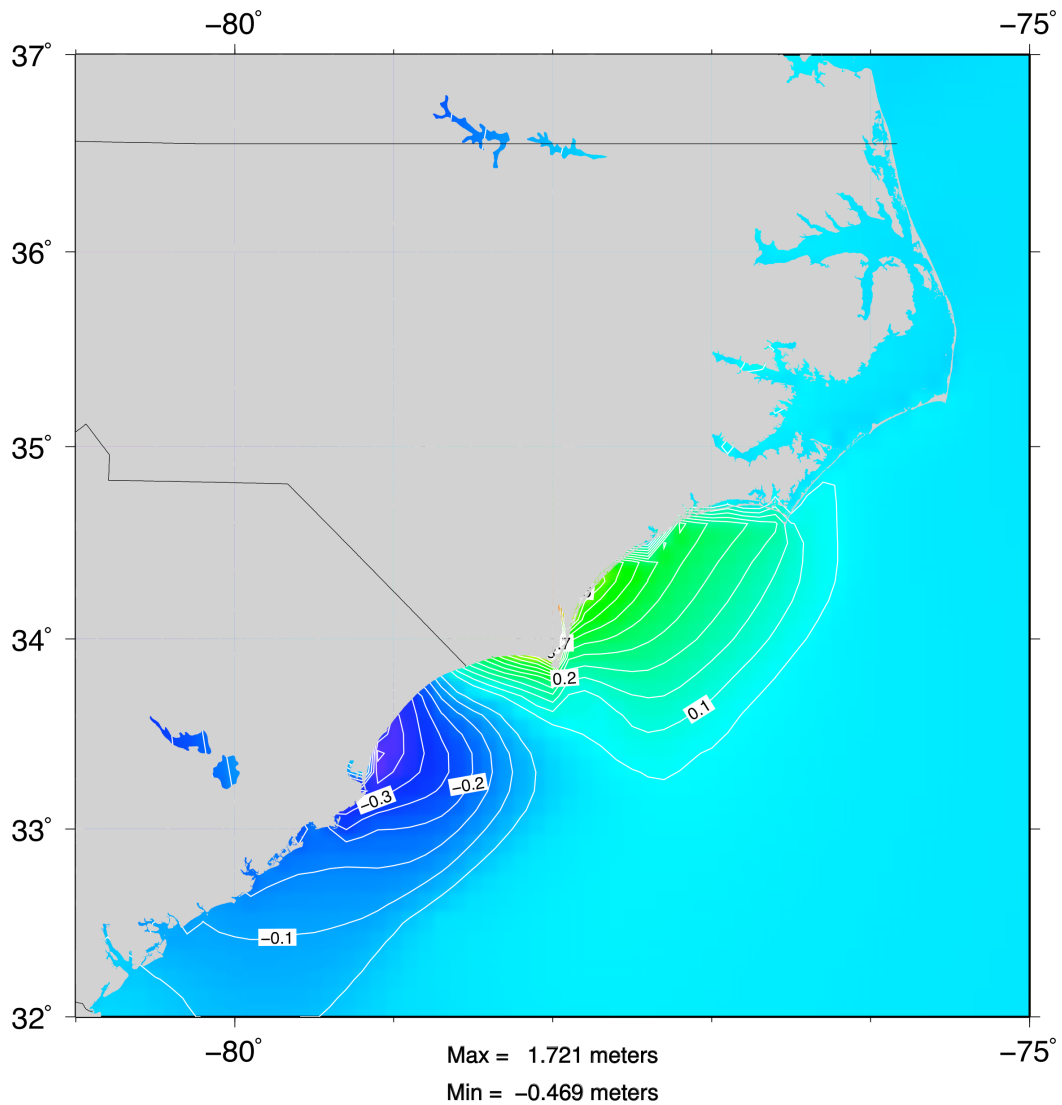


**FIG. 15.** Predicted storm surge (m) above tides from a 12-hour forecast of TS Ernesto, valid at 3Z on September 1, 2006.

### 6-hour Operational Forecast

When NHC forecast advisory #29 was issued at 21Z on August 31, the data from the advisory was extracted and the ADCIRC storm surge model was updated by running a 6-hour simulation from 15Z to 21Z with the nowcast data. After the update finished, a forecast run was performed with the forecast data from the advisory.

The 10-minute averaged synthetic asymmetric vortex winds generated from NHC's 6-hour forecast advisory, valid at 3Z on September 1, 2006, are shown in Fig. 16.

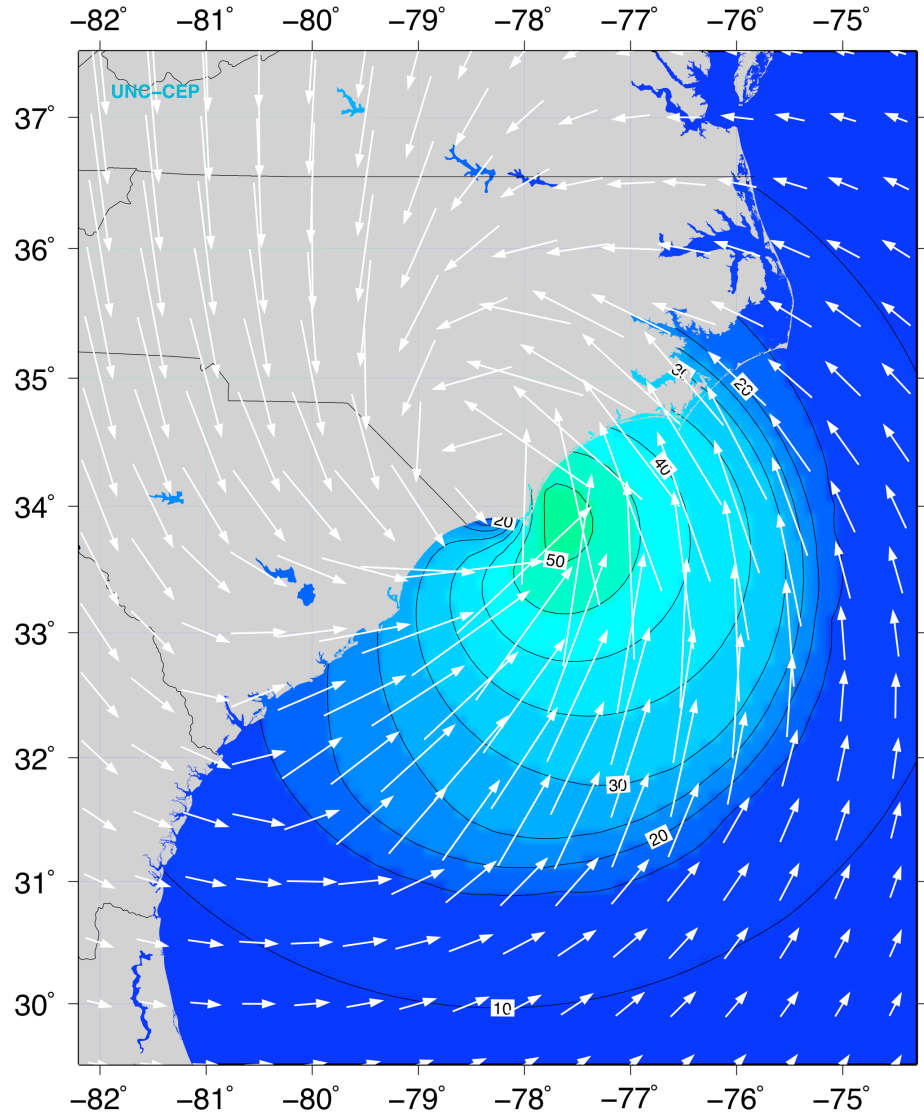


**FIG. 16.** The 10-minute average synthetic winds (kts) generated from the NHC's 6-hour forecast advisory valid at 3Z on September 1, 2006.

The center of the storm has moved eastward along the coast and is now located in the Holden Beach area along the southern coast of North Carolina. The highest predicted wind speeds have shifted offshore and their intensity has increased to 54.53 knots.

The predicted sea surface height and currents for the 6-hour forecast run are displayed in Fig. 17. The large-scale sea surface height maximum has moved up the coast and increased in magnitude. The surge up the Cape Fear River, about 0.90 meters, is smaller than in the 12-hour forecast, even though the winds have intensified. This is because the currents are now more perpendicular to the coastline, across the river's mouth, instead of flowing up the river.

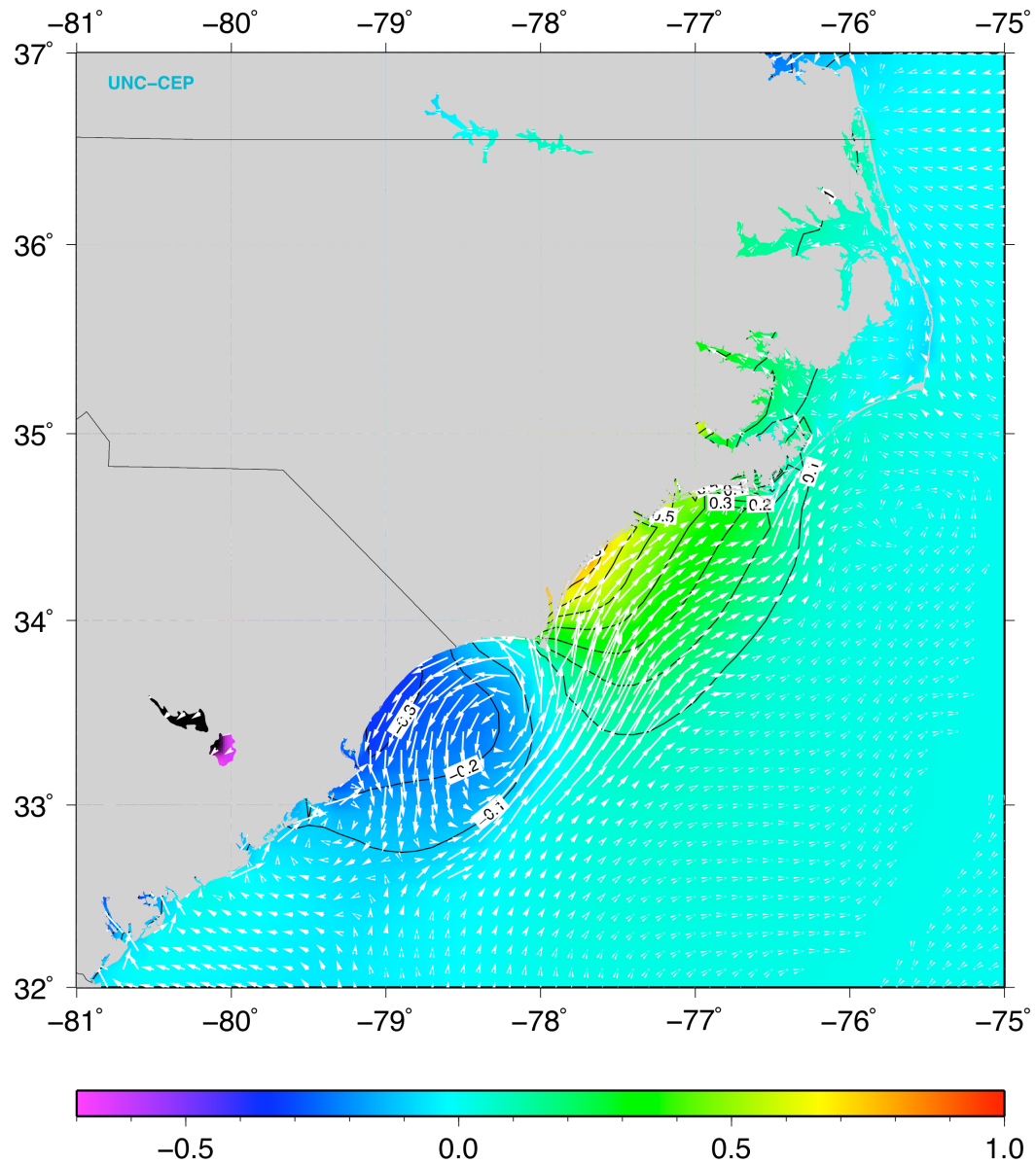


**FIG. 17.** Predicted sea surface elevation (m) and currents (m/s) from a 6-hour forecast of TS Ernesto, valid at 3Z on September 1, 2006.

The 6-hour forecast predicts that the storm surge above tides (Fig. 18) has diminished to 1.3 meters with the maximum shifted further east along the coast than in the 12-hour forecast.

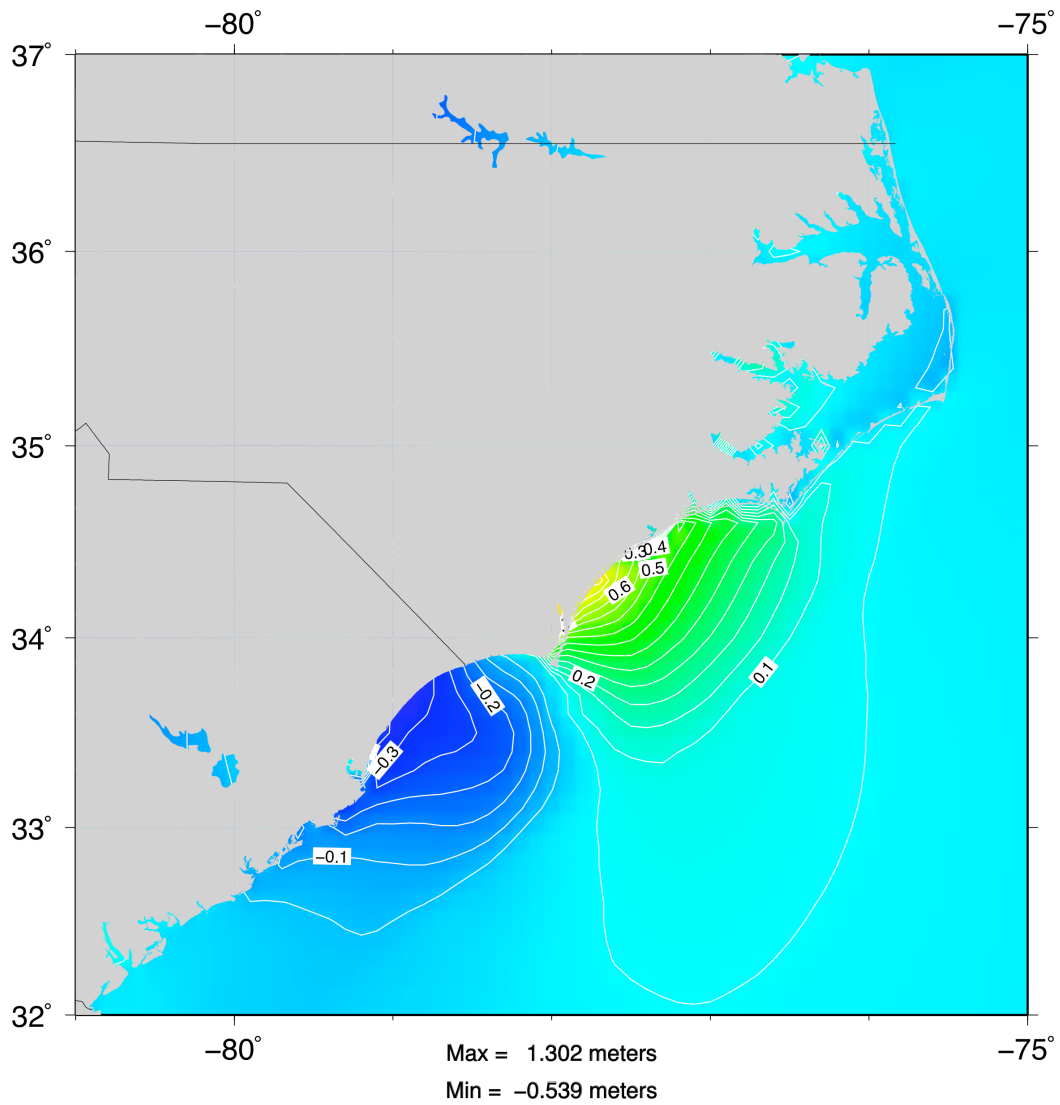


**FIG. 18.** Predicted storm surge (m) above tides from a 6-hour forecast of TS Ernesto, valid at 3Z on September 1, 2006.

### *Event Nowcast Simulations*

Immediately after forecast advisory #30 was issued for TS Ernesto at 3Z on September 1, its data was parsed and used to update the ADCIRC hotstart files from 21Z on August 31, 2006 to 3Z on September 1. Then another forecast was simulated. Once NHC forecast advisory #31 was released, the model was once again updated to 9Z.

The 10-minute averaged synthetic asymmetric vortex winds from the nowcast simulation, valid at 3Z on September 1, 2006, are shown in Fig. 19. It shows the center of TS Ernesto close to landfall, which officially occurred 40 minutes later.

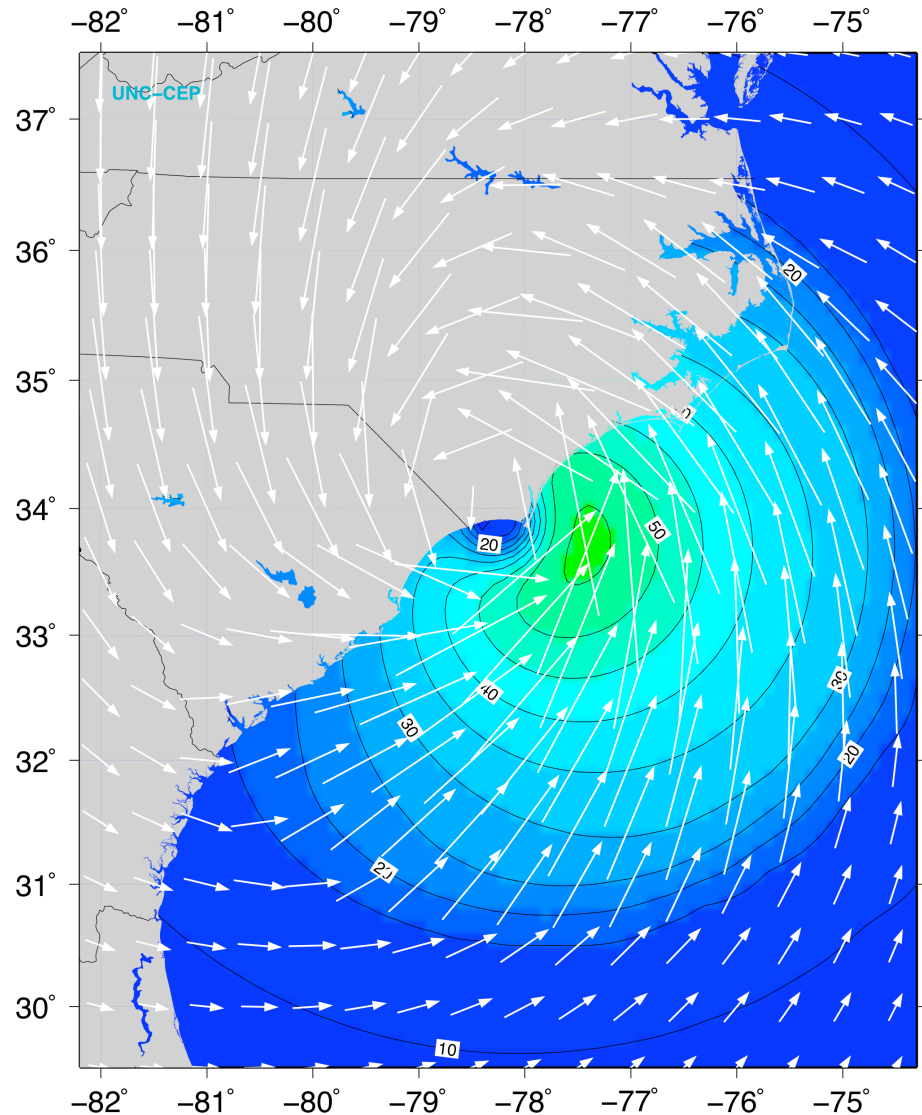


**FIG. 19.** Nowcast 10-minute averaged synthetic winds (kts) generated from the NHC's forecast advisory valid at 3Z on September 1, 2006.

The sea surface heights that were generated from an ADCIRC simulation driven by winds from the 3Z NHC forecast advisory, just 40 minutes prior to landfall, are displayed in Fig. 20. The storm surge is greater than 1 m in a swath near Topsail Beach along the southeastern coast of NC. There are some small isolated peaks of high sea surface elevation further to the northeast and a sound-side maximum of 1.48 m close to Emerald Isle, NC. Also evident in Fig. 20 is a large gradient across Pamlico Sound, high elevations up the Neuse River, and strong currents in the Croatan Sound and Alligator River.

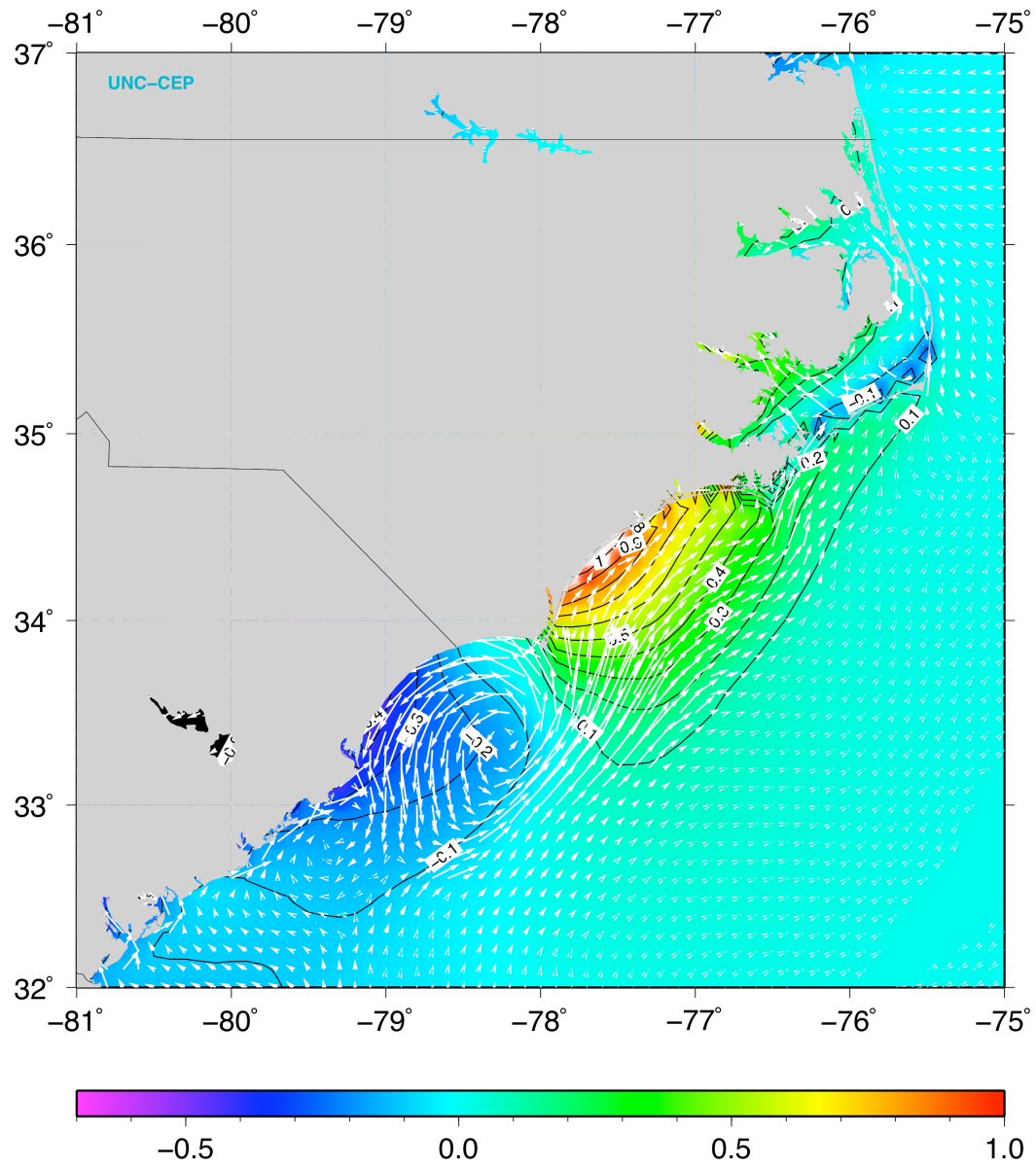


**FIG. 20.** Nowcast sea surface elevation (m) and currents (m/s) produced by TS Ernesto, valid at 3Z on September 1, 2006.

The storm surge above tides for the nowcast simulation is shown in Fig. 21. The maximum at 3Z was 1.15 meters, lower than in the previous ADCIRC forecasts. However, higher surface elevations are distributed more broadly along the NC coast instead of occurring at isolated peaks.

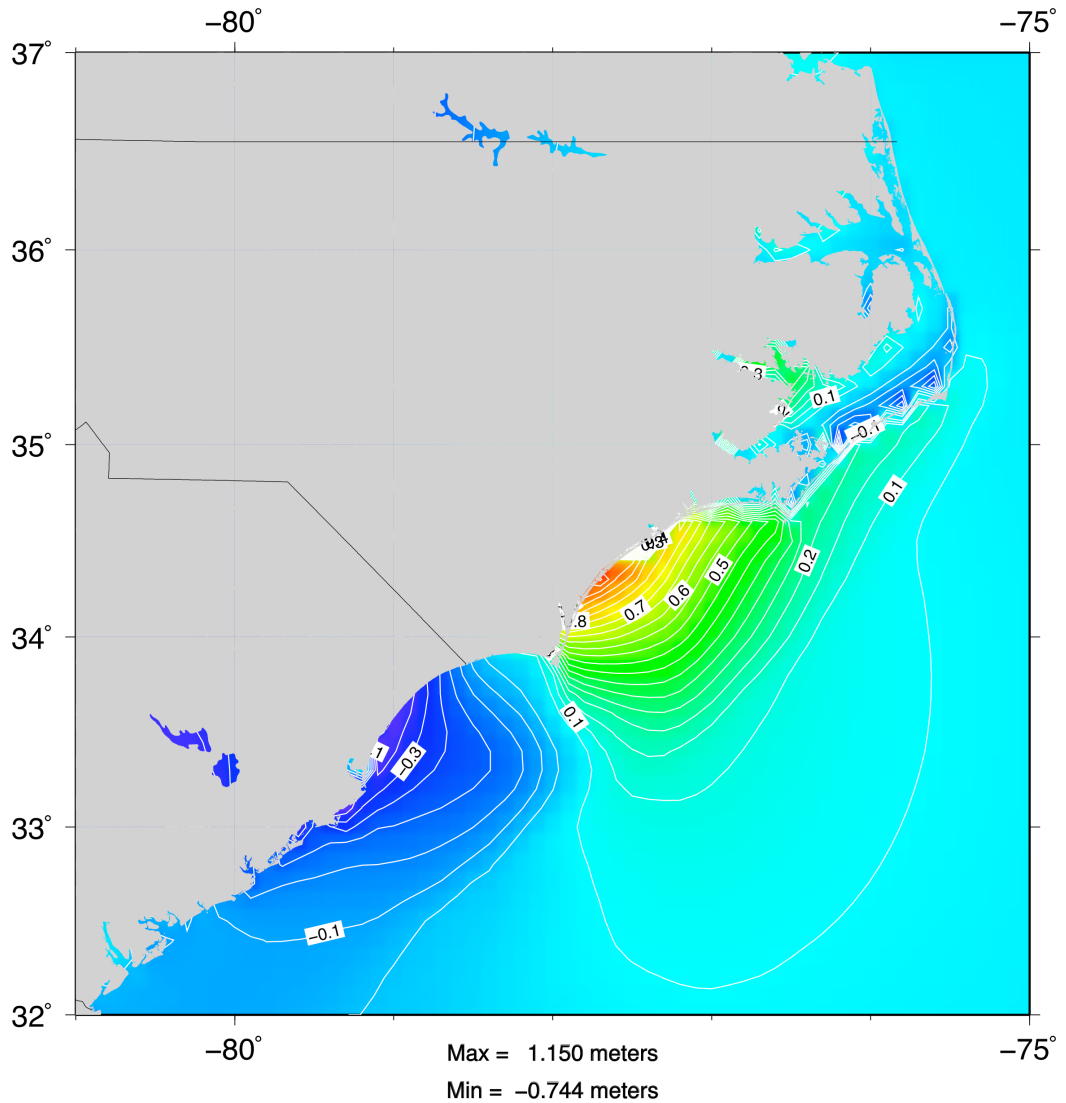


**FIG. 21.** Nowcast storm surge (m) above tides produced by TS Ernesto, valid at 3Z on September 1, 2006.

The sea surface heights from the ADCIRC 12-hour, 6-hour and 0-hour forecasts (the latter defined as the nowcast) are compared with the NOAA/NOS-CO-OP observations at Wrightsville Beach, NC in Fig. 22. It displays the evolution of the sea surface elevations with decreasing forecast lead time. As expected, the simulated sea surface height approaches the observations as the forecast times approach the time of the storm's landfall. The maximum sea surface height in the 12-, 6-, and 0-hour forecasts is 0.57, 0.74, and 0.99 m, respectively, while the highest elevation observed at Wrightsville Beach is 1.22 m, which occurs slightly after the maximum predicted by the model. The difference between the 12-hour forecast and the nowcast is 0.42 m, while the difference between the 6-hour forecast and the nowcast is only 0.25 m.

## Tropical Storm Ernesto ADCIRC vs Observations at Wrightsville Beach, NC

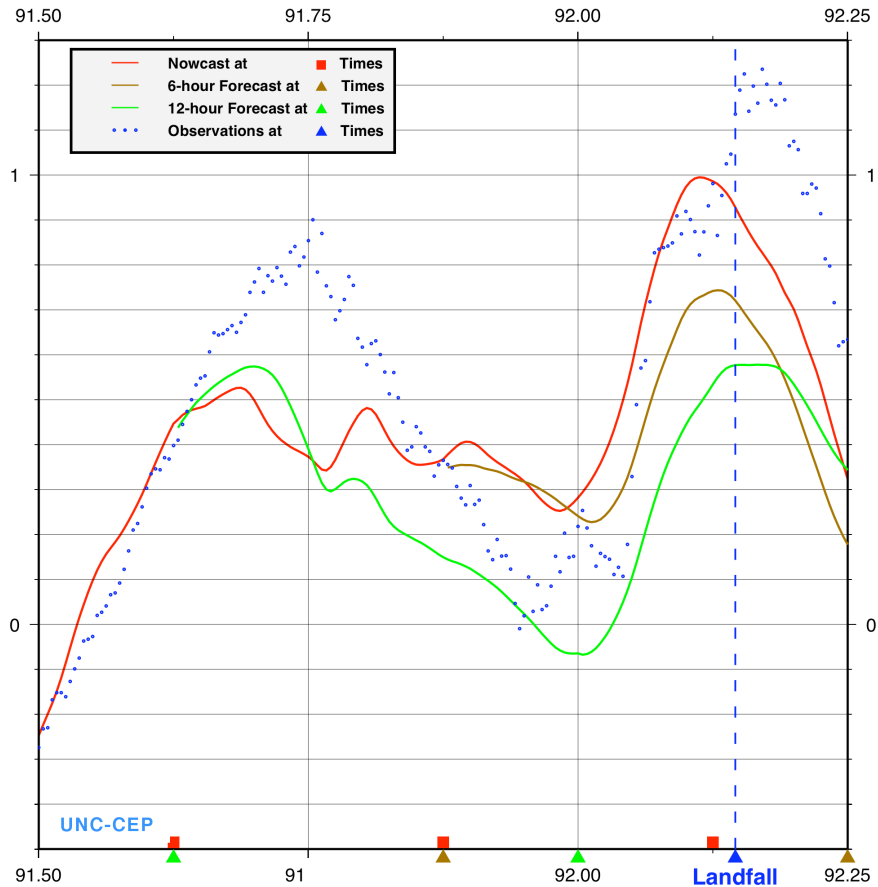
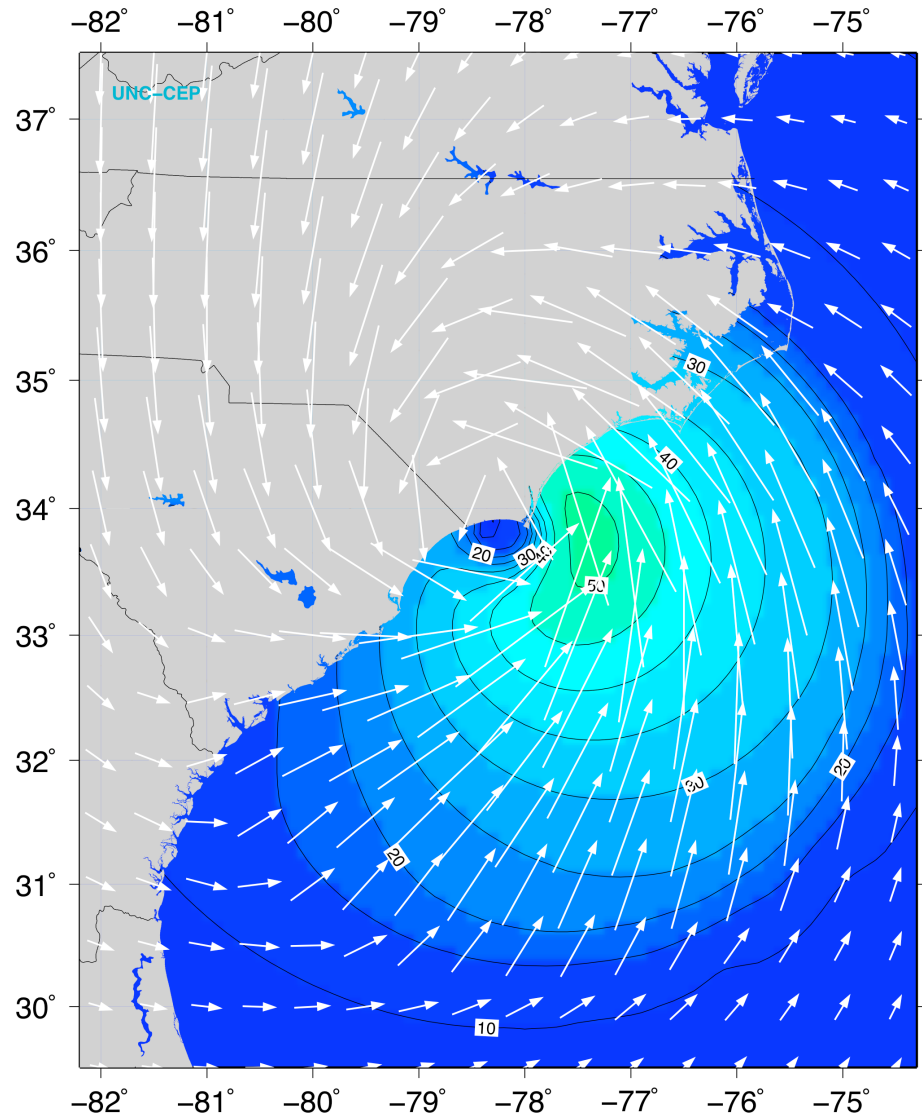


**FIG. 22.** Evolution of the sea surface elevations (m) predicted from a 12-hour ADCIRC forecast (green), 6-hour forecast (brown) and nowcast (red) simulations of TS Ernesto vs. NOAA/NOS/CO-OP observations (blue dots).

### Hindcasts

In order to quantify and qualify the results we obtained from our operational predictions run during the 2006 hurricane season, we ran two cases retrospectively with different types of wind forcing. In the first case, we compared our real-time NCFS forecasts with simulations driven by NHC's official best track wind information (in "best track hindcast" mode) to evaluate how errors in NHC's track/intensity forecasts impact the quality of the storm surge predictions. In the second case, we drove the model with H\*Wind analyses to determine whether the synthetic asymmetric vortex winds forcing could compare with forcing from a complete, data-rich analysis of the wind field.

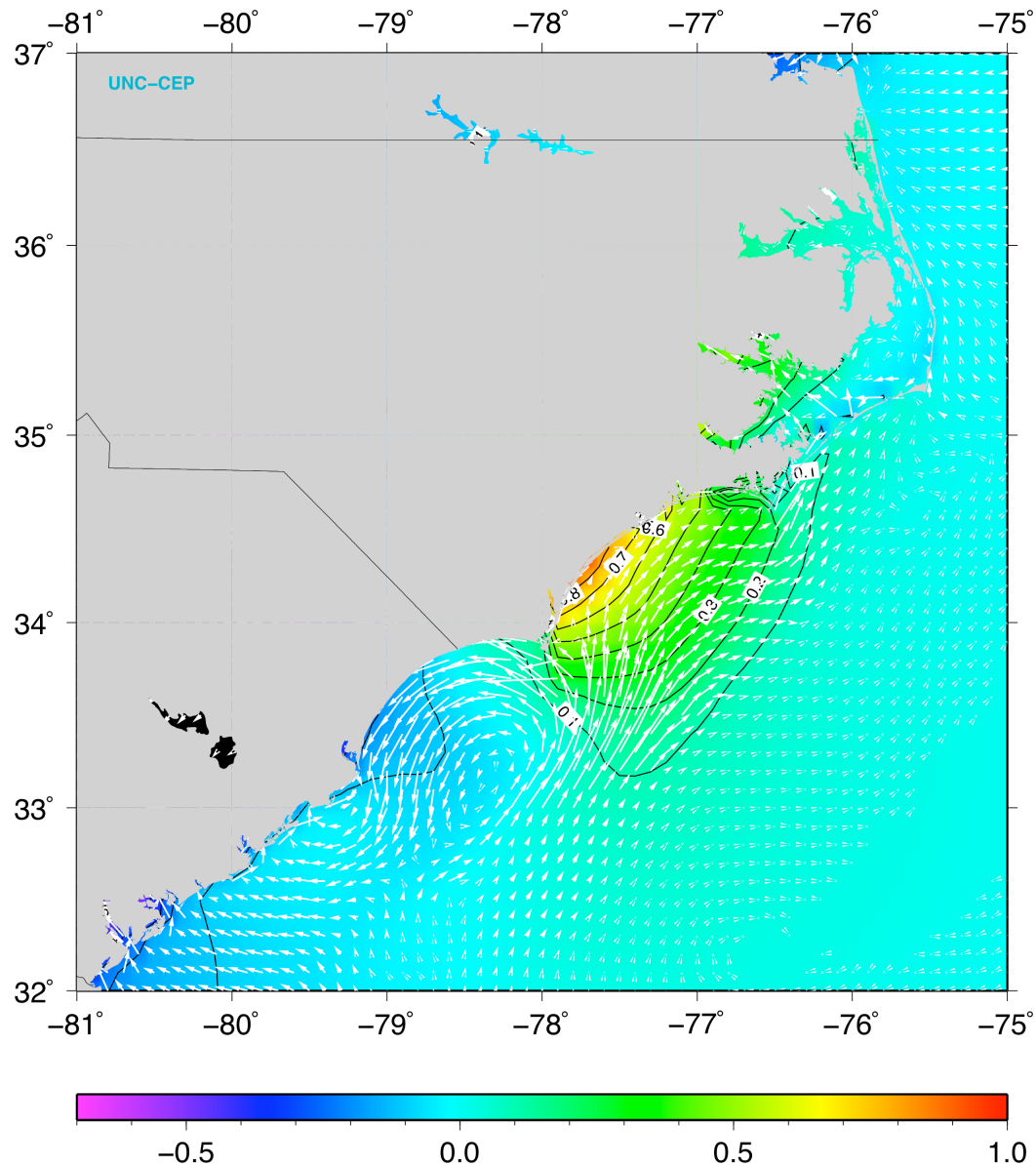
The synthetic winds derived from the best track data at 3Z September 1 are shown in Fig 23.



**FIG. 23.** The 10-minute averaged synthetic winds (kts) generated from the best track data at 3Z on September 1, 2006.

These winds are slightly lower than the synthetic winds produced from the real-time NHC forecast advisories (Fig. 19). The areal extent of the 45 kt isotach is reduced and the overall width of the storm is smaller. On the other hand, the eye diameter is larger in the best track rendition. The best track storm center is further offshore than the storm constructed from the operational NHC advisory winds.

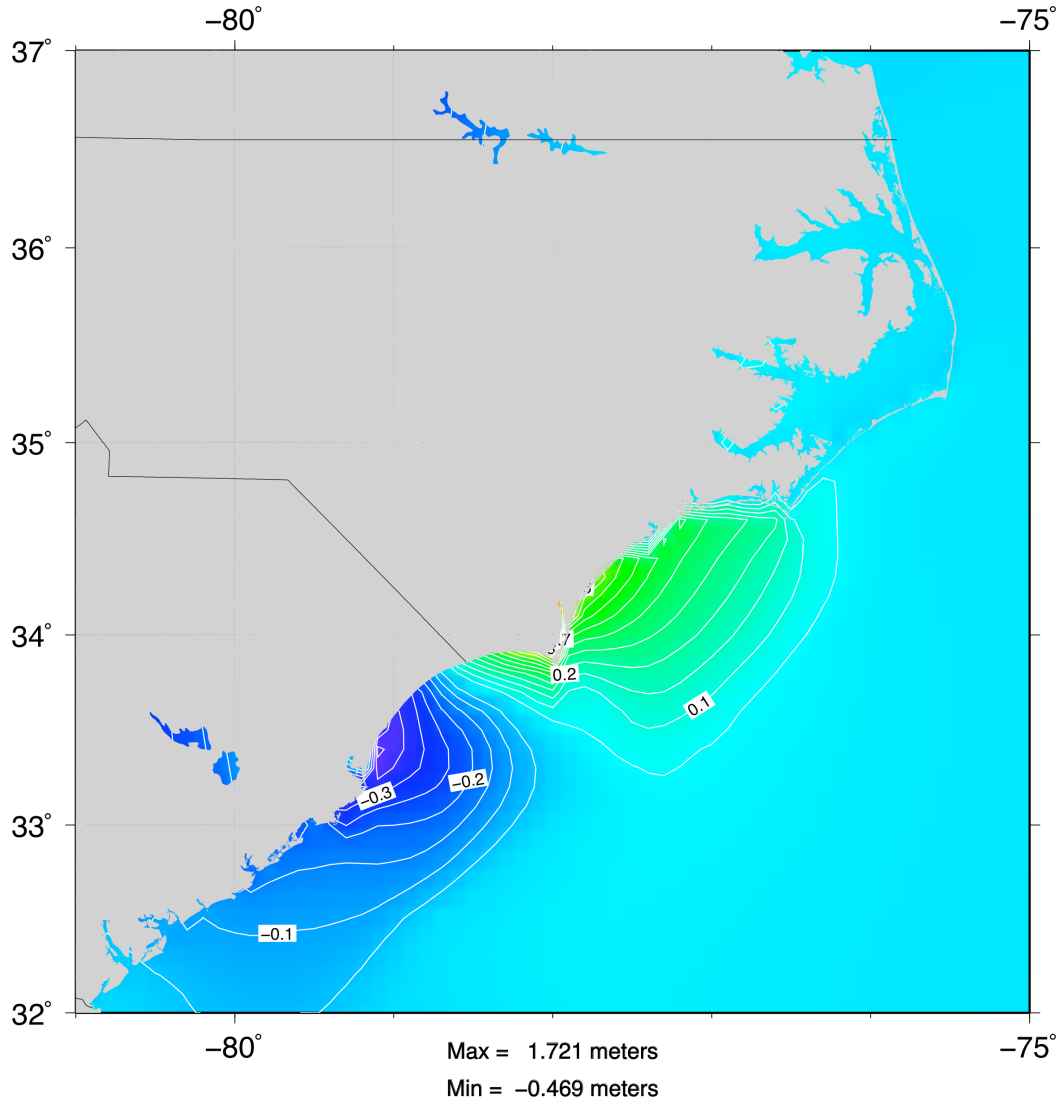
The sea surface height and currents forced with the best track winds are displayed in Fig. 24.



**FIG. 24.** Sea surface elevation (m) and currents (m/s) forced with best track winds from TS Ernesto, valid at 3Z on September 1, 2006.

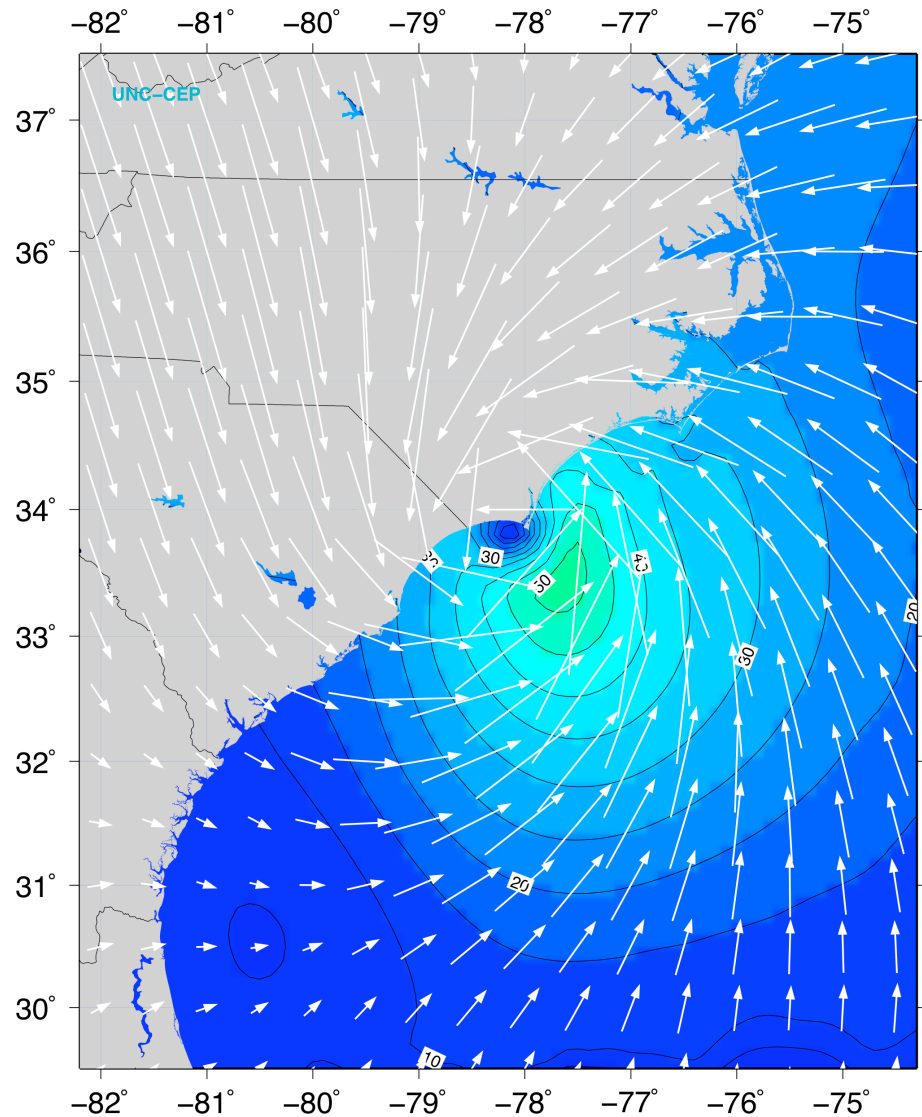
The sea surface height maximum in the right front quadrant of the storm and the draw down on the west side of the storm are both reduced in magnitude. However, higher elevations occur in the Pamlico Sound to the lee of the barrier islands, while lower elevations occur along the coast and up the Neuse River in the simulation driven by best track winds, when compared against the case forced with real-time NHC advisory data.

Even though the storm surge along the coast with the best track winds (Fig. 25) appears to be much smaller than in the asymmetric NHC winds case (Fig. 21) and it is not so widely spread offshore, it reveals that the best track simulation produces a maximum surge of 1.721 m up the Cape Fear River.



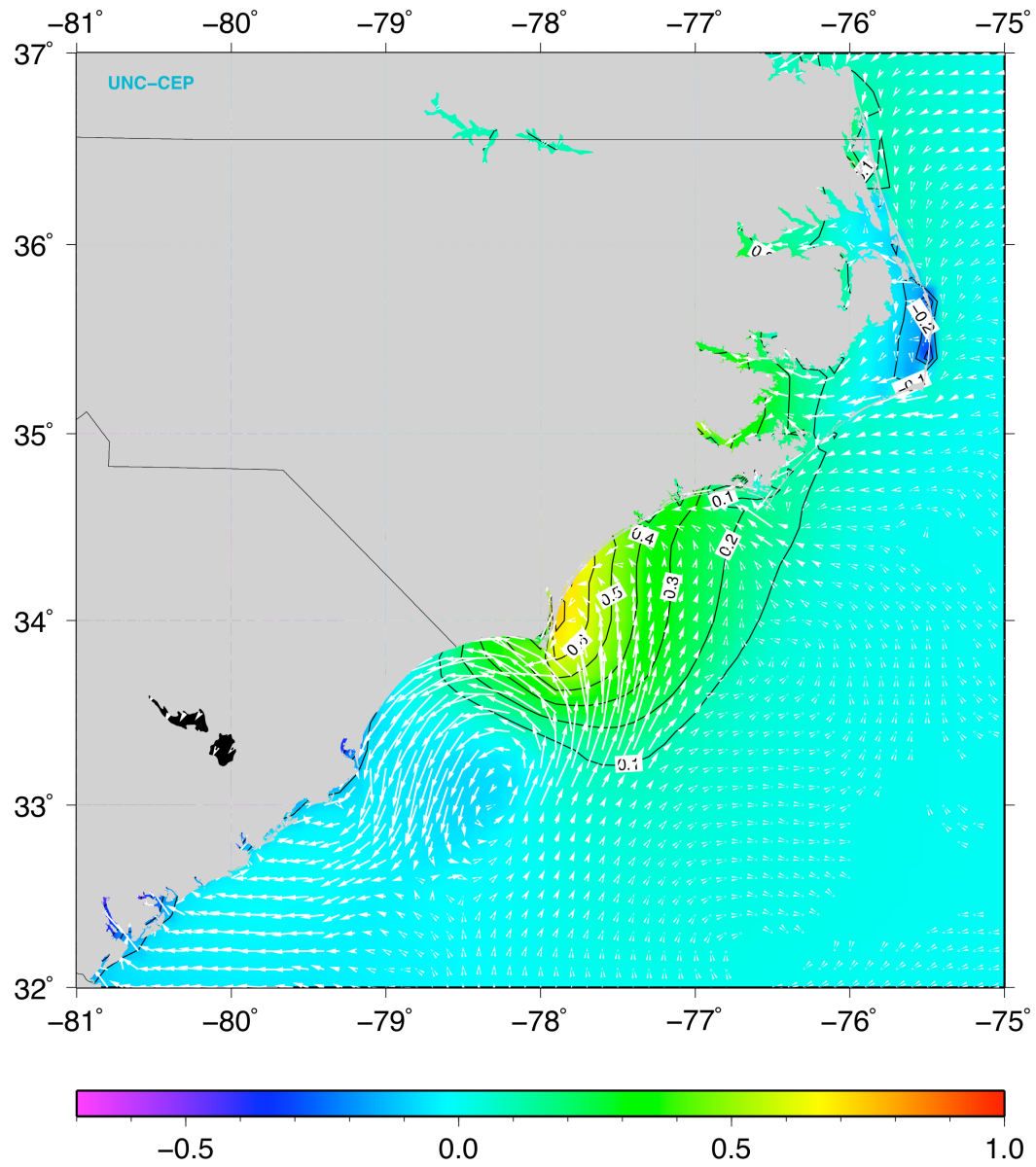
**FIG. 25.** Simulated storm surge (m) above tides forced with best track winds from TS Ernesto, valid at 3Z on September 1, 2006.

Fig. 26 shows the ADCIRC winds generated from the H\*Winds analysis for September 1 at 3Z. The storm is less intense but has the same general distribution of winds. The maximum wind intensity is 52.23 knots, compared to the NHC advisory-derived winds of 56.14 knots.



**FIG. 26.** ADCIRC winds (kts) generated by H\*Winds analysis for 03Z September 1, 2006.

Note, in Fig. 27, that the sea surface height is also smaller in the H\*Winds driven storm surge simulation, with a maximum of 0.925 m. The gradients in the Pamlico Sound exhibit a different distribution due to a more easterly wind direction and the draw down to the west of the storm is smaller in magnitude, consistent with the lower intensity of the winds in that area.



**FIG. 27.** Sea surface elevation (m) and currents (m/s) from ADCIRC simulation forced with H\*Winds for TS Ernesto, valid at 3Z on September 1, 2006

The maximum storm surge above tides generated by the H\*Winds driven simulation, shown in Fig. 28, is 0.798 m, the smallest value obtained in all the simulations for this particular time. This suggests that the H\*Winds forcing produces underestimates of storm surge.

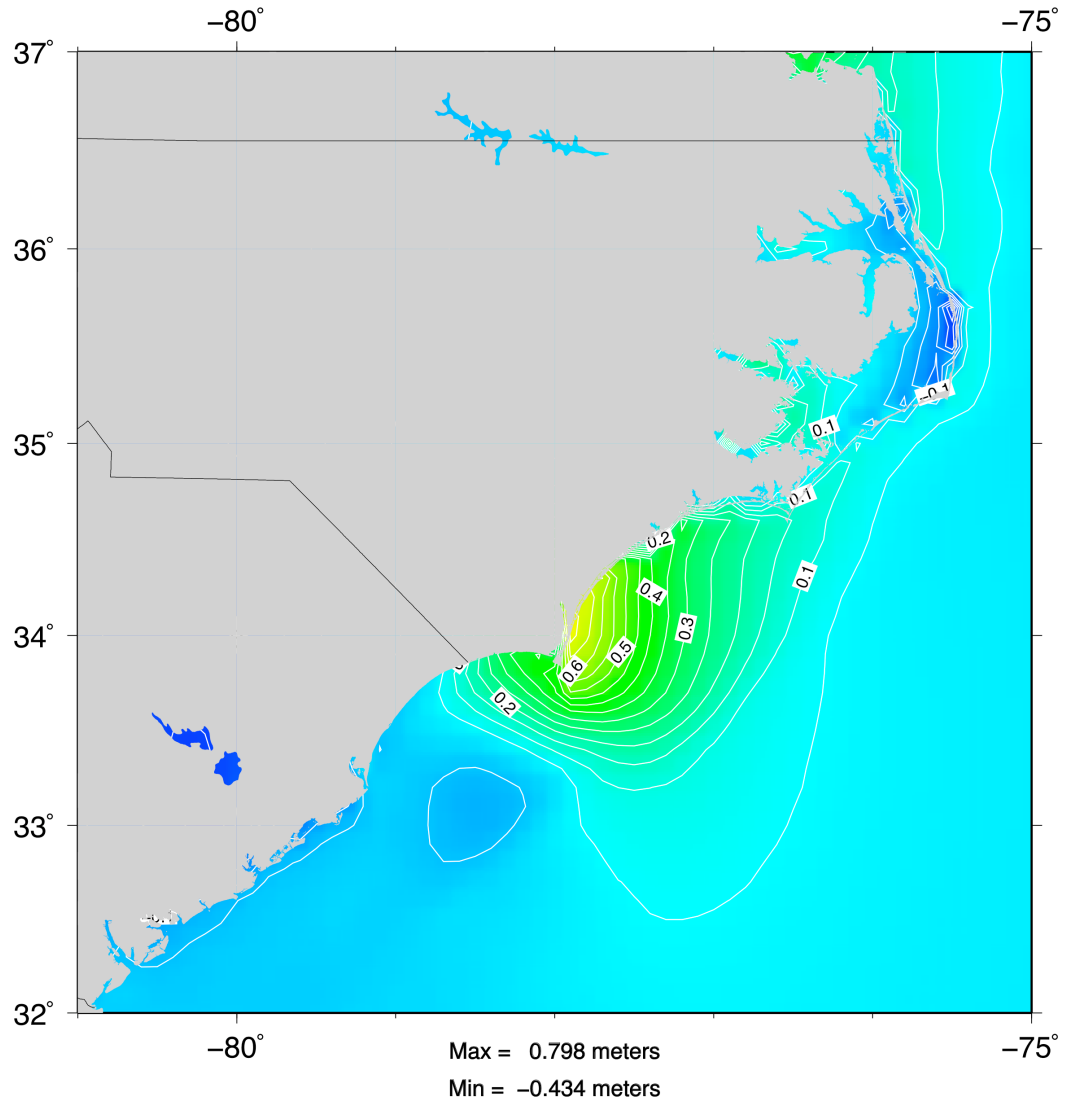


**FIG. 28.** Simulated storm surge (m) above tides forced with H\*Winds for TS Ernesto, valid at 3Z on September 1, 2006.

Next, we compare the model results to the actual observations at several stations along the NC coast from simulation day 88 to 92.375, which correspond to the calendar period of 0Z August 28, to 9Z September 1, 2006. Fig. 29a shows the ADCIRC model tides compared with the NOAA predicted tides at Wrightsville Beach, NC. There is an offset of about 10 cm between the two due to a different reference datum being used in each system. This is important to point out since the ADCIRC surface elevation could be adjusted by this amount to correct/calibrate the model's storm surge predictions in the future.

## Tropical Storm Ernesto ADCIRC vs Observations at Wrightsville Beach, NC

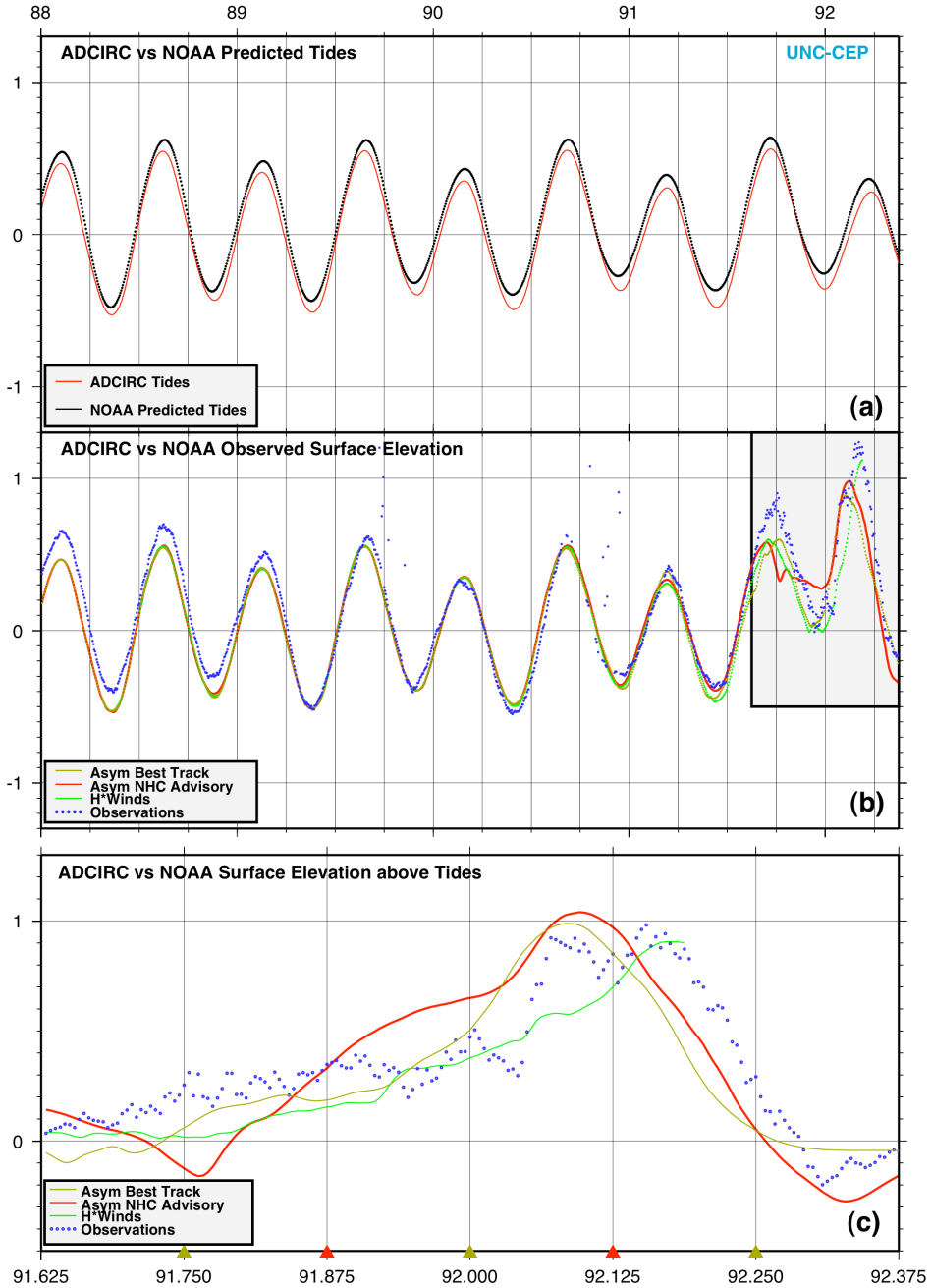


**FIG. 29.** ADCIRC model sea surface elevations (m) vs. NOAA/NOS/CO-OP observations (m) at Wrightsville Beach, NC from simulation day 88 (August 28, 2006 at 0Z) until simulation day 92.375 (September 1, 2006 at 9Z). (a) ADCIRC model tides (m) vs. NOAA predicted tides (m), (b) NOAA tidal station observations (m) vs. ADCIRC model elevations (m) produced by simulations driven with best track data, NHC advisories, and H\*Winds. (c) NOAA observed minus predicted surface elevation (m) and ADCIRC surge above tides (m) using different wind forcing: best track, NHC advisories, and H\*Winds analyses.

Fig. 29b shows a comparison between the actual NOAA tidal station observations and the ADCIRC model elevations produced by simulations driven by different wind forcing: (1) best track dataset, (2) NHC advisories, and (3) H\*Winds. The offset between the observed and model sea surface heights is noticeable. The maximum sea surface elevation produced by the model simulation forced with NHC advisory winds was 0.99 m at Wrightsville Beach and the surge above tides was 1.06 m vs. the observed sea surface elevation of 1.22 m and surge of 0.98 m, a difference of only 0.08 m or 8%. The maximum predicted surge occurs somewhat earlier than the observations when the tides are slightly lower.

We zoomed in on the time period when TS Ernesto was closest to the NC coast (grey square in Fig. 29b) and calculated the surge above tides by removing the model tides from the model elevations, and the NOAA predicted tides from the NOAA observed elevations (Fig. 29c). The predicted storm surge agrees well with the 3-5 feet (0.91-1.52 meters) that was predicted and observed. The red triangles at the bottom of the graph show the times when the NHC forecast advisories were issued and automatically "kicked off" an operational ADCIRC model run. The brown triangles show the times at which the corrected best track data is available.

In general, at the time when an NHC advisory was issued or best track data was available, the observations agree with the model results. The simulations in which the NHC advisories are in good agreement with the observations are initialized at 9Z and 3Z, and at 0Z for the best track. Since the storm made landfall at 3:40Z, then went inland and slowly decayed, the data available from the advisories cannot reproduce the peak at 3:40Z because the model has to interpolate the wind data between 3Z and 9Z. The best track forced simulation faithfully follows the signal produced by the ADCIRC simulation driven with the synthetic winds generated from NHC advisories. It is in even better agreement with the observations at the times that track fixes are available. The H\*Winds forced simulation underpredicts the storm surge prior to landfall but performs best at landfall.

After running numerous tests, it was discovered that using a background pressure of 1009 mb (obtained from the best track data), instead of the US Standard Atmosphere value of 1013 mb, improved the predicted sea surface elevation significantly, bringing it closer to the observations. Unfortunately, there is no information about the background pressure in the NHC forecast advisories so a real-time source of this information will be sought in the future.

**TABLE 2.** A summary of the maximum/minimum sea surface height and surge above tides (m) for the NOAA tidal station at Wrightsville Beach, NC, the corresponding model recording station and for the domain shown in the previous figures, accompanied by the maximum winds for the various simulations performed: 12-hour forecast (FOR-12), 6-hour forecast (FOR-6), nowcast with NHC forecast advisory derived asymmetric winds (NOW-NHC), nowcast with asymmetric winds derived from the best track dataset, and H\*Winds analyses. Times are on Sept 1, 2006.

Simulation	SSH Max (m)	Surge above tides Max (m)	Surge above tides Time (Z)	SSH Min (m)	SSH Max (m)	Surge above tides Min (m)	Surge above tides Max (m)	Wind Max (kts)
	Wrightsville	Wrightsville	Wrightsville					
<b>FOR-12</b>	0.57	0.530	2:30	-0.692	1.595	-0.469	1.721	51.78
<b>FOR-6</b>	0.74	0.780	2:24	-0.787	0.901	-0.539	1.302	54.53
<b>NOW-NHC</b>	0.99	1.060	2:24	-0.714	1.484	-0.744	1.150	56.14
<b>NOW-BTK</b>	0.88	0.971	2:24	-0.666	1.185	-0.469	1.721	51.79
<b>NOW-HW</b>	1.12	0.906	4:12	-0.874	0.925	-0.434	0.798	52.23
<b>OBS</b>	1.22	0.982	3:42					

## **3.4 Additions to the ADCIRC Model to Increase its Accuracy**

Three important enhancements were created for the ADCIRC model to improve the accuracy of the NCFS storm surge predictions. The first is the development of a method for processing the LIDAR high-resolution digital elevation model (DEM) data produced by the North Carolina Floodplain Mapping Program ([http://www.ncfloodmaps.com/default\\_swf.asp](http://www.ncfloodmaps.com/default_swf.asp)). The second addition is a directional surface roughness parameterization that modulates the wind speed at a given location based on the types of landuse encountered upwind. The third enhancement is a spatially varying distribution of Manning's roughness coefficient used for computing the bottom/channel bed friction.

### **3.4.1 Generation of a Node Point Shapefile for ArcGIS**

A preliminary processing step was required to create these new high-resolution datasets. GIS specialist Limei Ran generated a shapefile (a digital vector file for storing geometric location and associated attribute information) for the ADCIRC model node points by carrying out the following tasks.

1. A Java program (ToArcgis.Java) was developed to read the grid and boundary information file (fort.14) used in the ADCIRC model. The Java program takes the fort.14 input file and outputs three files -- nodes.dat, nodes\_att.csv, and elements.dat -- to be used to create ArcGIS shapefiles and attribute data.
  - a. nodes.dat is an ArcGIS generate text format for point shapes.
  - b. nodes\_att.csv is a csv (comma separated value) text file containing bathymetry data for nodes.
  - c. elements.dat is an ArcGIS generate text format for element shapes.
2. A public domain software program (gen2shp) was obtained from Jan-Oliver Wagner to convert ArcInfo generated text format to a shapefile format for ArcGIS.
3. The shapelib 1.2.8 software package, an open source package developed by Frank Warmerdam, was downloaded from the <http://shapelib.maptools.org/> web site. Gen2shp uses libraries from the shapelib package.
4. Programs gen2shp and shapelib were configured for use on the UNC baobab Linux cluster.
5. Program gen2shp was run with the nodes.dat file to generate a node shapefile.
6. Program txt2dbf was run to create an attribute dbf file from nodes\_att.csv to replace the dbf file created by gen2shp.
7. The generated node shapefile with node ID and bathymetry information was processed in the ArcGIS system for projection transformation before it was used for the LIDAR elevation extraction and surface roughness calculations.

### **3.4.2 Computation of LIDAR Elevation for ADCIRC Nodes**

Unfortunately, due to delays in processing, merging and quality-controlling the LIDAR elevation data on the part of state contractors, only small samples of this data were acquired by RENCI prior to project termination. Nevertheless, GIS specialist Limei Ran developed a methodology for creating high-resolution terrain for the ADCIRC model using a precision-truncated, rounded-up version of the dataset obtained from the NC Department of Transportation (<http://www.lib.ncsu.edu/gis/ncdot.html>).

1. The previously developed ADCIRC model node shapefile was overlaid with a NC county shapefile to compute the counties in which the nodes fall. There were 29 counties in NC that contain ADCIRC model nodes. There are a total of 227,240 nodes in the current ADCIRC grid and boundary information (fort.14) file. Of these, there are 151,149 nodes in NC where there is LIDAR elevation data.
2. LIDAR data grid cells with a 20 ft by 20 ft (6 meter by 6 meter) horizontal resolution and a vertical accuracy of one foot were downloaded from the NC Department of Transportation web site.
3. The node shapefile was transformed to the same projection system as the LIDAR data (Lambert Conformal Conic).
4. The node shapefile was overlaid with each LIDAR dataset to obtain the elevation data for each node.
5. A text file was created from the overlaid output dbf file which contains both bathymetry data and LIDAR elevation data.

Plots of the LIDAR elevation values (red indicates positive, blue indicates negative) in this text file, the terrain currently used by the ADCIRC model, and the difference between the two are displayed in Fig. 30. Most features are represented correctly but some critical hydraulic features, like rivers, canals and channels that connect inland bodies of water, are not clearly delineated. This becomes more noticeable in the difference field shown in Fig. 30c. Note, for example, the deteriorated representation of the Intracoastal Waterway near the Alligator River. Deficiencies like these are expected. More specialized bathymetric LIDARs that employ a blue-green wavelength of laser light are required to penetrate water. Therefore, some manual editing of the topographic values will be required to create an optimum dataset for ADCIRC.

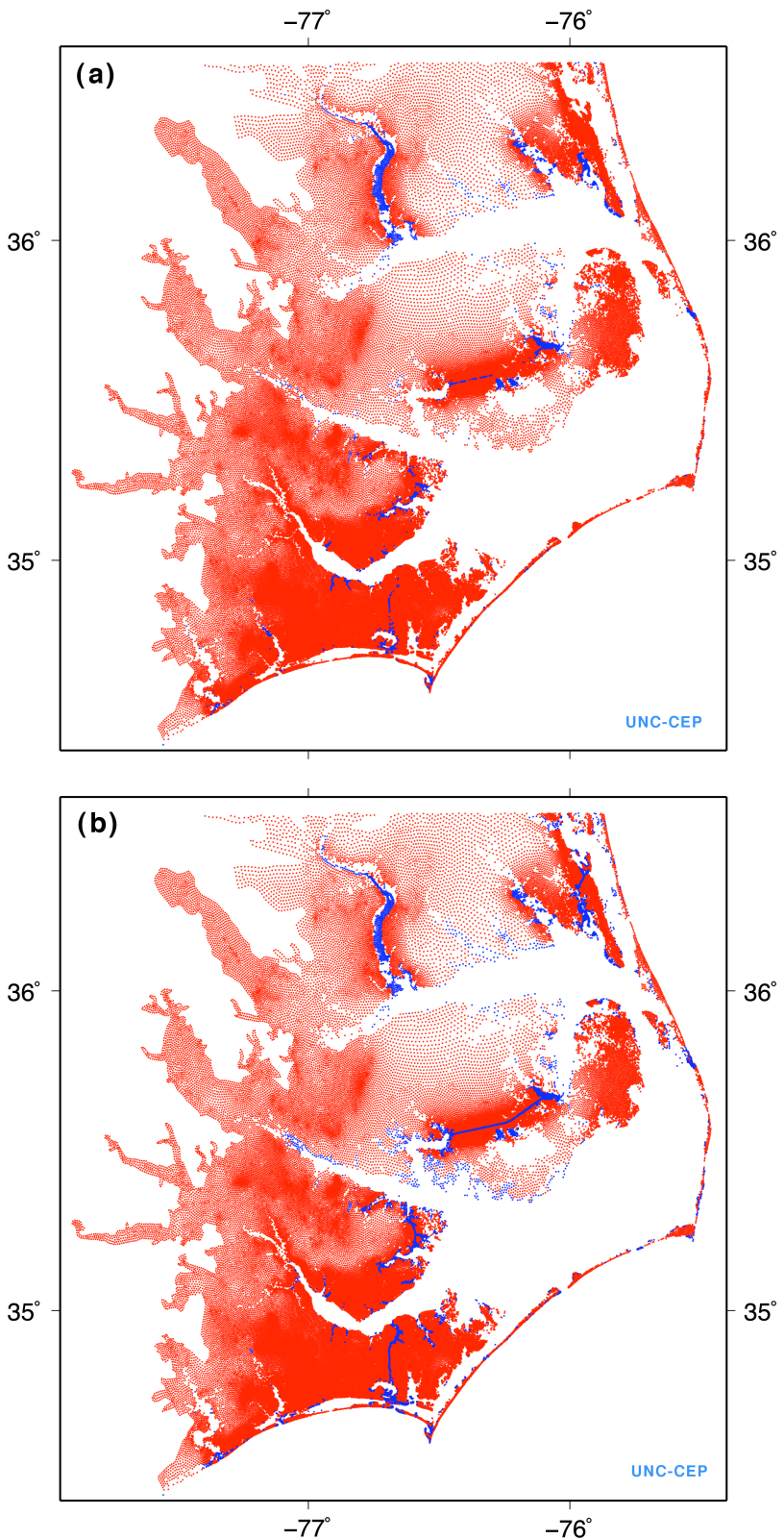


**FIG. 30.** Elevation values (red indicates positive, blue indicates negative) from (a) LIDAR, and (b) current ADCIRC model grid.

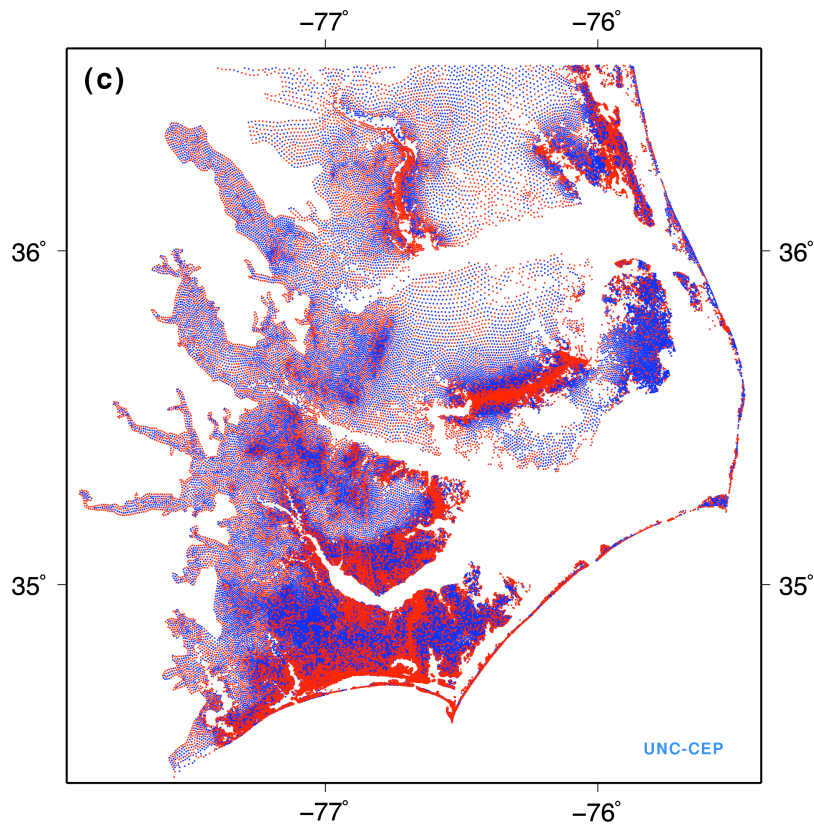


**FIG. 30c.** Difference between the LIDAR elevation (Fig. 30a) and ADCIRC model terrain (Fig. 30b) values (red indicates positive, blue indicates negative).

Another issue that has not yet been addressed is how to combine the LIDAR terrain data with the bathymetry currently used in ADCIRC when the two datasets are measured relative to different vertical reference datums (geoids). It is imperative to resolve this discrepancy so the model can be used to simulate inundation processes. Consultant John Atkinson (Ayres Associates, Fort Collins, CO) provides the following succinct explanation of the problem:

Technically speaking, the [water elevation computed by the ADCIRC] model is relative to the geoid, and the U.S. realization of this is NAVD 88. However, most [numerical] modelers use Mean Sea Level (MSL) since this is familiar to what they expect to observe, even though MSL varies in space and is not the geoid.

Bathymetry is generally relative to Mean Lower Low Water (MLLW); this is so that ship captains can plan for the shallowest depth their boat will encounter so they will not run aground. Therefore, the bathymetric datum needs to be raised to the mean water datum, which increases the water column depth in the model. One needs to examine a tide gauge in their region of interest (or several if its a large region) to determine the difference between MLLW and MSL.

Topography is generally relative to NAVD 88. In North Carolina this datum tends to be above MSL (by about 13 cm at the Outer Banks). Therefore you will need to lower the topography by some amount like this to adjust it to the mean water datum. Again, examine NOS tide gauges (with benchmarks) to determine the differences between MSL and NAVD 88.

Other topographic datasets, such as the USGS 7.5 minute DEM, are referenced to the older

NGVD 29 geodetic datum, so further investigation will be required to resolve this issue. NOAA's Office of Coast Survey and National Geodetic Survey offers a standard conversion tool named VDatum (<http://nauticalcharts.noaa.gov/csd1/vdatum.htm>) that can be used to correct this discrepancy among 28 different vertical datums. However, any labor-intensive calibration efforts should probably be delayed until a more precise, digitally corrected LIDAR dataset is released by the NC Floodplain Mapping Program.

### **3.4.3 Calculation of Directional Surface Roughness Length Values and Manning Roughness Coefficients**

An algorithm for wind speed reduction induced by spatially varying land friction based on landuse data was obtained. The data was preprocessed to account for wind exposure in 30 degree wind direction increments. Tables were built for the wind speed reduction values along these 12 "lines of sight" for each model node in the ADCIRC grid domain. Consultant John Atkinson, who has implemented a similar algorithm to compute these factors for Louisiana, collaborated with UNC-CEP scientists on this task.

Described in detail by Westerink et al. (2006), this technique reduces hurricane winds to account for the higher surface roughness that exists over land. This gradual upwind modulation is consistent with the fact that the boundary layer does not adjust to a new roughness instantaneously. Simulating this effect is crucial in coastal regions because winds that transition from land to water would suddenly accelerate and be incorrectly simulated at full marine force in the nearshore zone without it, while marine winds that penetrate inland would suddenly decelerate and be unrealistically diminished.

UNC-CEP GIS specialist Limei Ran performed the following tasks to generate the directional surface roughness dataset and Manning roughness coefficients.

1. 2001 National Land Cover Dataset (NLCD) coastal landuse data at a horizontal resolution of 30 meters was obtained from the NOAA Coastal Change Analysis Program (CCAP). A sample of this data for Beaufort County, NC is displayed in Fig. 31. The ERDAS Imagine NLCD data was converted into a TIFF image file in ArcGIS for subsequent Java processing.
2. The ArcGIS node shapefile was transformed to the same projection (Albers Conical Equal Area) as the NLCD landuse use data. The x and y coordinates of the ADCIRC model nodes were computed and added to the shapefile attribute table. A text data file with node ID, x and y was exported from the node shapefile into ArcGIS.

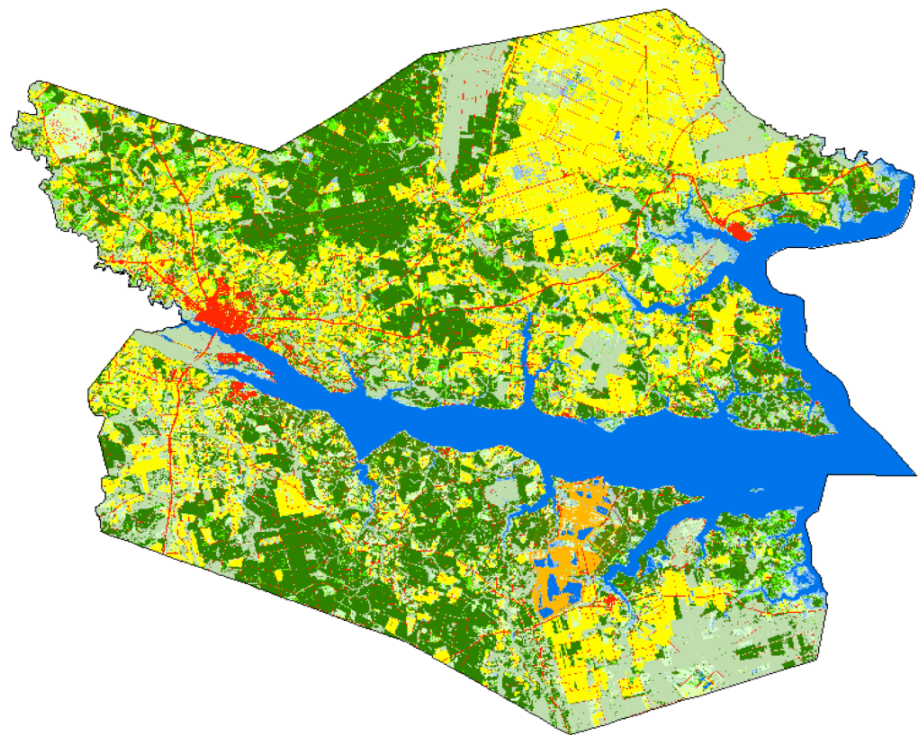


**FIG. 31.** 2001 NLCD 30-meter resolution landuse data for Beaufort County, North Carolina.

3. Surface roughness length and hydrologic Manning-n data for each landuse type were obtained from consultant John Atkinson and values published in other studies. There are 29 landuse classes for the NLCD data set (Table 3). A text data table was created with class ID, class name, Manning-n, and surface roughness length items.
4. Because the NLCD data file is too large to be processed in ArcGIS on a desktop computer system, open source Java image processing packages were used to develop a Java program to compute the surface roughness values. Three Java source packages were downloaded for the spatial and image processing:
  - a. GeoTools from <http://geotools.codehaus.org/> was downloaded for geotiff spatial processing.
  - b. The Java Image I/O API package was downloaded to provide a pluggable architecture for working with images stored in files.
  - c. The Java Advanced Imaging API was downloaded to provide a set of object-oriented interfaces that support a simple, high-level programming model which lets you manipulate tiff images easily.
5. A Java-based program that calls classes from the downloaded software packages was developed to compute average Manning-n and surface roughness length values in 12 directions (similar to a clock's face) for each model node. The computation was based on the information provided by Dr. Rick Luettich.

**TABLE 3.** NLCD landuse classes with assigned values for the Manning coefficient and surface roughness length.

NLCD Class Number	NLCD Class Name	Manning Coefficient n	Surface Roughness Length
11	Open Water	0.001	0.001
12	Perennial Ice/Snow	0.010	0.012
21	Developed - Open Space	0.020	0.100
22	Developed - Low Intensity	0.050	0.300
23	Developed - Medium Intensity	0.100	0.400
24	Developed - High Intensity	0.150	0.550
31	Barren Land (Rock/Sand/Clay)	0.090	0.040
32	Unconsolidated Shore	0.040	0.090
41	Deciduous Forest	0.100	0.650
42	Evergreen Forest	0.110	0.720
43	Mixed Forest	0.100	0.710
51	Dwarf Scrub	0.040	0.100
52	Shrub/Scrub	0.050	0.120
71	Grassland/Herbaceous	0.034	0.040
72	Sedge/Herbaceous	0.030	0.030
73	Lichens	0.027	0.025
74	Moss	0.025	0.020
81	Pasture/Hay	0.033	0.060
82	Cultivated Crops	0.037	0.060
90	Woody Wetlands	0.100	0.550
91	Palustrine Forested Wetland	0.100	0.550
92	Palustrine Scrub/Shrub Wetland	0.048	0.120
93	Estuarine Forested Wetland	0.100	0.550
94	Estuarine Scrub/Shrub Wetland	0.048	0.120
95	Emergent Herbaceous Wetlands	0.045	0.110
96	Palustrine Emergent Wetland (Persistent)	0.045	0.110
97	Estuarine Emergent Wetland	0.045	0.110
98	Palustrine Aquatic Bed	0.015	0.030
99	Estuarine Aquatic Bed	0.015	0.030

6. The surface roughness values and averaged Manning-n value were computed by running the Java program with three input files – a Tiff image, node position file, and roughness table. The results for Beaufort County, NC are displayed in Fig. 32.

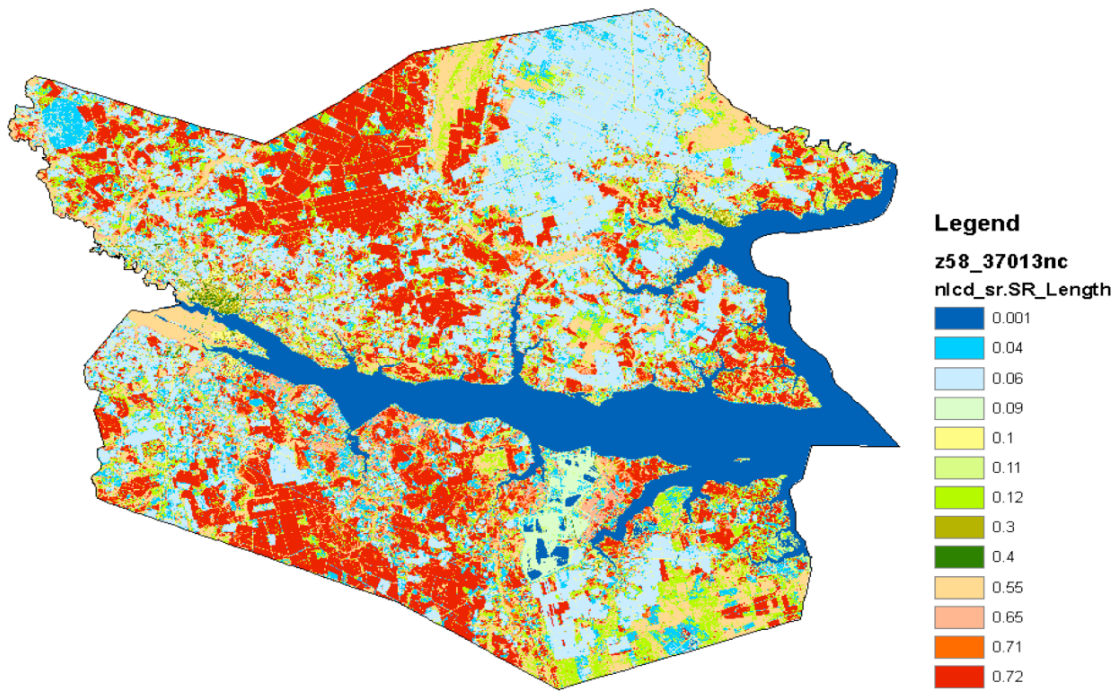


**FIG. 32.** Surface roughness length (m) computed from the 2001 NLCD 30-meter resolution landuse data for Beaufort County, North Carolina using the GIS/Java data processing techniques described in the text.

7. The directional roughness value was computed based on the landuse types with a range of 10 km upwind within an arc length of 30 degrees. Each cell is treated as a point (cell center). The angle  $\alpha$  from ADCIRC model node to the cell center is computed. The surface roughness coefficient for sector SR<sub>1</sub> is for  $\alpha \geq 345$  and  $\alpha < 15$  degree (north wind), SR<sub>2</sub> is for  $\alpha \geq 15$  and  $\alpha < 45$  degree (north-northeast wind) ... SR<sub>4</sub> is for  $\alpha \geq 75$  and  $\alpha < 105$  (east wind), etc. For the nodes on the edge of landuse grid centers, it is possible that for some directions there are no landuse data. In these cases, a missing flag value of -99999.00000 was used to indicate NODATA. As per Westerink et al. (2006), a Gaussian weighting function with higher amplitude within a 3 km range was used to compute distance-based weights:

$$w(i) = \frac{1}{\sqrt{2\pi}\sigma} e^{\left(-\frac{d(i)^2}{2\sigma^2}\right)} \quad (5)$$

where d(i) is the distance between the ADCIRC model node and the landuse pixel, and  $\sigma$  is set to 3 km.

The cell surface roughness length assigned to ADCIRC model nodes in the high-resolution portion of the grid in eastern NC is displayed in Fig. 33.

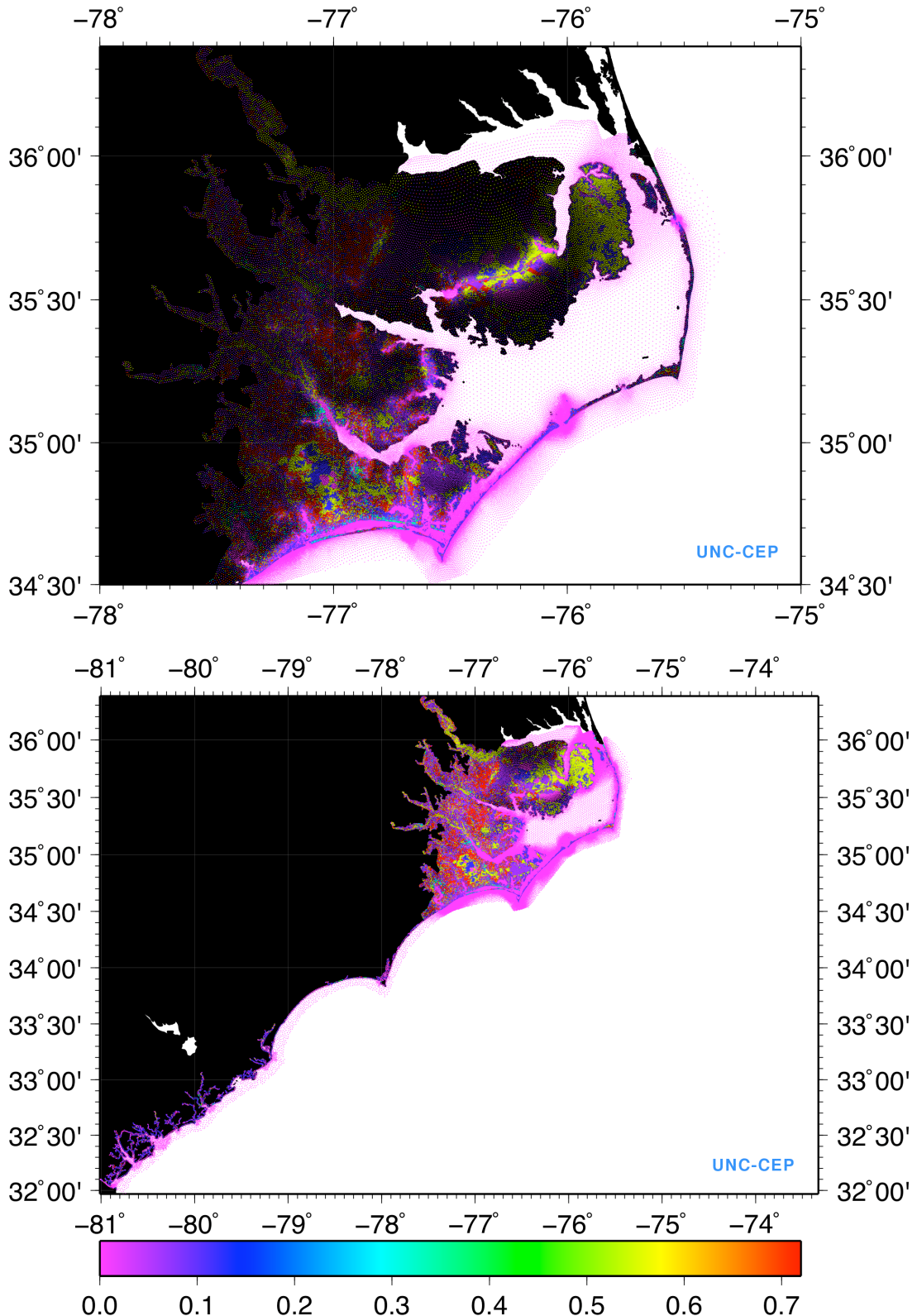


**FIG. 33.** Cell surface roughness length (m) assigned to ADCIRC model nodes in the high-resolution portion of the grid in eastern North Carolina.

The spatial distribution of surface roughness and the impact of the directional upwind parameterization can be seen more clearly by examining an ADCIRC model node (#70717 located at  $34.61^{\circ}$  N,  $76.54^{\circ}$  W) that falls on Cape Lookout, NC (Fig. 34), where there is a large variation in the surface characteristics that can immensely affect the winds depending on their direction (Fig. 35).



**FIG. 34.** Cape Lookout, North Carolina.

## Landuse at ADCIRC Nodes

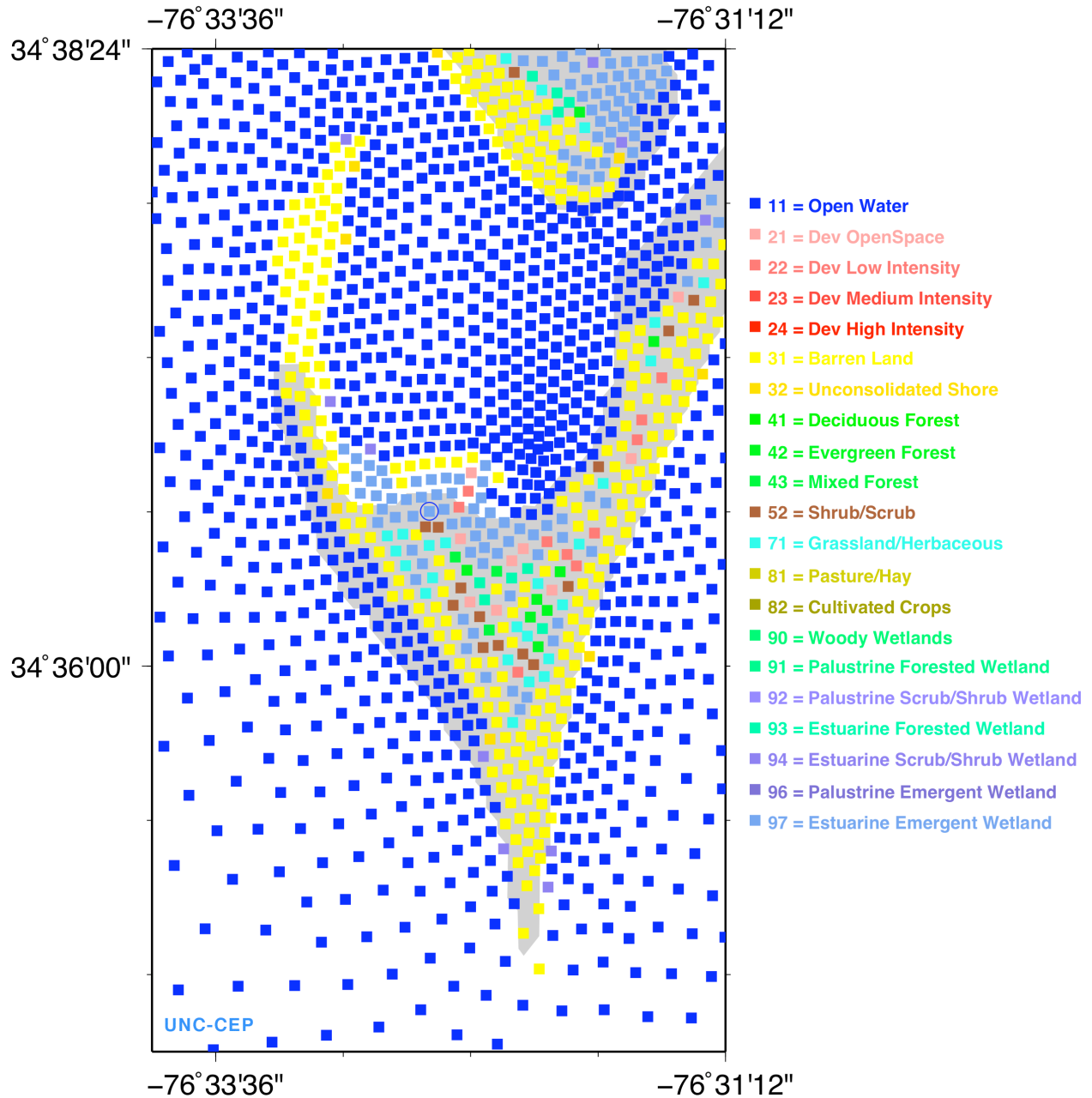


**FIG. 35.** Categories of landuse assigned to ADCIRC model grid nodes over Cape Lookout. Node #70717, located in the center of the figure, is circled.

The cell surface roughness length assigned to nodes in this area is displayed in Fig. 36.

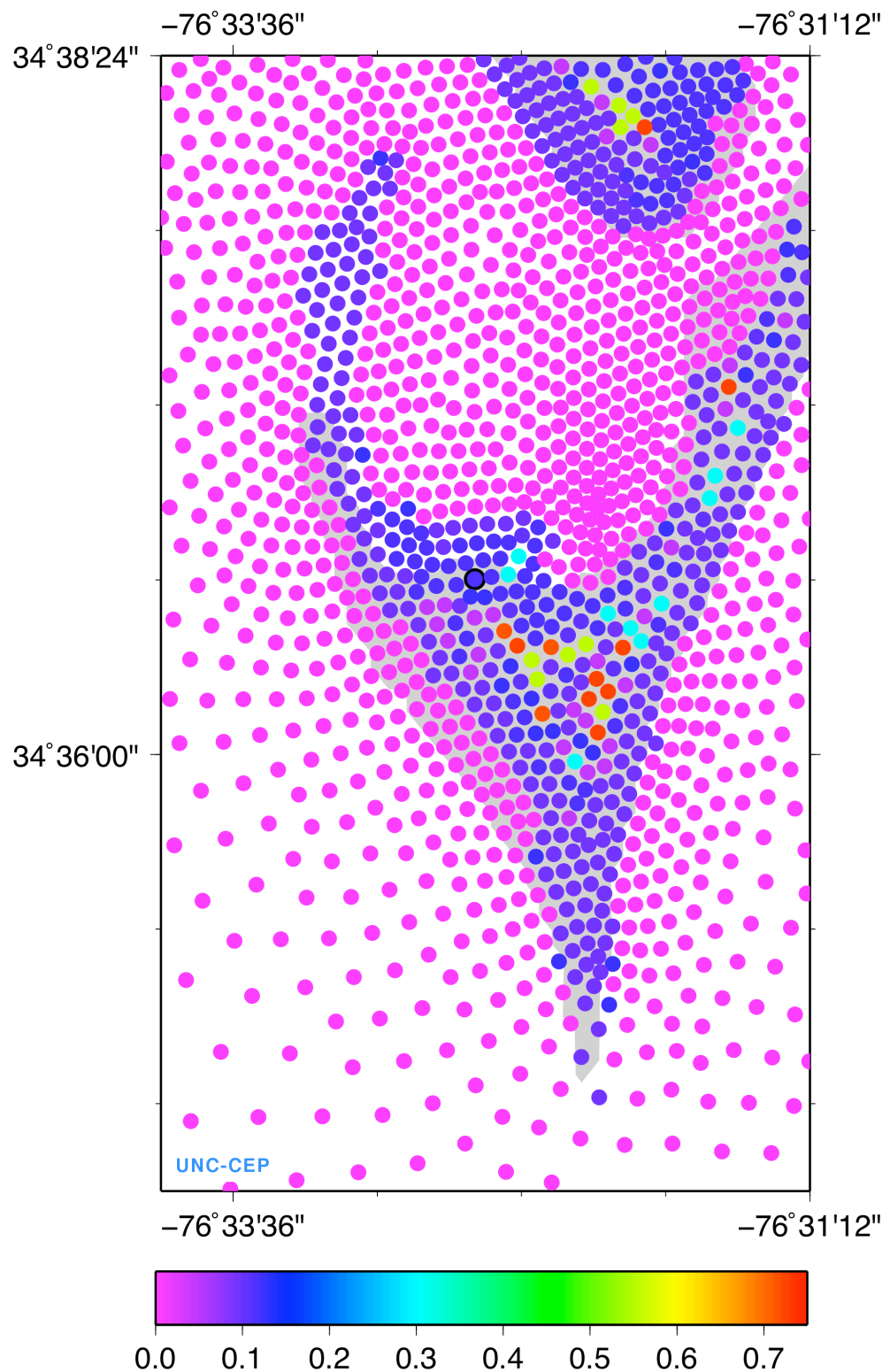


**FIG. 36.** Cell surface roughness length (m) assigned to ADCIRC model grid nodes in the Cape Lookout area.

A polar coordinate “rose” plot of the values of the surface roughness as a function of wind direction at ADCIRC model node #70717 is displayed in Fig. 37. The rose plot shows that the roughness is lowest for winds blowing from the southwest over water. The highest values occur when the winds traverse long stretches of developed or forested land within a 3 km radius of the node, such as in the northeast sector.

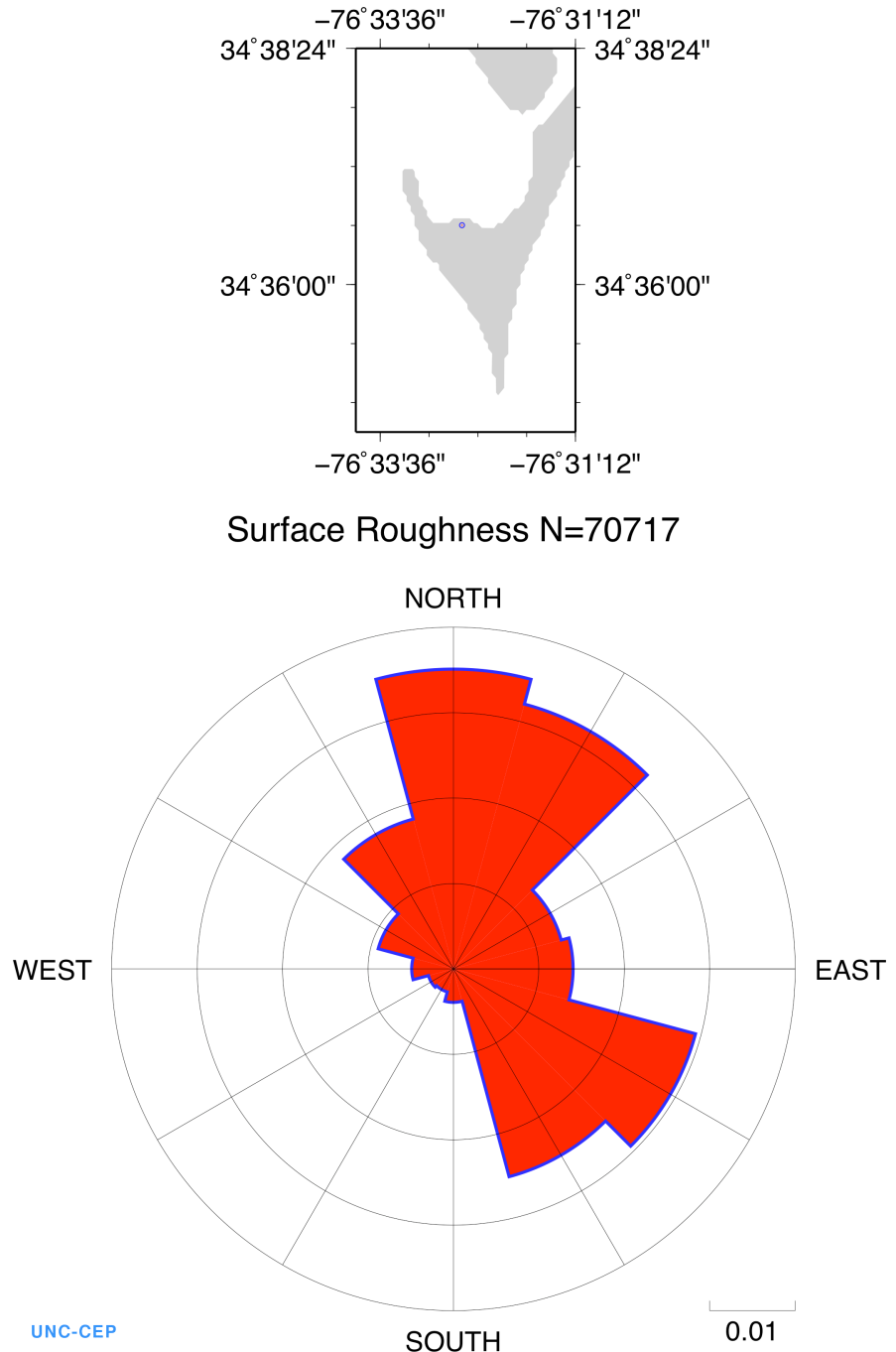


**FIG. 37.** Polar coordinate “rose” plot of the surface roughness as a function of wind direction at ADCIRC model node #70717.

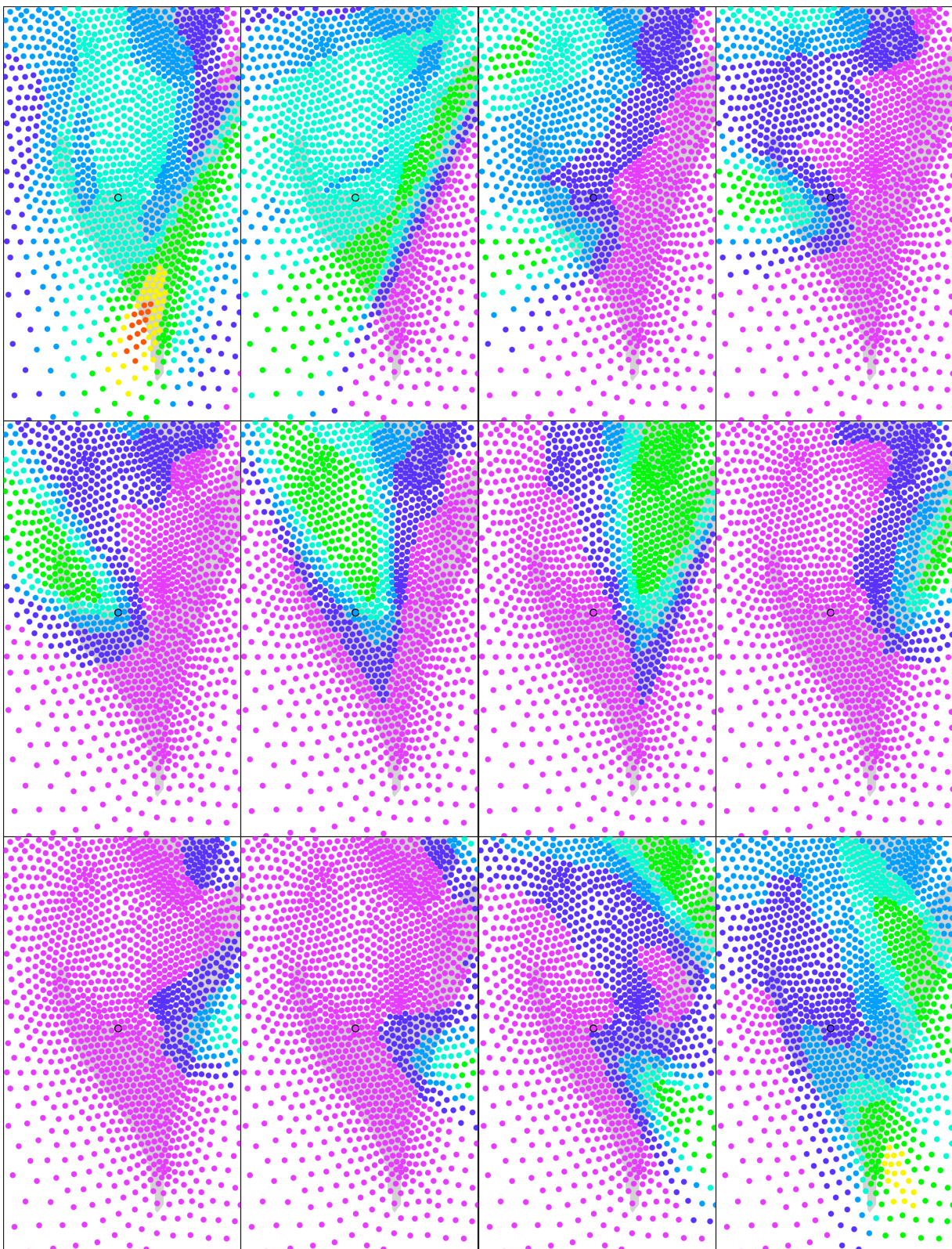


**FIG. 38.** Anisotropic surface roughness field for the 12 wind directions specified in  $30^\circ$  increments, starting from the north and proceeding clockwise.

Fig. 38 shows the anisotropic surface roughness field for the 12 wind directions specified in 30° increments, starting from the north and proceeding clockwise. Different features in the land surface modify the surface drag as the winds rotate anticyclonically.

Under large-scale heavily forested canopies, the water is sheltered from the wind and very little vertical momentum transfer occurs – the water surface is effectively decoupled from the wind field. Therefore, when an ADCIRC model node's landuse type falls in the 41-43 or 90-93 NLCD categories (indicated in bold in the landuse table), its surface canopy coefficient (VCanopy) is set to zero in the nodal attributes (fort.13) file and no wind stress is applied at the water surface.

The average Manning-n value was computed from 5 by 5 cell windows (150 meter by 150 meter squares). The drag coefficient for the spatially varying bottom friction induced by flow over channel bed material is calculated using the equation:

$$C_f = \frac{gn^2}{\sqrt[3]{H}} \quad (6)$$

where g is the gravitational constant, n is the Manning coefficient, and H is the total height of the water column (depth + surface elevation). The cell Manning coefficient assigned to ADCIRC model nodes in the NC high-resolution grid and the average Manning-n values are displayed in Figs. 39 and 40, respectively. These values may need to be adjusted higher in shallower waters. Note that all Manning coefficients were set to a minimum of 0.02 in the model's nodal attributes file to prevent numerical instabilities, as suggested by consultant John Atkinson.

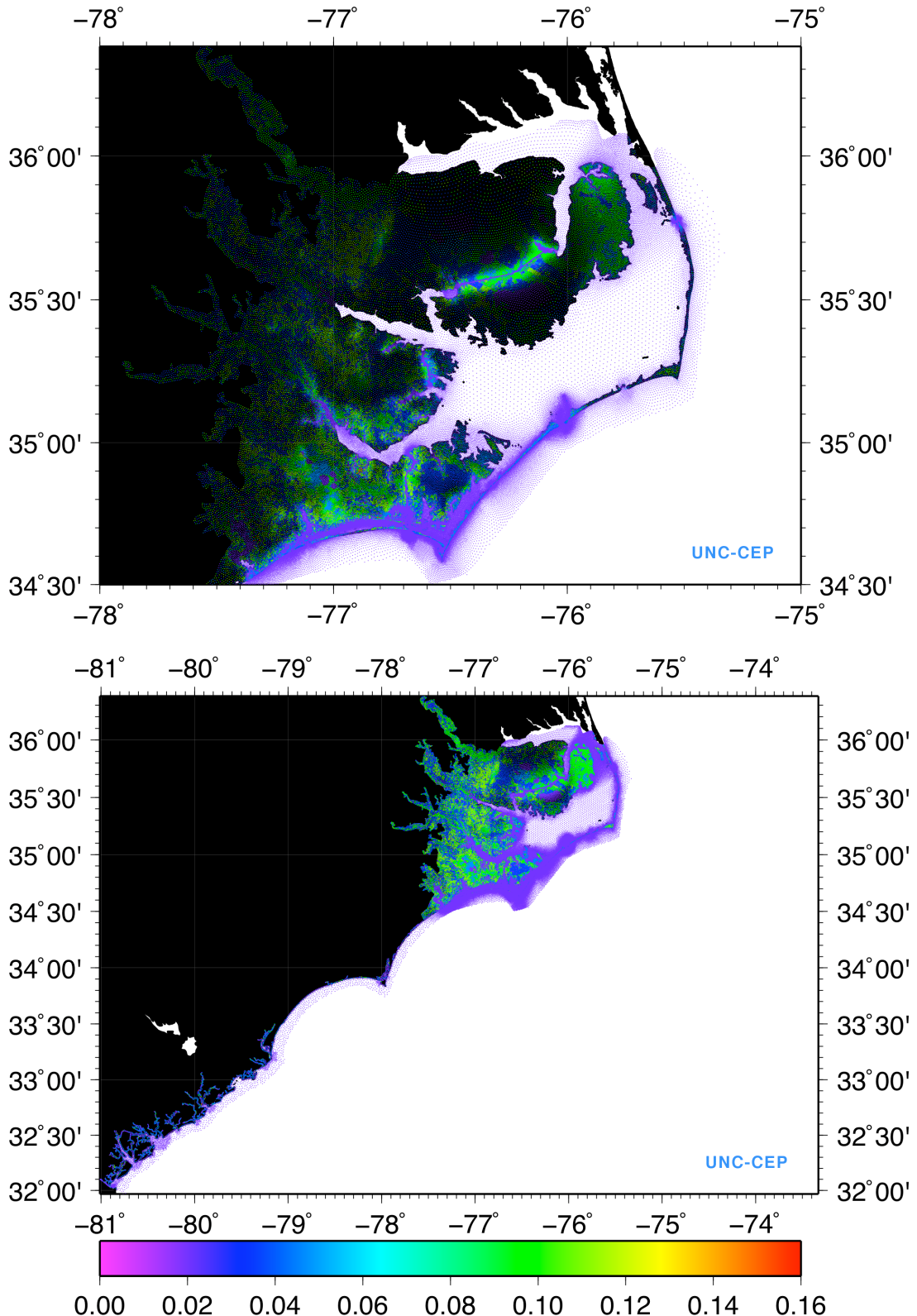


**FIG. 39.** Cell Manning coefficient values assigned to ADCIRC model nodes in the NC high-resolution grid.

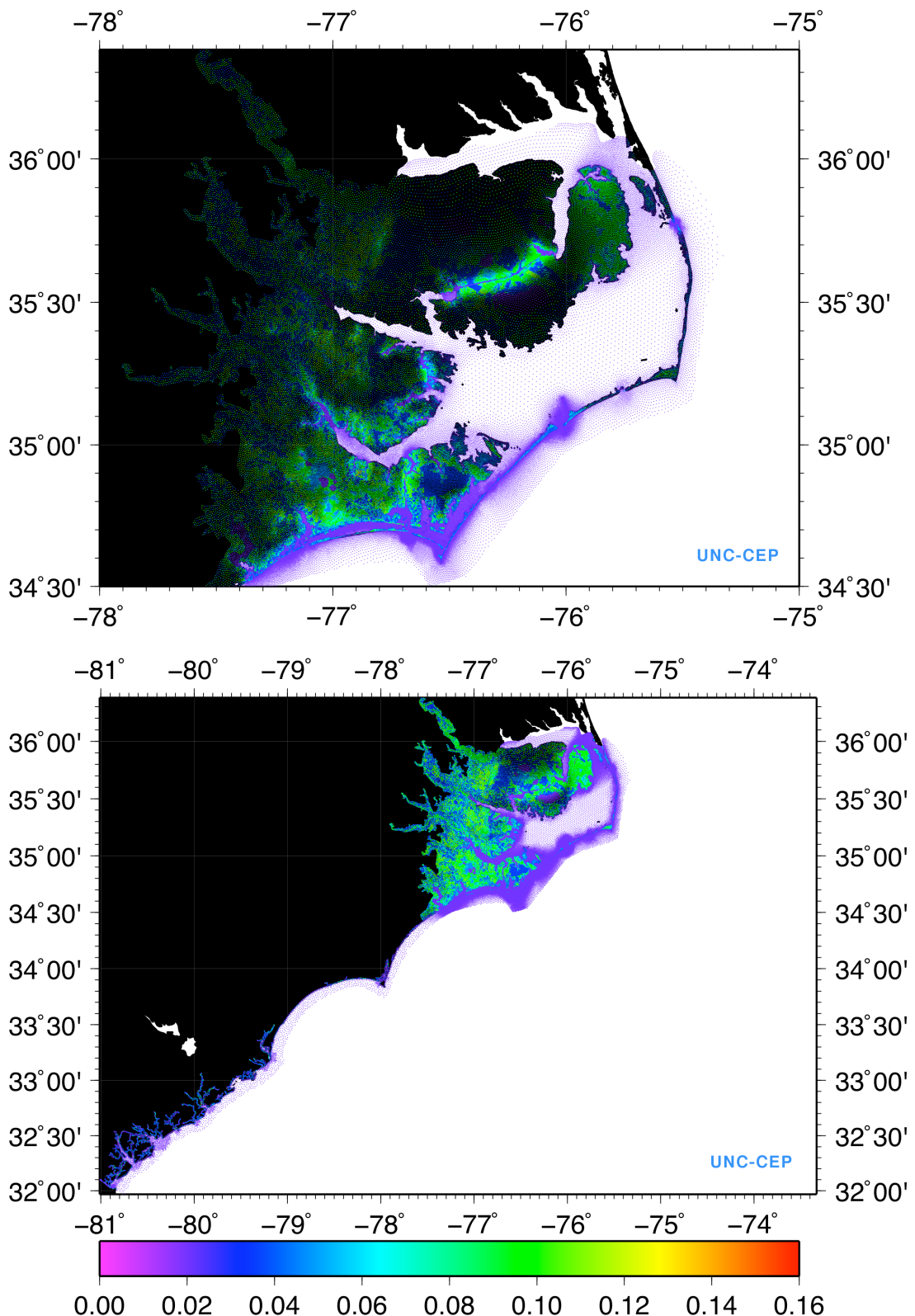


**FIG. 40.** Average Manning coefficient computed in  $5 \times 5$  cell windows (150 m x 150 m in size) for the high-resolution NC grid.

The cell and average Manning coefficients over Cape Lookout, in the vicinity of ADCIRC model node #70717 (circled), are shown in Figs. 41a and b.

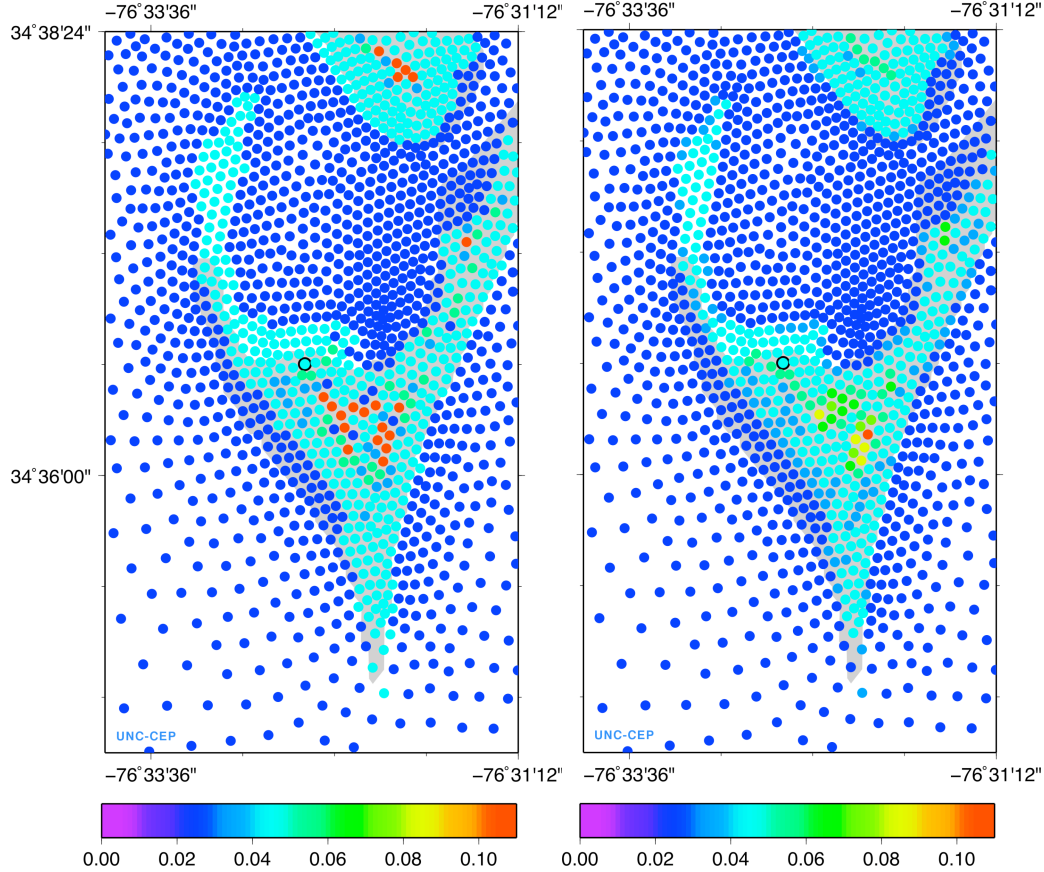


**FIG. 41.** The (a) cell Manning coefficient and (b) average Manning coefficient over Cape Lookout, NC.

### 3.5 Improved Storm Surge Simulation Results

A historical test case, Hurricane Ophelia, was used to evaluate the asymmetric winds algorithm and calibrate its performance, then assess the implementation of the three model nodal attributes: surface roughness length, forest canopy and Manning's coefficient.

Hurricane Ophelia's track is shown in Fig. 42. Ophelia formed on September 4, 2005 near the Bahamas from the remnants of a cold front in an elongated trough of low pressure. Due to the presence of weak steering currents, its motion was slow and erratic. It made several clockwise and counterclockwise loops during its gradual trek northward. Ophelia's intensity oscillated between tropical storm and hurricane strength until its fourth re-intensification off the NC coast, where it reached its peak intensity of 75 knots on September 14-15. Although it never made landfall, the northern portion of Ophelia's eye impinged on Cape Fear as it drifted in an east-northeast direction parallel to the NC coast from Wilmington to Morehead City, pummelling the coastline with high winds for two days. An upper-level trough associated with a cold front caused an abrupt change in Ophelia's track near Cape Hatteras on September 16 and swept the storm northward towards Massachusetts.

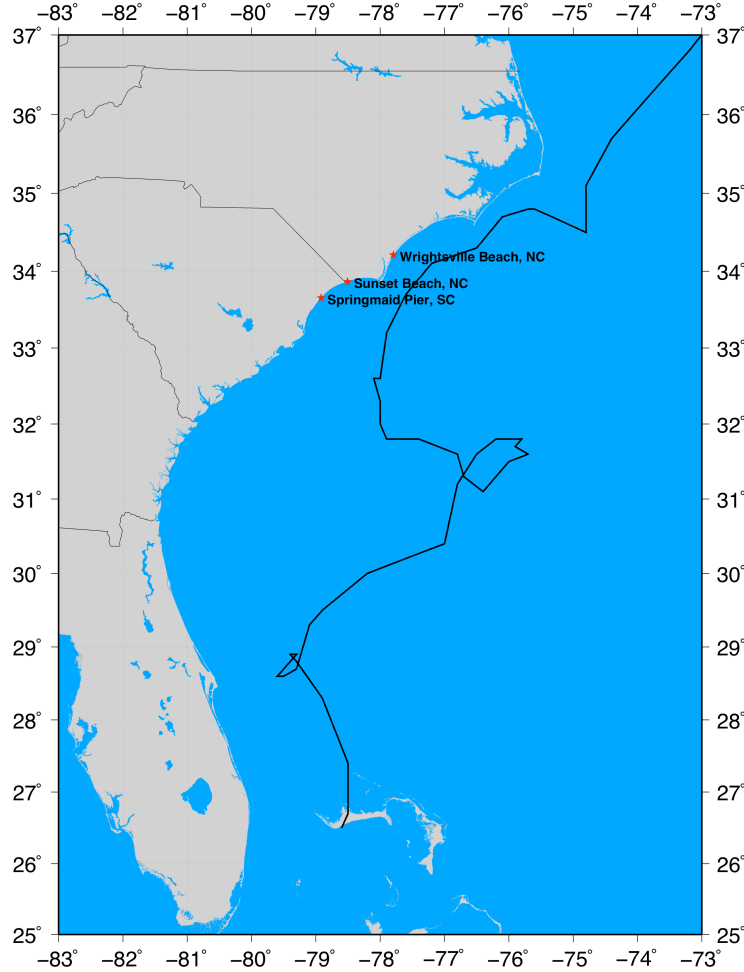


**FIG. 42.** Hurricane Ophelia's track from September 6-17, 2005. Data from the NHC advisories for this period were used to drive the ADCIRC storm surge prediction model.

Storm surge simulations were run with different methods of *initialization*: cold start mode (with no tides) and hotstart mode (starting with the tides-only hotstart file then continuing with the daily tides), with different *nodal attributes*: with/without the Manning-n coefficients (Mn) and surface roughness (Sr) plus canopy, and with different *wind forcing data*: the operationally released NHC forecast advisory data and the best track data obtained from NHC. The results were then compared with the observed sea surface elevations to try to assess the impact of the asymmetric winds model and the new enhancements to ADCIRC on the predicted storm surge.

For the hotstart mode, we first generated the open boundary conditions and tidal potential terms valid at 00Z June 1, 2005. We then spun up the tides for 102 days from 00Z June 1, 2005 until 00Z September 11, 2005 to create a hotstart file with tides. Once the model was spun up with the tides-only runs, we incorporated the synthetic asymmetric wind forcing based on Hurricane Ophelia's wind parameters from the advisories (eye location, highest sustained wind speed, 64/50/34 knot radii information, central pressure). We slowly ramped up the model over 6 hours using a hyperbolic tangent function to prevent initialization shock, then continued forcing the model with the winds at full strength. For cold start mode, we incorporated the same wind forcing but ran the model with no tidal forcing.

Figs. 43a and b show the 10-minute averaged winds from the ADCIRC model at 22:30 UTC on September 14, 2005 used in the Hurricane Ophelia storm surge simulations run with and without the Manning coefficient (Mn) and surface roughness (Sr) nodal attributes.

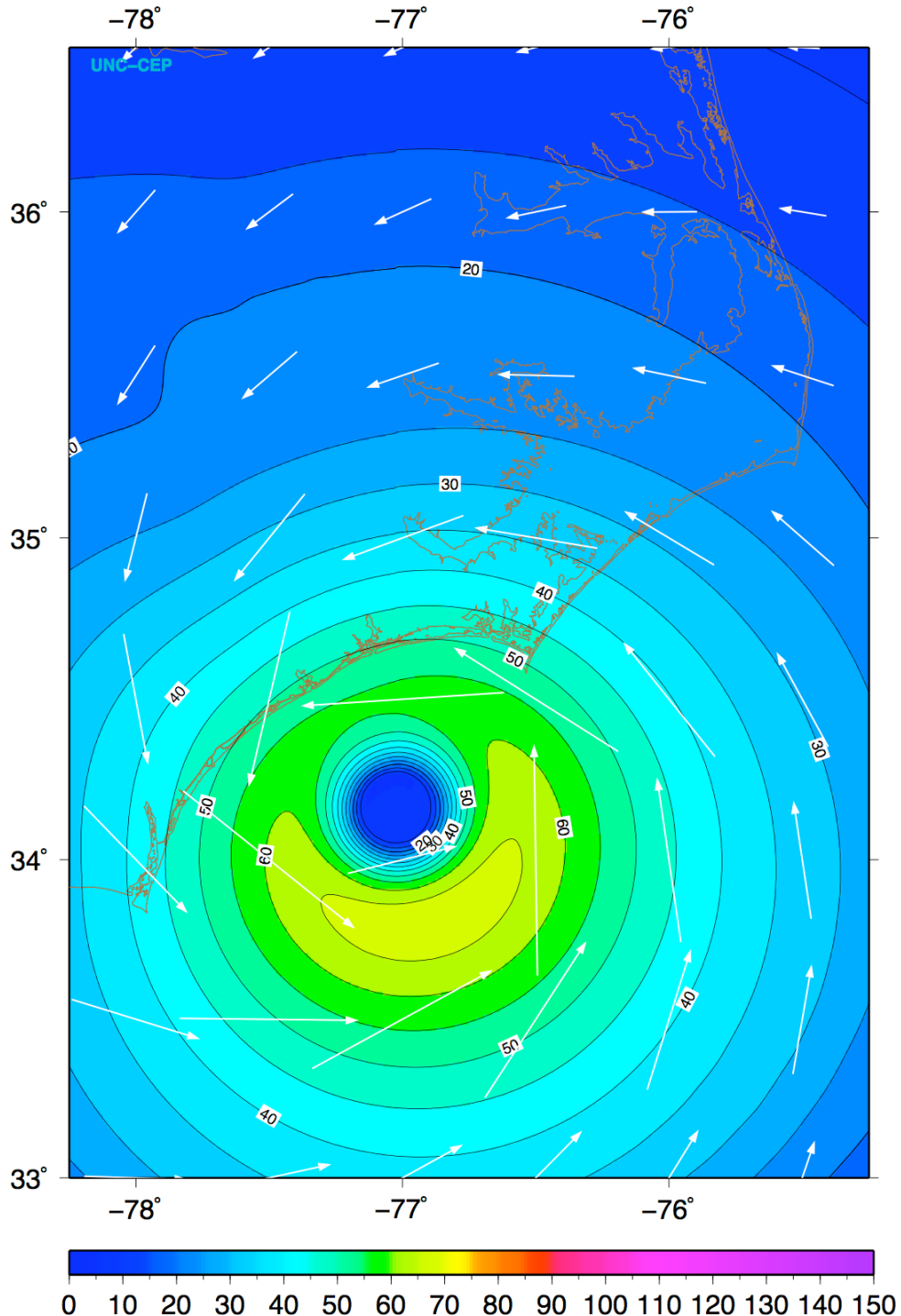


**FIG. 43a.** 10-minute averaged winds (kts) from the ADCIRC model at 22:30 UTC on September 14, 2005 without surface roughness (no Sr).

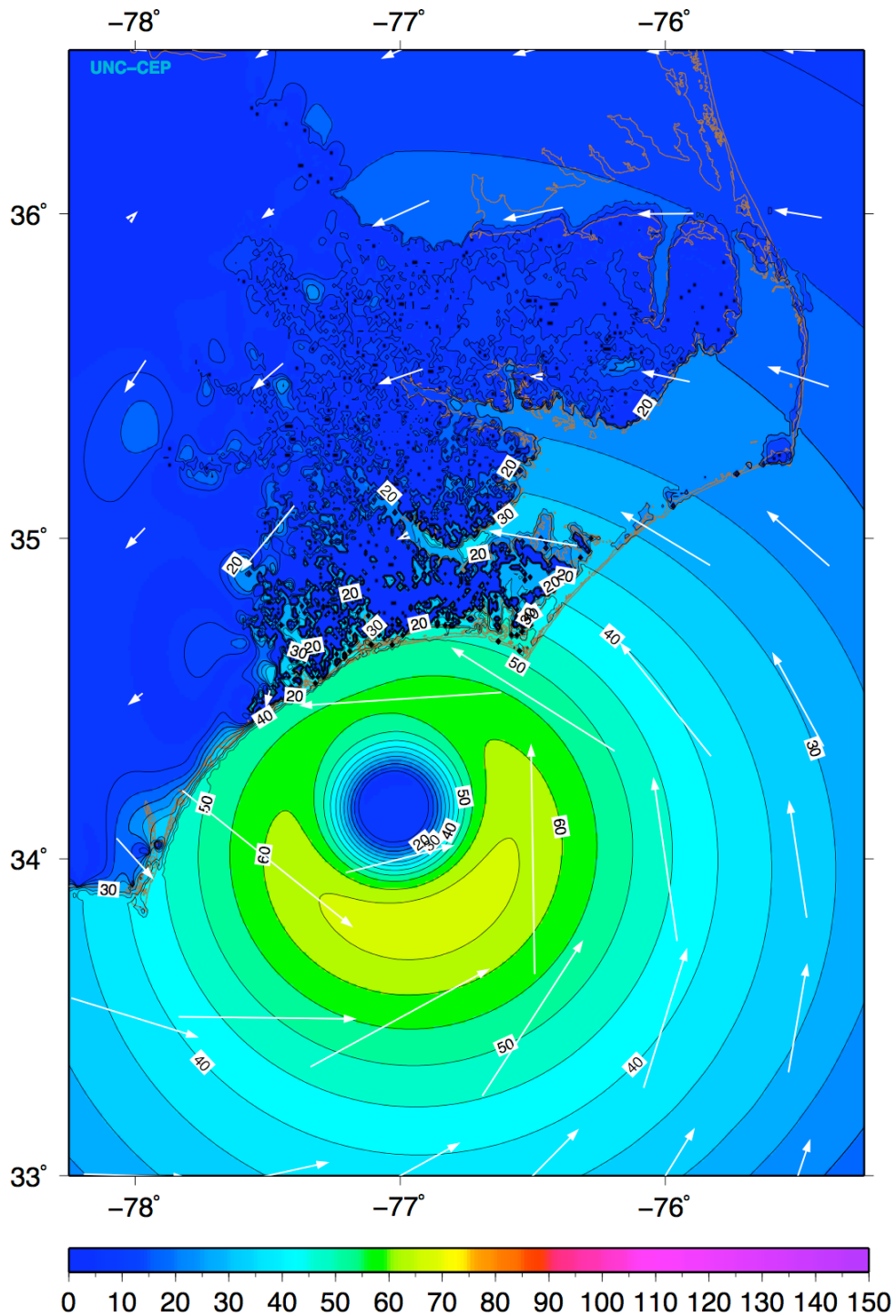


**FIG. 43b.** 10-minute averaged winds (kts) from the ADCIRC model at 22:30 UTC on September 14, 2005 with surface roughness (Sr).

Note that in Fig. 43a that there is no difference in strength between the winds offshore and those over land. This is unrealistic since winds normally diminish exponentially inland with increased surface roughness. Fig. 43b show the winds with both the Sr and Canopy (Can) nodal attributes. The surface canopy coefficient (VCanopy) in ADCIRC is set to 0 where the wind stress should

be zero due to sheltering from forest canopy, and 1 otherwise. The wind speeds are dramatically reduced inland. Detailed, landuse dependent structures emerge in the horizontal distribution of the winds. Small notches are cut into the isotachs to the immediate lee of the barrier islands, while complex acceleration/deceleration patterns occur where the land transitions from low-drag regions, such as the large cardioid-shaped area of cropland (indicated by the brighter blue color, 30+ knot winds) northeast of Beaufort, NC, to the high-drag forested areas downwind. Channeling up the Neuse River between the tree-lined banks is also clearly evident in the figure. This depiction is much more realistic and consistent with what really occurs when high winds are modulated by variations in the surface roughness. Therefore, the upwind exposure wind drag formulation used in ADCIRC successfully compensates for the lack of such a parameterization in the synthetic asymmetric wind model.

### *Effects of initialization: Cold Start vs. Hotstart*

In order to determine whether and how the incorporation of tides affect the surge results, we ran two cases (1) a cold start (no tides) for a period of 5.125 days, and (2) a hotstart simulation starting with the tides-only hotstart file at 00Z September 11, 2005, then driving the model with the synthetic asymmetric winds and including the tides without Mn and Sr nodal attributes from 00Z September 11 to 03Z September 17, 2005.

Figs. 44a and b show the sea surface elevation and currents for the cold start simulation and the hotstart simulation with tides, respectively. Since it does not include tides, the cold start surge along the coast north of the storm is about 0.6 m and the draw down along the southern part of the coast is between -0.3 and -0.4 m. The hotstart run has values of 1.2 m along the coast on the northern side of the storm. The cold start produced a maximum surface elevation of 2.189 m in the lee of the barrier islands, while the hotstart produced a maximum of 2.165 m at the same location, but note that the hotstart has the tides included. The observed sea surface height nearby, at the NOAA Beaufort tidal station, was 1.470 m. However, there is a strong sea surface height gradient in the area between the islands and the coast in this area, which could account for the difference. The surface currents have the same general pattern in both cases, with strong currents flowing towards the southwest along the NC coastline. There are differences in the Pamlico Sound, where the hotstart simulation predicts higher velocities penetrating through inlets between the barrier islands.

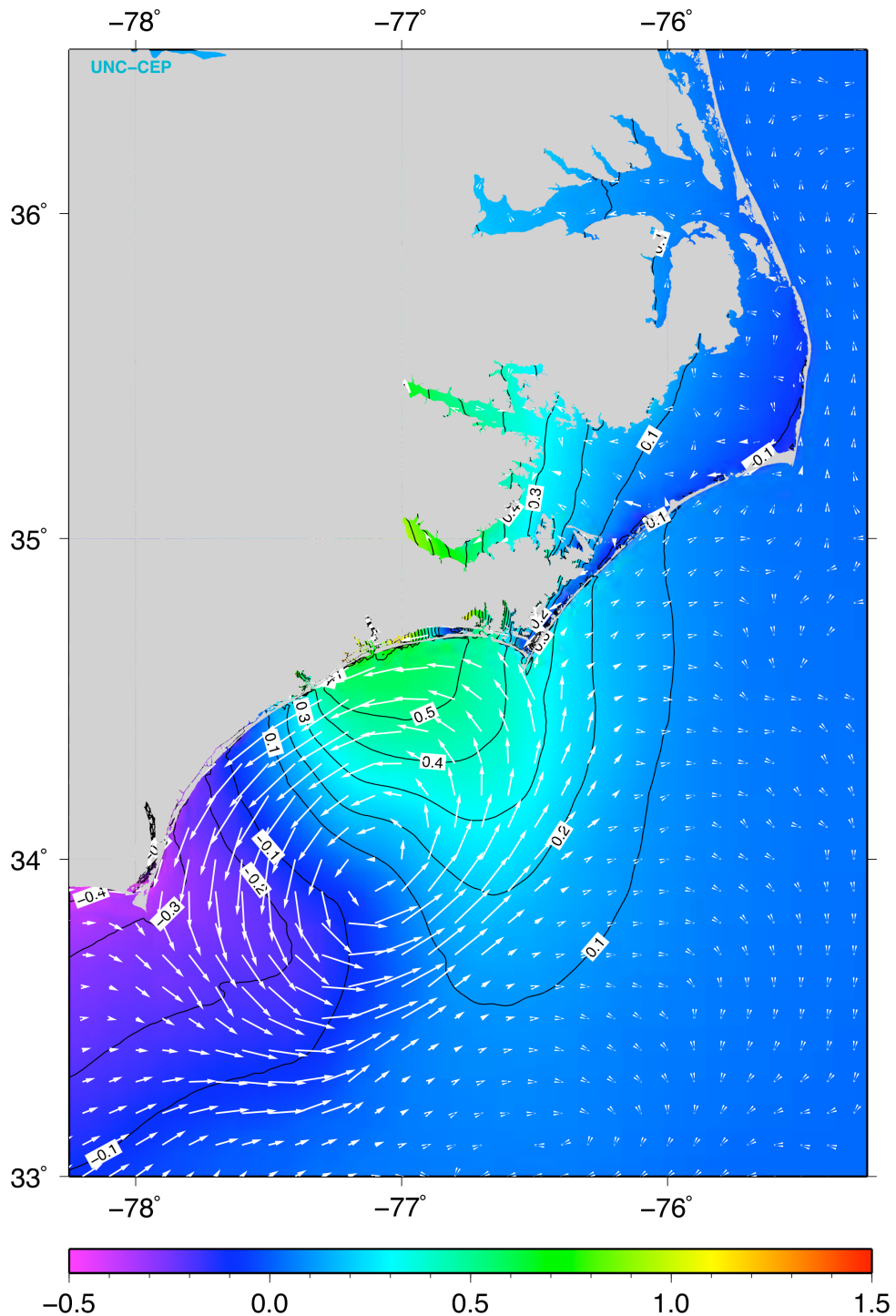


**FIG. 44a.** Sea surface elevation (m) and surface currents (m/s) from the ADCIRC model at 22:30 UTC on September 14, 2005 using NHC advisory derived winds - cold start without nodal attributes (no Mn, no Sr).

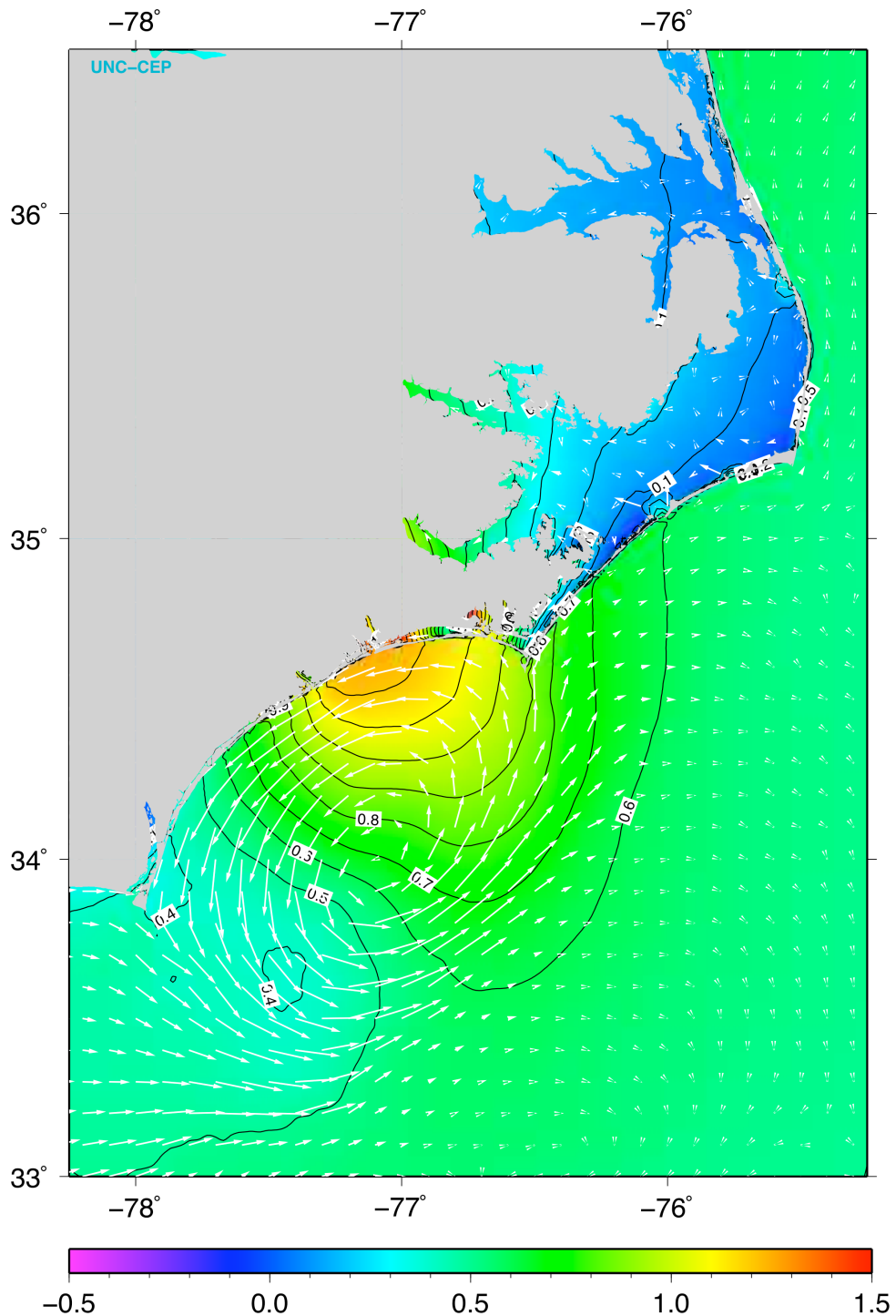


**FIG. 44b.** Sea surface elevation (m) and surface currents (m/s) from the ADCIRC model at 22:30 UTC on September 14, 2005 using NHC advisory derived winds - hot start without nodal attributes (no Mn, no Sr).

We calculated the surge above tides by removing the tides from the sea surface elevation after the fact (Fig. 45b) for Hurricane Ophelia at 22:30 UTC Sept 14, 2005 for the hotstart simulation. We then compared the surge results to the cold start sea surface elevation (Fig. 45a) for the same

time (same as Fig. 43a but displayed with a different color range and no surface currents for better comparison). The cold start surge maximum of 2.189 m is localized at an area in the lee of the barrier islands. The hotstart run surge maximum is in the same location but the value is much lower (1.2986 m) since the tides have been removed. The observed sea surge above tides at the NOAA Beaufort tidal station was 0.859 m.

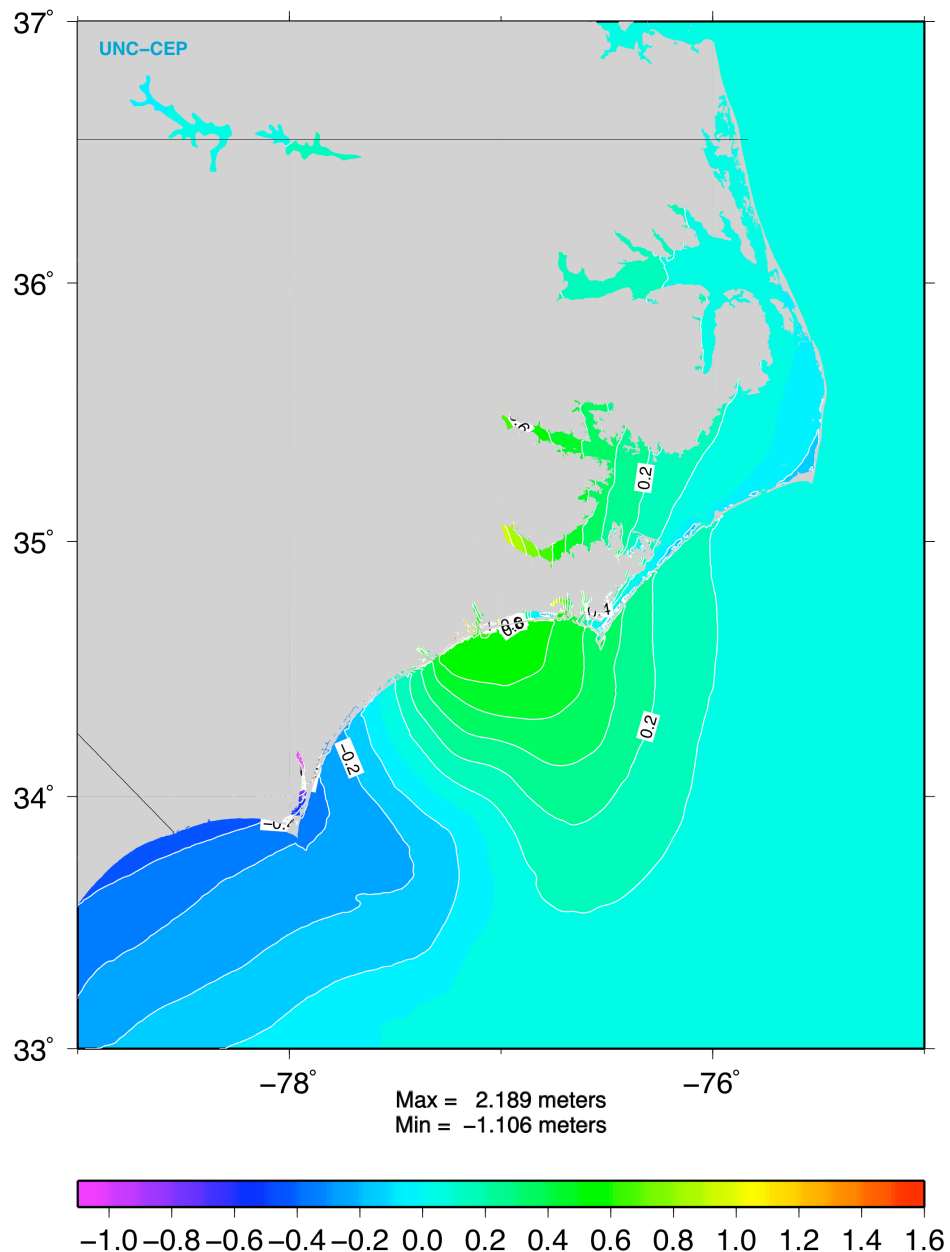


**FIG. 45a.** Surge above tides (m) from the ADCIRC model at 22:30 UTC on September 14, 2005 using NHC advisory derived winds - cold start without nodal attributes.

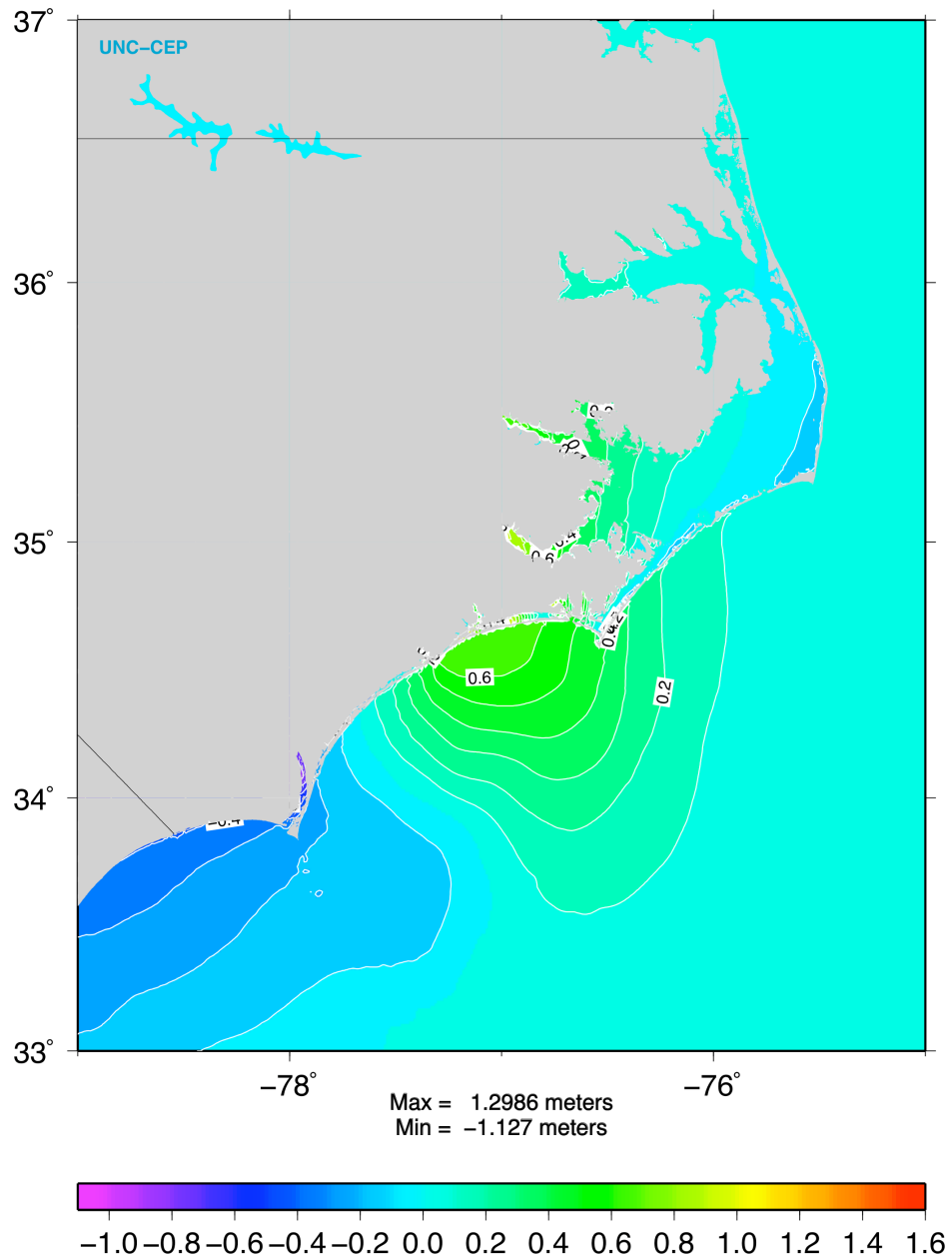


**FIG. 45b.** Surge above tides (m) from the ADCIRC model at 22:30 UTC on September 14, 2005 using NHC advisory derived winds - hot start without nodal attributes.

#### *Effects of nodal attributes: Mn and Sr vs NoMn and NoSr*

The sea surface elevation and surface currents for ADCIRC simulations run with Mn and Sr are shown in Fig. 46a.

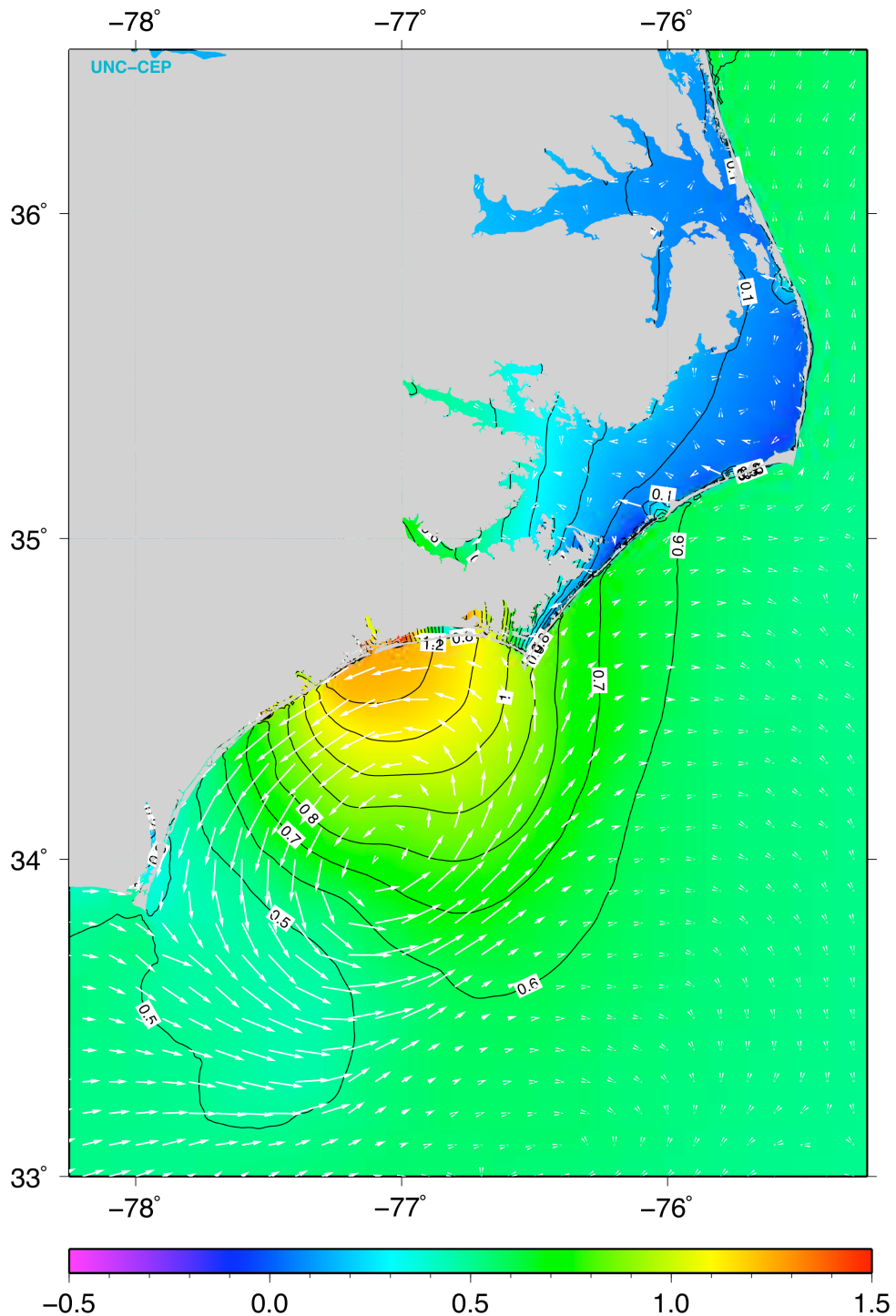


**FIG. 46a.** Sea surface elevation (m) and surface currents (m/s) from the ADCIRC model at 22:30 UTC on September 14, 2005 using NHC advisory derived winds with Manning coefficient ( $M_n$ ) and surface roughness ( $S_r$ ).

The sea surface currents follow the counterclockwise pattern of the hurricane winds, which causes the water to pile up along the NC coast north of the storm's eye and draw down southwest of the storm's center. The storm surge is higher at the coast when  $M_n$  and  $S_r$  are activated. In the

case without Mn and Sr Fig. 44b, the overestimated draw down southwest of the hurricane was produced by erroneously high offshore winds not damped by the landuse.

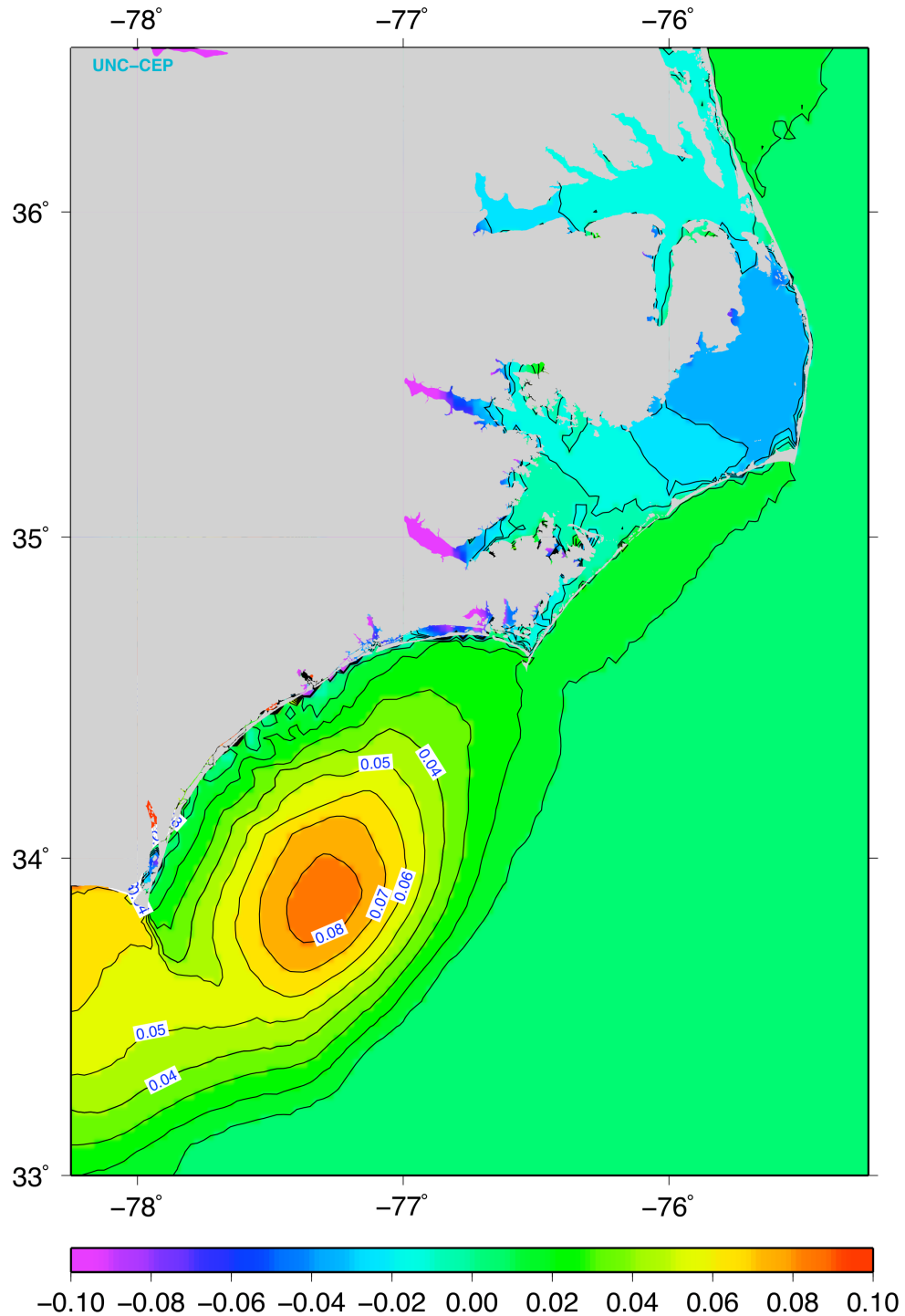


**FIG. 46b.** As in Fig. 46a, but sea surface height difference field (m) with - without Manning coefficient (Mn) and surface roughness (Sr).

We compared the sea surface elevations with and without Mn and Sr by calculating the difference field shown in Fig 46b. Three distinct patterns are apparent. First, the difference field shows the Manning effect in shallow water evidenced by the higher values of sea surface elevation in the location of the eye, but no effect in deeper water. Second, the surface roughness effect is seen in the southern part of NC where the winds offshore produce less of a draw down with these nodal attributes activated than without. In the Pamlico Sound, where the winds diminished in the Mn + Sr case, the difference is negative since the lower winds cause less water to be driven against the mainland coast inside the sound than without Mn and Sr.

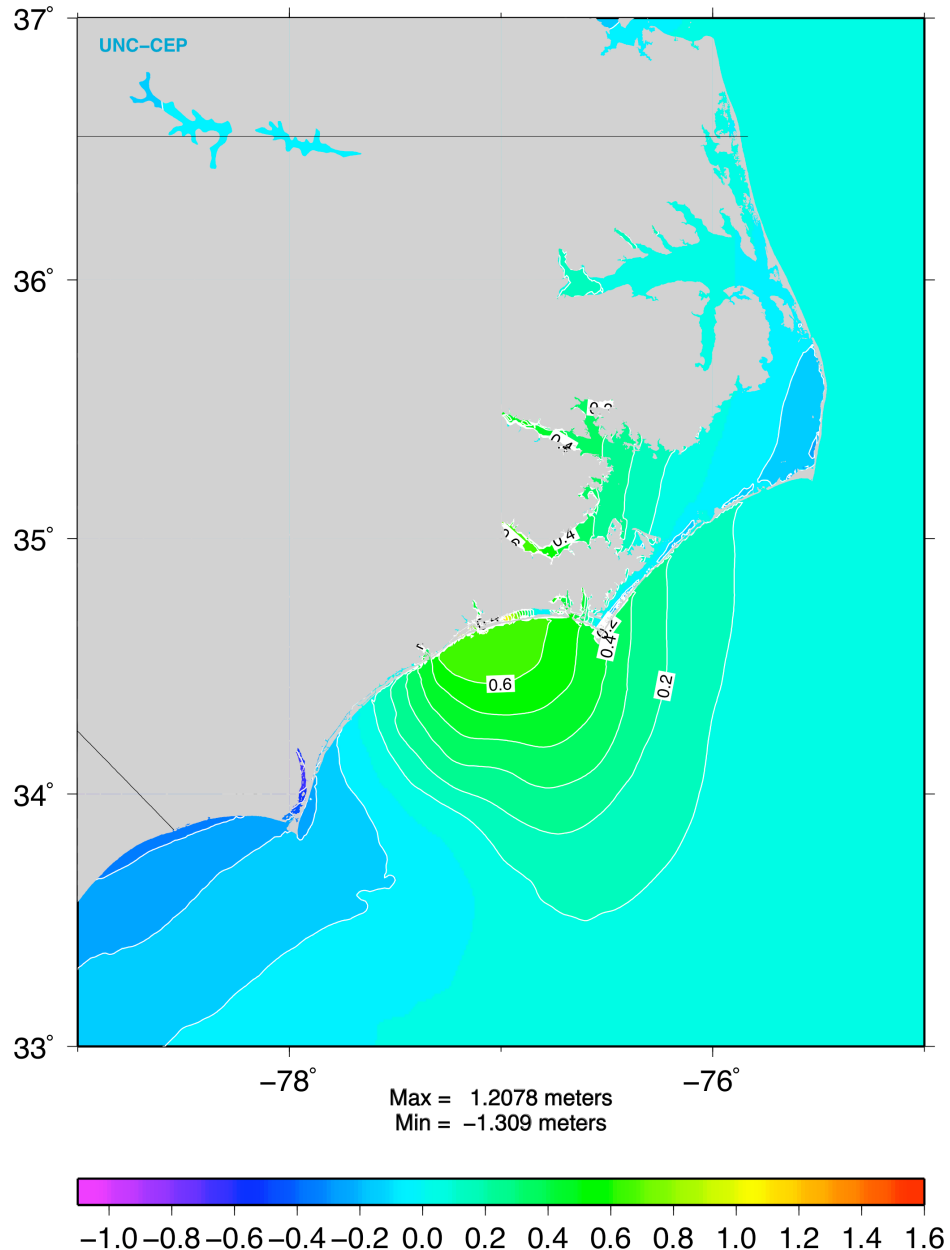


**FIG. 46c.** As in Fig. 46a, but surge above tides (m) with Manning coefficient (Mn) and surface roughness (Sr).

The surge above tides with the Mn and Sr is shown in Fig. 46c. The maximum surge is 1.208 m (3.96 ft). The NHC public advisory had predicted a maximum coastal storm surge flooding of 5 to 7 feet above normal tide levels. In the Pamlico Sound, the onshore winds cause a greater depletion of water in the eastern side of the sound with the Mn and Sr nodal attributes than without (Fig. 46c and Fig. 45b). One possibility might be that, since winds in this area are from the southeast, stronger flow occurs through the inlets in the case without Mn or Sr, resulting in larger sea surface elevation.

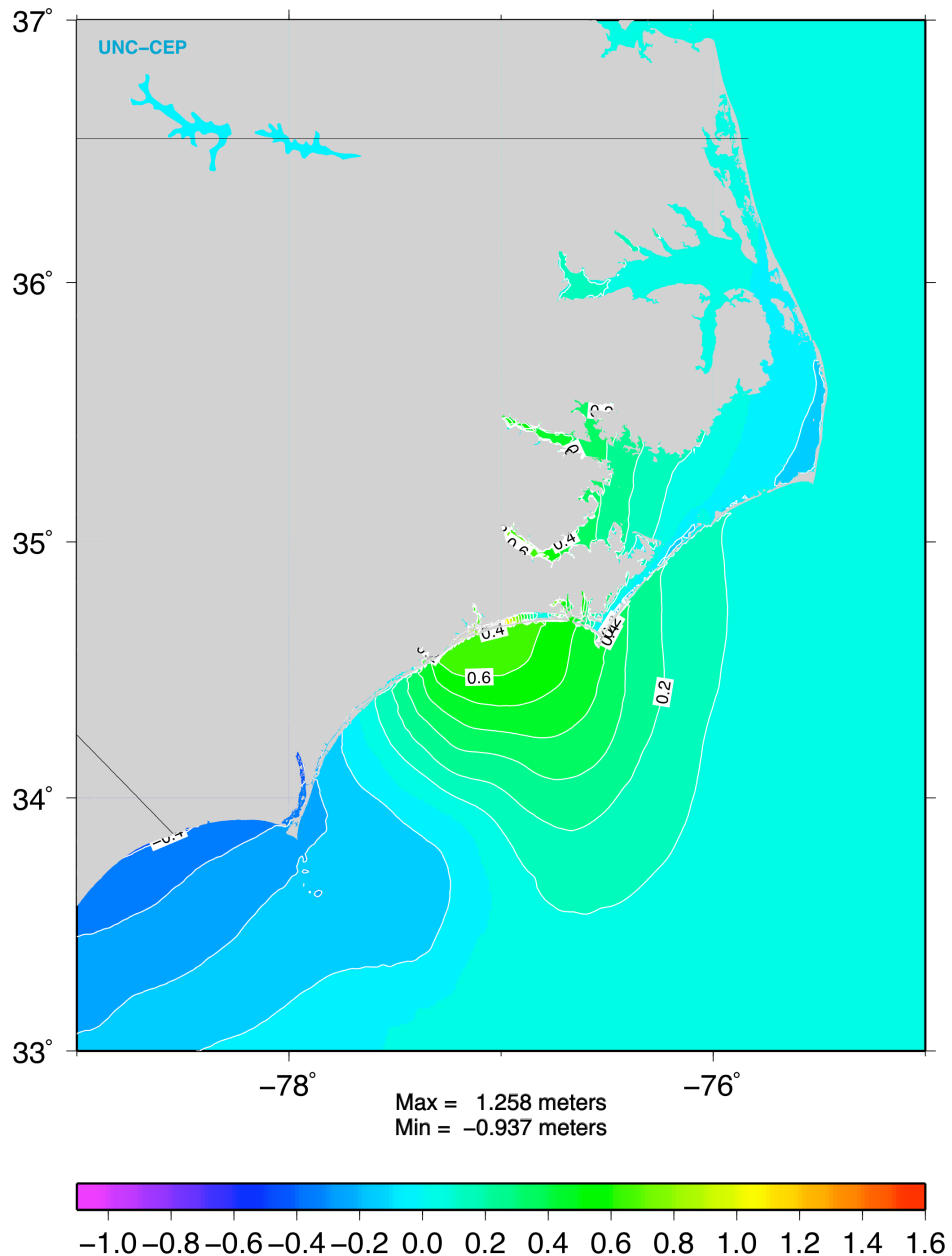


**FIG. 46d.** As in Fig. 46a, but surge above tides (m) with surface roughness (Sr) only.

Fig. 45d shows that for the same simulation with Sr but no Mn, the pattern in the Pamlico Sound is very similar to the simulation with no Mn and no Sr, implying that the lower sea surface elevation is due to the inclusion of a spatially varying Manning coefficient. Further investigation, including calculations of the mass transport through the inlets and channels, should be conducted to account for this difference.

#### *Effects of wind forcing: Best track vs. NHC advisory derived winds*

Fig. 47a shows the sea surface elevation using Mn + Sr but forced with the corrected best track winds. The sea surface heights driven by the best track winds are about 10 cm lower than in the simulation forced with the wind data from the operational NHC advisories. The magnitude of the sea surface depression along the coast is also slightly smaller than the one produced by NHC derived winds. The storm surge up the coast and draw down generated by the best track wind data is slightly lower than the one generated by the NHC advisory derived winds.

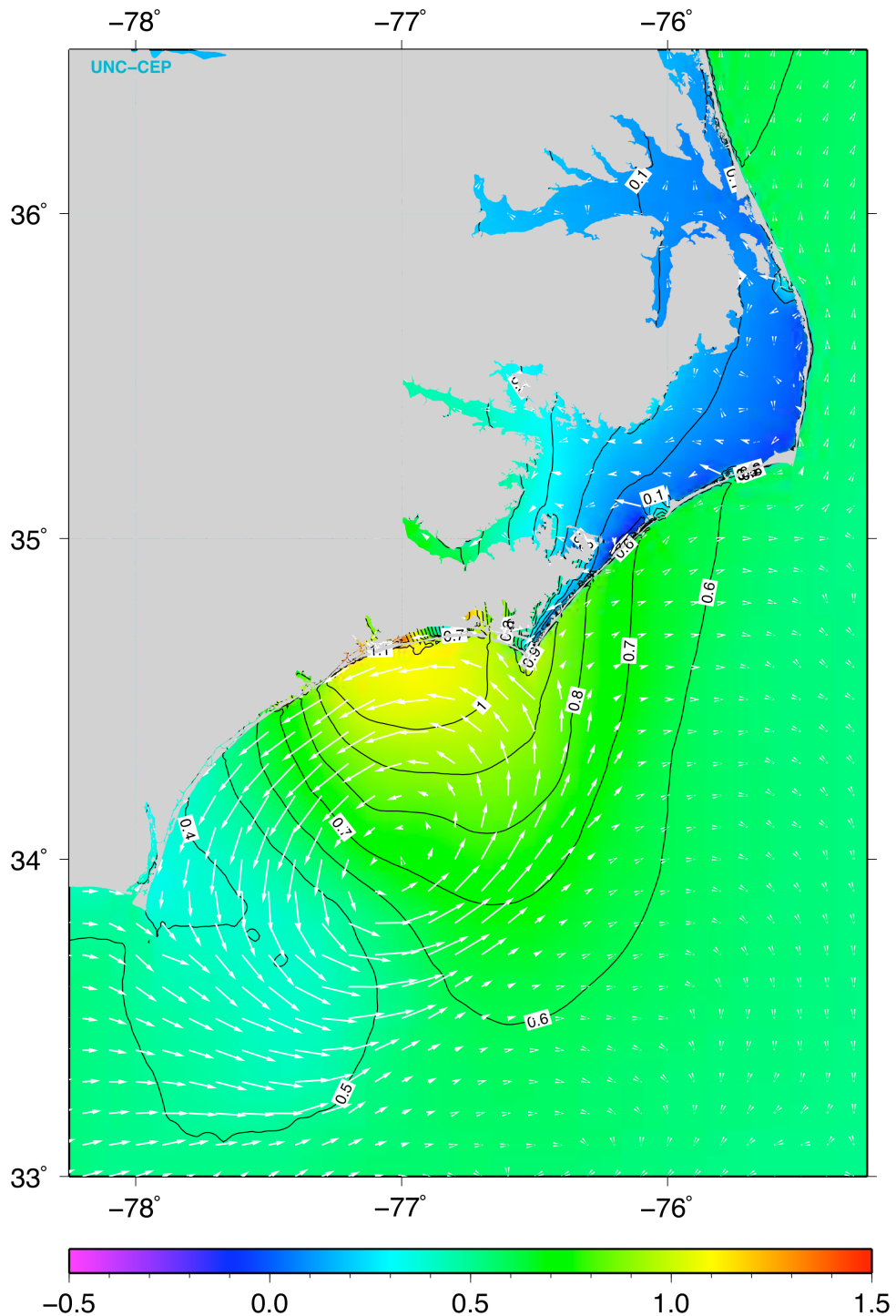


**FIG. 47a.** Sea surface elevation (m) and surface currents (m/s) and with Manning coefficient ( $M_n$ ) and surface roughness ( $S_r$ ) from the ADCIRC model at 22:30 UTC on September 14, 2005 using best track derived winds.

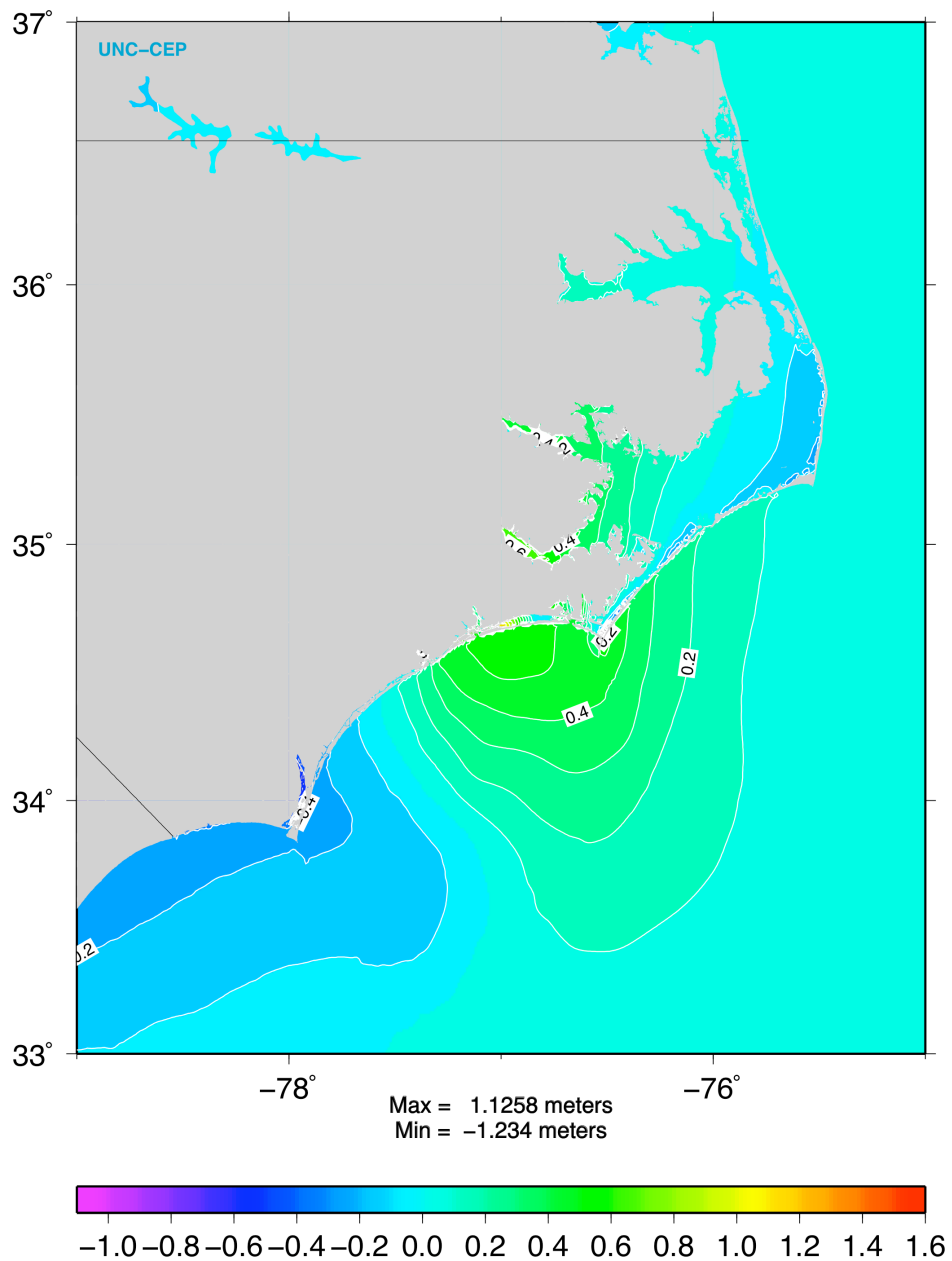


**FIG. 47b.** Surge above tides (m) with Manning coefficient ( $M_n$ ) and surface roughness ( $S_r$ ) from the ADCIRC model at 22:30 UTC on September 14, 2005 using best track derived winds.

#### *Comparison between observations and model elevation*

Tidal station data was extracted from the NOAA web site ([http://tidesandcurrents.noaa.gov/station\\_retrieve.shtml?type=Tide+Predictions](http://tidesandcurrents.noaa.gov/station_retrieve.shtml?type=Tide+Predictions)) for all stations along the NC coast. An example of the Wrightsville Beach record is shown in Fig. 48.

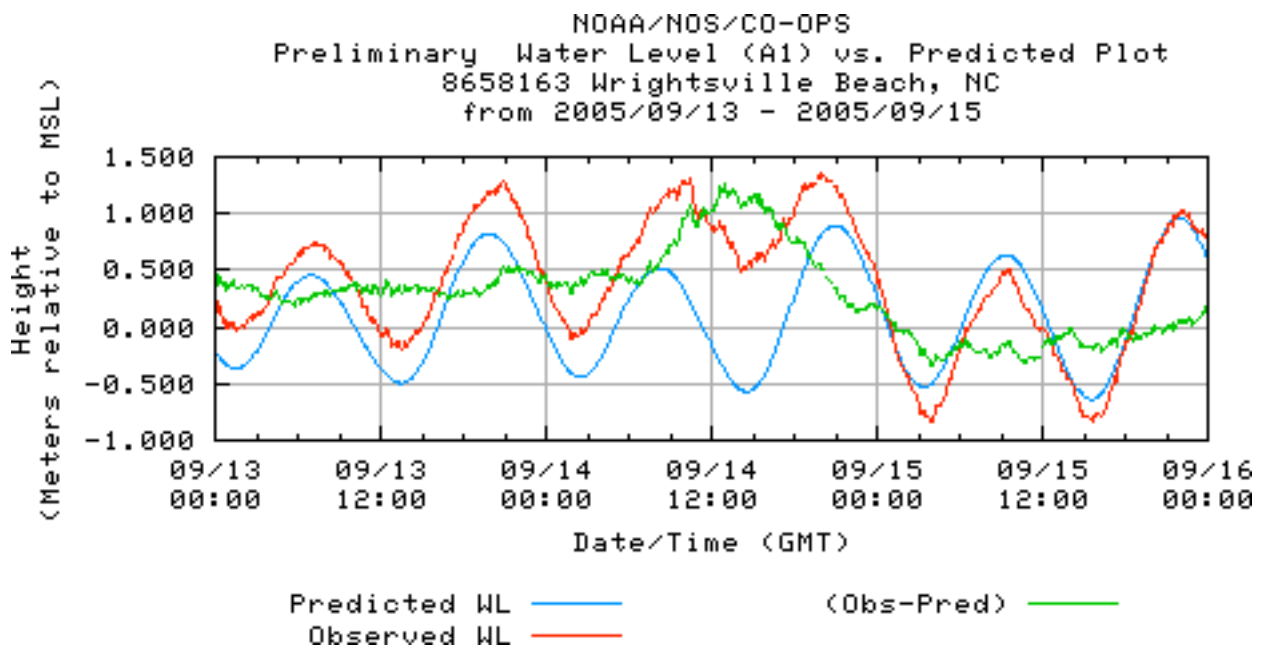


**FIG. 48.** Predicted, observed and observed minus predicted sea surface elevation (m) at Wrightsville Beach during Hurricane Ophelia from NOAA/NOS/CO-OP data.

The elevation due solely to tides was removed from the hotstart and best track simulations to allow comparisons with the cold start simulation, since it has no tides. In addition, the predicted tides were subtracted from the observed tides at each NOAA tidal station.

The elevation residuals for three different stations at the coast (Wrightsville Beach, NC, Sunset Beach, NC, and Springmaid Pier, SC; see Fig. 42 for locations) were then compared for different test cases. The residuals for cold start with no Sr, no Mn, hotstart with no Sr, no Mn, hotstart Sr and Mn, and hotstart forced by best track winds with both Sr and Mn are shown in Fig. 49.

The cold start elevation exhibits a phase shift with respect to the hotstart elevation residuals and observations at all stations in the time series far away from the strong hurricane forcing, but it is in phase during the strong wind forcing. This suggests that with lower forcing there are nonlinear dynamic processes that interact with the tidal forcing, leaving the residual of the observations in phase with the model elevation residuals when tides are incorporated in the simulations, which does not occur with cold starts. During the period of the storm the cold start surge above tides is in phase with the observations and the amplitude is in agreement for these particular stations.

The hotstart with Sr and Mn enhances lower amplitudes more prevalently than the simulations without Mn or Sr when the stations are west or south of the storm in the draw down area. The best track wind driven simulation agrees fairly well with the NHC advisory wind forced runs, even though the best track data has been corrected and recorded at the 6-hour intervals 0Z, 6Z, 12Z and 18Z while the NHC forecast advisories are issued at 3Z, 9Z, 15Z and 21Z. This time difference between the data sources may explain why the peak sea surface height at Wrightsville Beach at around 12Z is better resolved in the best track simulation than in the NHC advisory run, and the peak at 15Z is better resolved in the NHC advisory run than in the best track run.

## Hurricane Ophelia Surge Above Tides

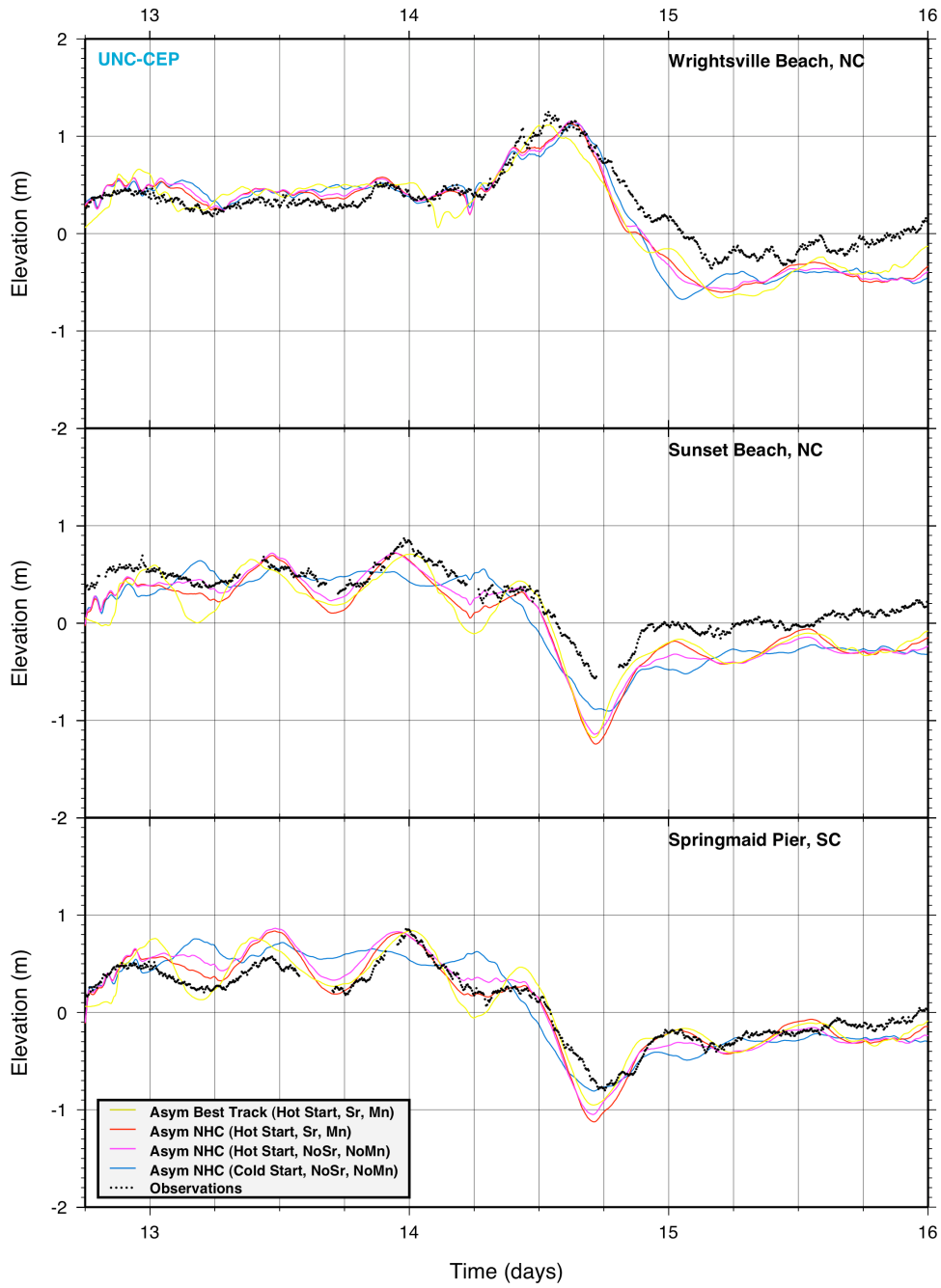


**FIG. 49.** Sea surface height residuals (m) at Wrightsville Beach, NC, Sunset Beach, NC and Springmaid Pier, NC during Hurricane Ophelia from ADCIRC model simulations with different initialization modes, different nodal attributes and different wind forcing.

In all cases, the model surge above tides is pretty much in phase with the observations at all three stations, while the magnitudes of the draw down are slightly lower than in the observations. The highest winds approached closer to Wrightsville Beach than the other stations so the storm surge signal is noticeably higher there. The amplitude is pretty much in agreement, especially when the

data source time is near the time the highest winds reach the shore and produce the highest storm surge.

Cross correlations between observed and model sea surface height residuals were calculated at different stations for several storms.

Fig. 50 shows the cross correlations between sea surface observations with the predicted tides removed and model elevation with the model tides removed at Wrightsville Beach, NC, calculated for Hurricane Ophelia. The correlation between the observed height residual and the asymmetric wind driven model height residual is encouragingly high. There is very good agreement at all lags. The best track correlation value is slightly lower at increasing lag.

### Hurricane Ophelia Cross-Correlations NOAA Tidal Station at Wrightsville Beach vs ADCIRC Storm Surge Model Sept 11-17, 2005

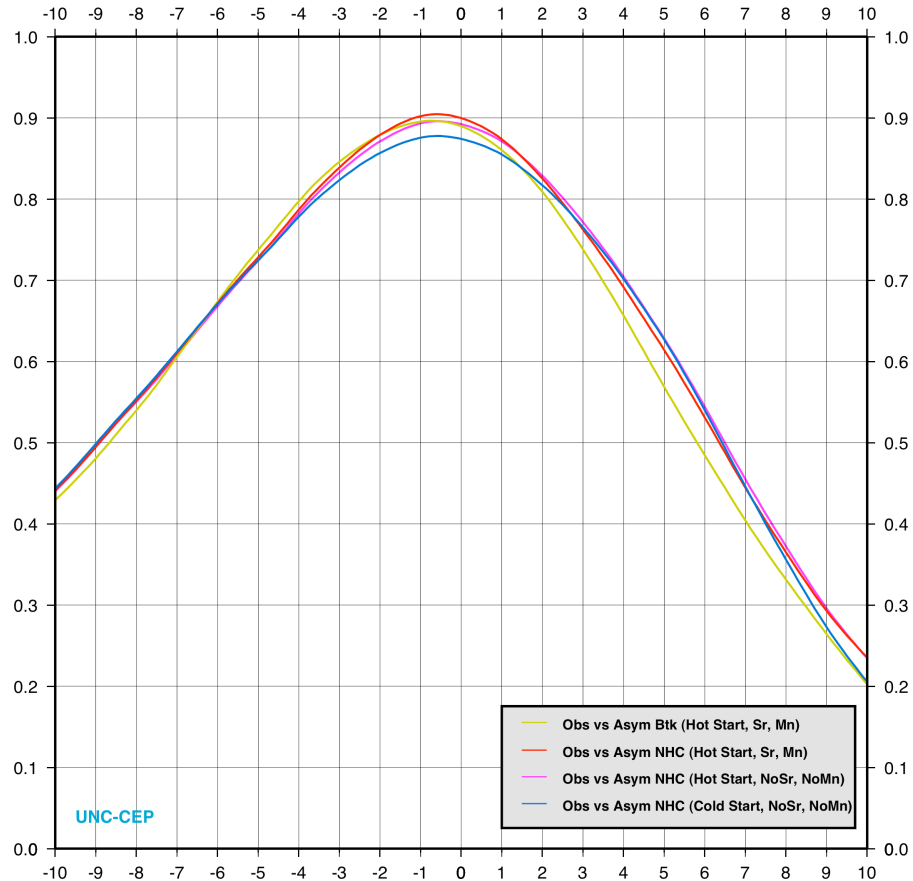


**FIG. 50.** Cross correlations between observed and model sea surface height residuals at Wrightsville Beach, NC for cold start (no Mn, no Sr), hot start (no Mn, no Sr), hot start (Mn, Sr) forced with NHC advisory derived winds and Best Track (Mn, Sr) wind data.

The correlations at 0 lag between the observed residuals and the hotstart simulation with no enhancements (no Mn, no Sr) is 0.892, while the cold start correlation is lower at 0.874. The highest correlation between observations and the model elevation residuals is achieved when both the spatially varying Manning coefficient and directional surface roughness are used. In this case, the values reach 0.900, which slightly exceeds the correlation obtained with the best track wind forcing that included the Manning coefficient and surface roughness. More stations and more storms need to be analyzed to validate these results and reach a more concrete conclusion.

A summary of the cross correlations between the NOAA/NOS/CO-OPs observed minus predicted sea surface elevation and ADCIRC surge above model tides simulation results, at lag 0 and maximum correlation and corresponding lag in hours is shown in Table 4.

**TABLE 4.** Summary of the cross correlations between the NOAA/NOS/CO-OPs observed minus predicted sea surface elevation and ADCIRC surge above model tides simulation results, at lag 0 and maximum correlation and the corresponding lag in hours at Wrightsville Beach, NC.

Simulation Type	Correlation	Maximum	Lag at
	At 0 Lag	Value	Maximum Value
<i>Cold Start</i>	0.874	0.878	-0.6
<i>Cold Start + Sr</i>	0.874	0.878	-0.6
<i>Hotstart</i>	0.892	0.896	-0.6
<i>Hotstart + Sr</i>	0.892	0.896	-0.6
<i>Hotstart + Sr + Mn</i>	0.900	0.905	-0.8
<i>Hotstart Btk + Sr + Mn</i>	0.890	0.897	-0.7

The correlations between the observations and the model elevations exhibit a slight shift in time, with the maximum correlation being at -0.6 and -0.8 time lags (36-48 minutes). Note that positive (negative) lag means that the second time series (model) lags (leads) the first (observations). In this case, even when the observed hurricane signal at Wrightsville Beach appears to be slightly ahead of the model elevation on September 14 prior to 15Z, the model elevation signal leads the hurricane produced draw down signal in the later part of the record. This causes the peak of the correlation to be shifted towards negative lags.

**TABLE 5.** Summary of the RMS error between the NOAA/NOS/CO-OPs observed minus predicted sea surface elevation and ADCIRC surge above model tides simulation results.

Simulation Type	Mean	Mean	RMS	RMS
	(model)	(observations)	(m)	(means removed)
	(m)	(m)		(m)
<i>Cold Start</i>	0.104	0.248	0.239	0.192
<i>Cold Start + Sr</i>	0.104	0.248	0.240	0.192
<i>Hotstart</i>	0.104	0.248	0.229	0.178
<i>Hotstart + Sr</i>	0.104	0.248	0.229	0.179
<i>Hotstart + Sr + Mn</i>	0.010	0.248	0.226	0.170
<i>Hotstart Btk + Sr + Mn</i>	0.105	0.248	0.221	0.169

The RMS error at Wrightsville Beach, calculated for both the observed and model residuals in simulations run with and without Mn and Sr, and cold start and hotstarts with tides for the full length of the run, are shown in Table 5.

Also displayed in the table is the mean of the residuals for both time series, and the RMS calculated with their means removed. The cold start simulations have the highest error while the simulation forced with the best track winds has the lowest RMS (0.221). The simulation driven with the NHC forecast advisory derived winds has the second lowest amount of error (0.226). The RMS error, with the means of the residuals removed, are also lowest for the best track run (0.169) while the hotstart with both Mn and Sr is very close.

We can infer from these results that the addition of tides and the landuse dependent enhancements (Sr + Canopy + Mn) improve the results of the simulations. The portion of the grid where Wrightsville Beach is located has lower resolution than further north. With increased grid resolution, these results can be improved. More comparisons between observations should be carried out along the coast to determine what other factors could improve the results further.

### 3.6 ADCIRC Performance Benchmarks

We ran a series of benchmarks on different number of processors to provide performance measurements to RENCI management and a similar series of ADCIRC storm surge simulations on the UNC Topsail cluster to assess the model's scalability.

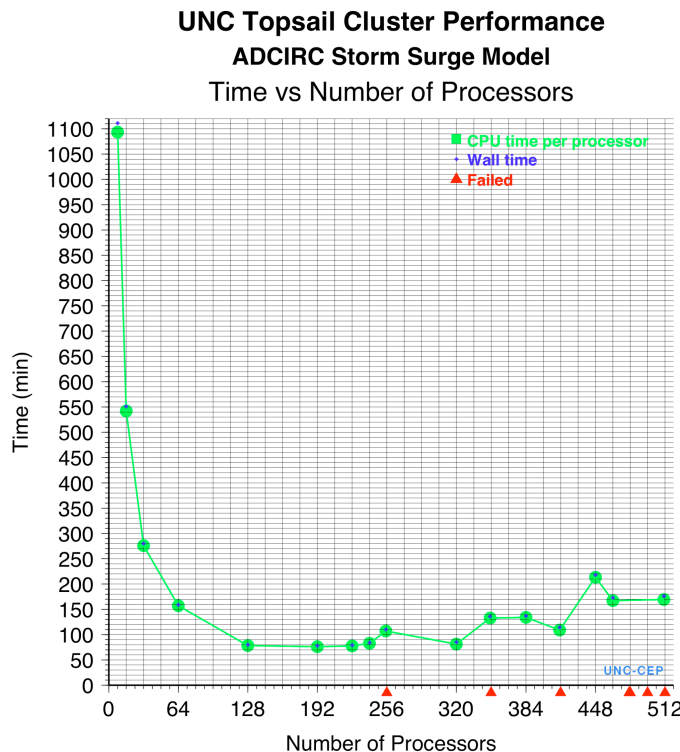


**FIG. 51.** ADCIRC parallel performance (time in minutes) on the UNC Topsail cluster for different numbers of processors.

Presented in Fig. 50 is a summary of the CPU times (green dots) and wall times (blue crosses) for the exact same simulation run on different numbers of processors. The model's performance increases dramatically until the 128-processor mark, then remains flat until it is distributed over 448 processors, where it starts to degrade due to interprocessor communication latency.

## 3.7 WRF-ARW Model Implementation

One of the original objectives of this project was to gradually replace the atmospheric forcing used to drive ADCIRC with more realistic, high-resolution meteorological fields generated by the HWRF model, the hurricane version of WRF-NMM. Unfortunately, requests to obtain this model from the NCEP Environmental Modeling Center (EMC) were denied because the model is currently undergoing intensive development and will not be released to the public prior to its scheduled operational deployment in the summer of 2007. Therefore, the decision was made to implement the advanced research version of WRF in the NCFS, which offers several strategic advantages of its own. Unlike WRF-NMM, WRF-ARW is widely used in the university research community and maintained by NCAR, so the latest cutting-edge modeling technologies are more rapidly integrated into its Eulerian core. Since it employs Arakawa-C horizontal grid staggering, which is much simpler than the NMM's rotated Arakawa-E grid and used in models from many other scientific disciplines, it is a better choice for coupling to models such as the Hybrid Coordinate Ocean Model (HYCOM) and the Community Multiscale Air Quality (CMAQ) in the future.

### 3.7.1 Modifications for Operational Use

The original version of WRF-ARW implemented in the NCFS employed an extremely high-resolution vertical coordinate distribution consisting of 66 levels with grid spacing on the order of 5 mb in the planetary boundary layer. This configuration was ideal for running test simulations of Hurricane Katrina, in which we were able to reproduce the winds and cloud water vapor in great detail (Fig. 52).

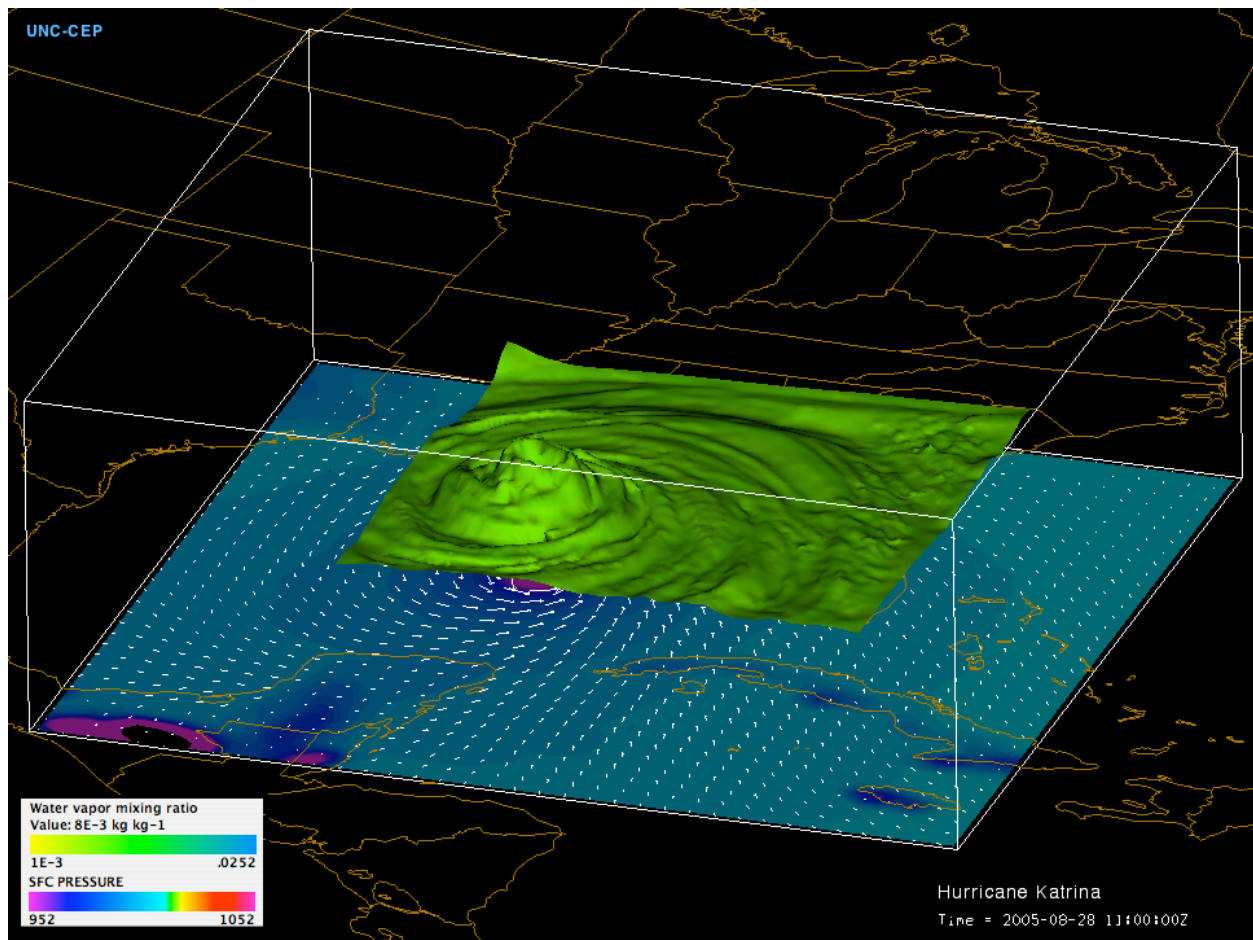


**FIG. 52.** WRF-ARW nested simulation of Hurricane Katrina just prior to landfall, valid at 11 UTC August 28, 2005. Winds (white vectors) and surface pressure (color-filled contours) are from the 12 km outer grid, while the cloud water vapor (green isosurface) is from the 4 km inner nest.

WRF was also run in real-time, in concert with the ADCIRC storm surge model, to produce operational forecasts of the winds and precipitation as Tropical Storm Ernesto made landfall along the NC coast on September 1, 2006 (Fig. 53).

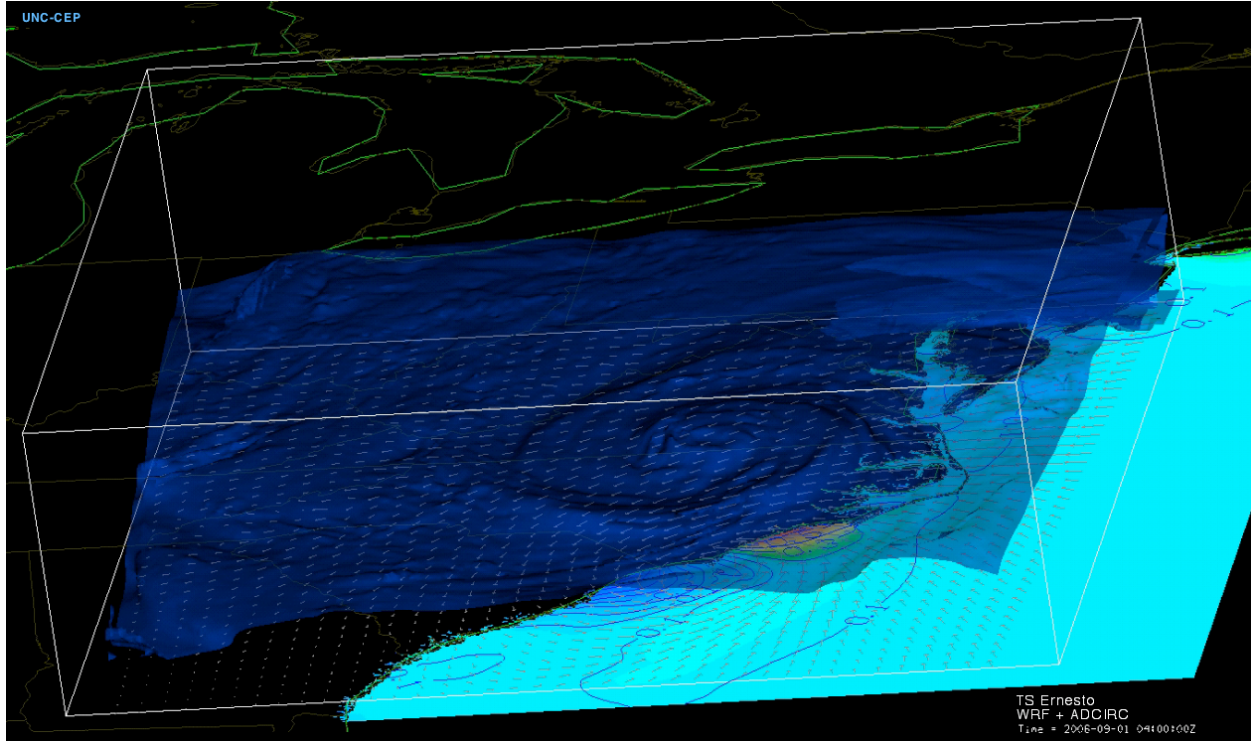


**FIG. 53.** Results from real-time operational predictions of the clouds (blue isosurface of water vapor) and surface winds (grey vectors) produced by the WRF numerical weather prediction model, and storm surge (color-filled contours) produced by the ADCIRC coastal ocean model as Tropical Storm Ernesto made landfall along the North Carolina coast on September 1, 2006.

Although this configuration was optimum for scientific research, it was too computationally intensive for operational use at RENCI and it generated excessively large output files. Therefore, one of the first tasks was to reduce the number of vertical levels in the model, while maintaining the quality of the simulations. This was accomplished by adapting a vertical coordinate stretching algorithm designed for the University of Oklahoma's Advanced Regional Prediction System (ARPS) cloud-/mesoscale atmospheric model for use in configuring WRF. A hyperbolic tangentially stretched distribution consisting of 45 levels was specified that retains ample resolution in the PBL (14 levels beneath 900 mb), gradually transitions to coarse resolution at mid-levels, then constricts again aloft where tropopause folding and stratospheric intrusions of high potential vorticity air and ozone occur (see Table 6 below).

**TABLE 6.** Vertical levels used in the operational version of the WRF-ARW numerical weather prediction model. A hyperbolic tangentially stretched distribution was specified to retain resolution in the planetary boundary layer.

Level	Uniform Z	Stretched Z	Layer DZ	Pressure	Layer DP	Sigma-P
45	20119.00	20576.96	.00	50.00	.00	.0000
44	19661.75	19661.75	915.21	57.75	7.75	.0080
43	19204.50	18746.54	915.21	66.71	8.97	.0174
42	18747.25	17834.87	911.67	77.03	10.31	.0281
41	18290.00	16927.48	907.39	88.88	11.85	.0404
40	17832.75	16025.27	902.22	102.47	13.59	.0545
39	17375.50	15129.29	895.98	118.02	15.55	.0706
38	16918.25	14240.81	888.48	135.77	17.75	.0890
37	16461.00	13361.31	879.49	155.96	20.20	.1100
36	16003.75	12492.54	868.77	178.86	22.90	.1338
35	15546.50	11636.52	856.03	204.71	25.85	.1606
34	15089.25	10795.54	840.98	235.92	31.20	.1930
33	14632.00	9972.22	823.32	267.39	31.48	.2257
32	14174.75	9169.47	802.75	301.37	33.97	.2610
31	13717.50	8390.44	779.03	337.69	36.32	.2987
30	13260.25	7638.49	751.95	376.11	38.42	.3385
29	12803.00	6917.10	721.39	416.29	40.19	.3803
28	12345.75	6229.73	687.37	457.81	41.52	.4234
27	11888.50	5579.66	650.07	500.16	42.35	.4673
26	11431.25	4969.82	609.84	542.77	42.60	.5116
25	10974.00	4402.62	567.20	585.02	42.25	.5554
24	10516.75	3879.77	522.85	626.32	41.30	.5983
23	10059.50	3402.17	477.60	666.10	39.78	.6396
22	9602.25	2969.81	432.36	703.87	37.77	.6788
21	9145.00	2581.80	388.01	739.24	35.37	.7155
20	8687.75	2236.43	345.37	771.93	32.69	.7495
19	8230.50	1931.30	305.13	801.78	29.85	.7805
18	7773.25	1663.46	267.83	828.75	26.97	.8085
17	7316.00	1429.65	233.82	852.89	24.14	.8335
16	6858.75	1226.38	203.26	874.34	21.45	.8558
15	6401.50	1050.21	176.18	893.29	18.94	.8755
14	5944.25	897.76	152.45	909.95	16.66	.8928
13	5487.00	765.86	131.89	924.56	14.62	.9079
12	5029.75	651.63	114.23	937.38	12.81	.9212
11	4572.50	552.45	99.18	948.62	11.24	.9329
10	4115.25	466.01	86.44	958.50	9.89	.9432
9	3658.00	390.30	75.71	967.23	8.73	.9522
8	3200.75	323.57	66.73	974.98	7.75	.9603
7	2743.50	264.34	59.23	981.89	6.92	.9674
6	2286.25	211.35	52.99	988.11	6.22	.9739
5	1829.00	163.54	47.82	993.76	5.64	.9798
4	1371.75	120.00	43.54	998.92	5.16	.9851
3	914.50	80.00	40.00	1003.68	4.76	.9901
2	457.25	40.00	40.00	1008.45	4.78	.9950
1	.00	.00	40.00	1013.25	4.80	1.0000

After a series of meetings with other atmospheric research scientists at state universities and potential consumers of WRF output products, a decision was made to further increase computational performance by removing several unnecessary variables from the model's registry

and history output stream. The explicit cloud microphysics scheme was also changed from an advanced formulation that predicts 8 classes of water substances to the Ferrier microphysics algorithm, which only advects cloud water vapor and total condensate, then derives concentrations for the other hydrometeors. The latter scheme, used operationally at NCEP, is designed for computational speed and has proven to be robust under a wide range of weather scenarios but, most importantly, it drastically reduces the size of the WRF output files. Finally, in order to broaden community interest in (and the applicability of) WRF output products, the original grid was transformed to the NC Department of Air Quality (NCDAQ) map projection on three (12, 4, and 1.333 km) two-way nested telescoping grids (Fig. 54).

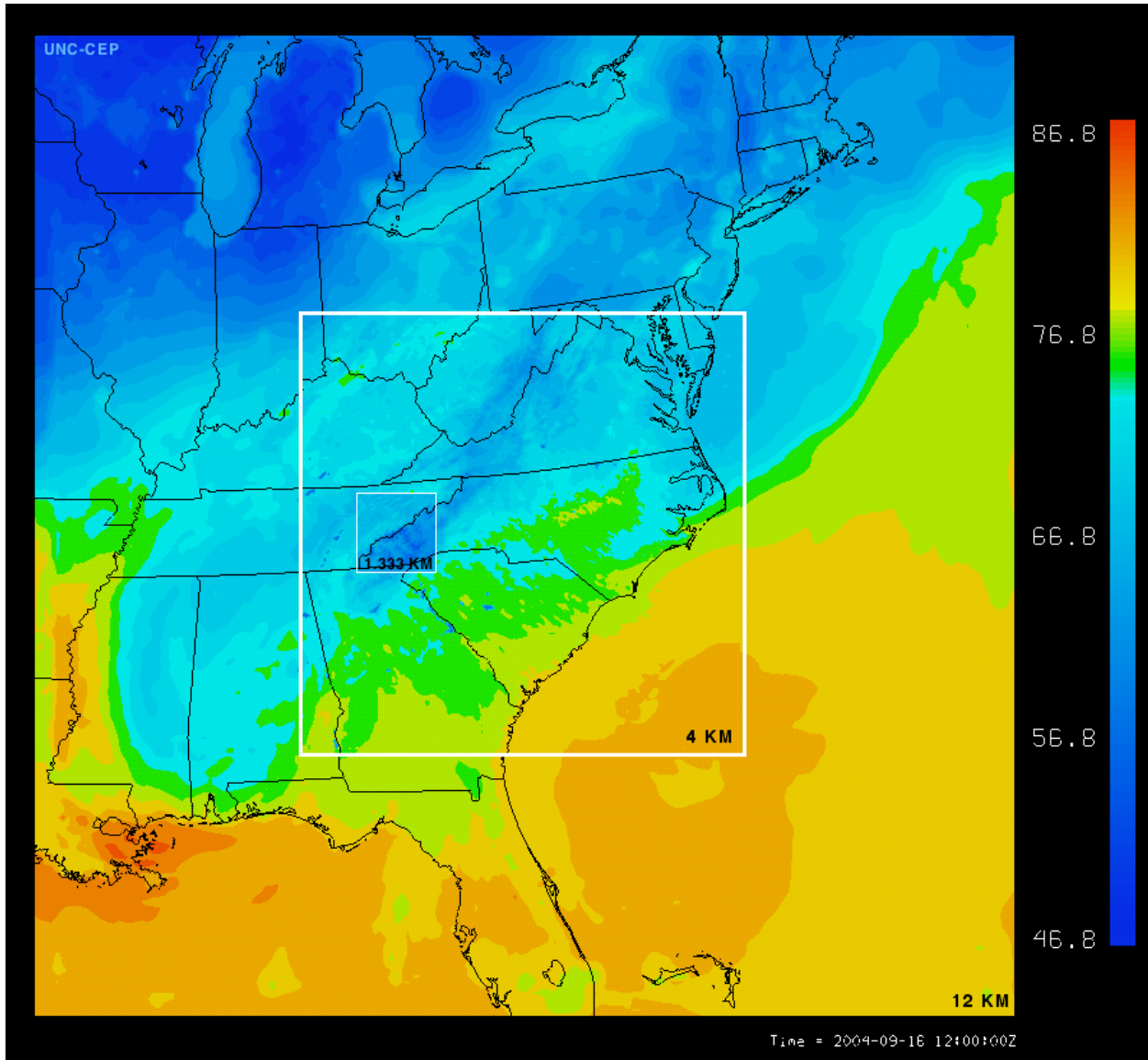


**FIG. 54.** The NC Department of Air Quality grid implemented in the NCFS operational version of WRF, consisting of three (12, 4, and 1.333 km resolution) two-way nested telescoping grids.

The combination of these three major modifications reduced WRF output file size from approximately 10 GB to 4.25 GB for a 24 hour simulation and pared down execution time by

about 30%, even though an additional 1.333 km inner nest over the western NC mountains (Fig. 55) was added to the operational workflow for interfacing with the hydrology models at RENCI.

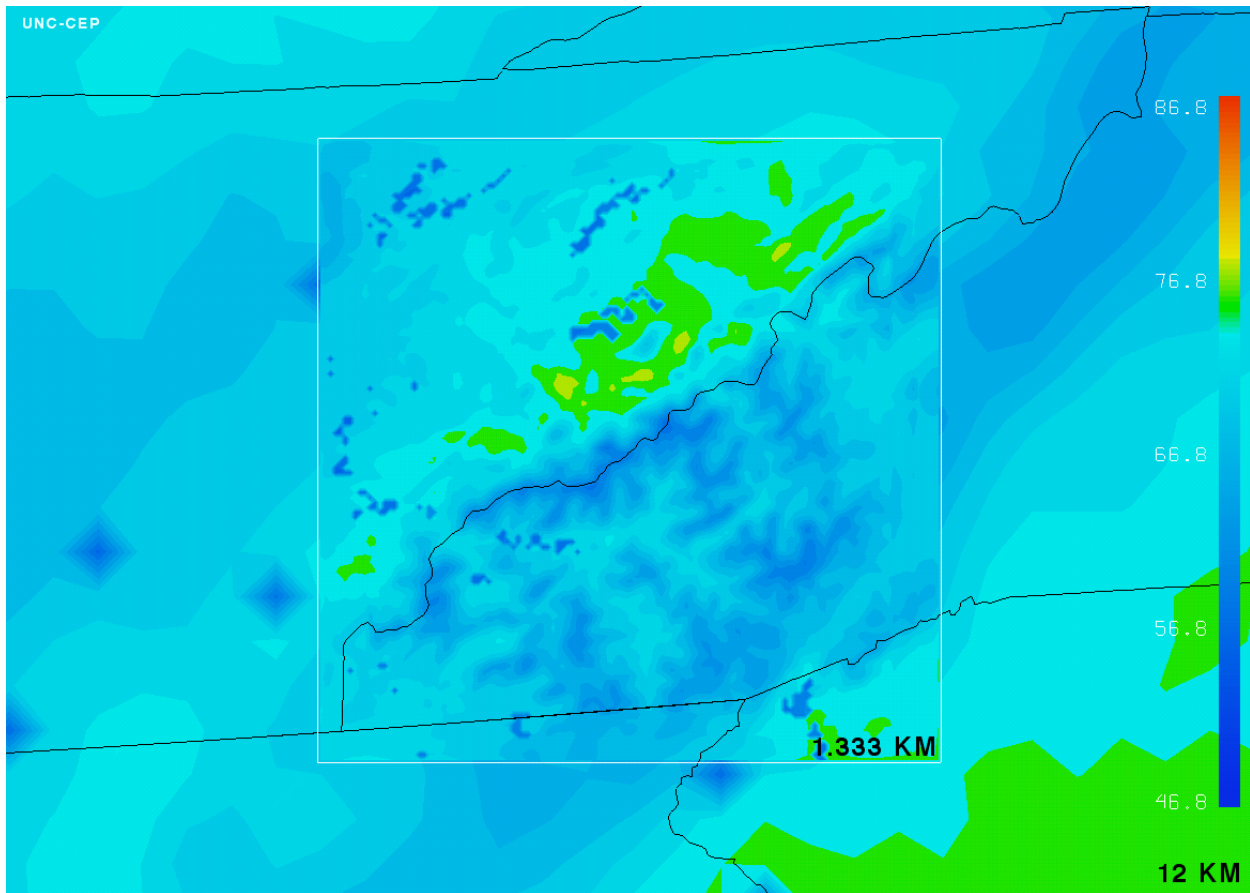


**FIG. 55.** Comparison of the inner 1.333 km nested grid, deployed over the western mountains of NC to support hydrology modeling, with its 12 km “grandparent” grid. Note the superior level of detail in the predicted surface temperature (°F) over mountainous terrain.

The short wave radiation, turbulence and planetary boundary layer schemes were also adjusted to further improve the quality of the numerical weather predictions. A new native Infiniband version of WRF was compiled to increase runtime performance.

### 3.7.2 Initialization

Initial and boundary conditions for the simulations were prepared using the WRF-SI (Standard Initialization) package. Setting up this software is not trivial – an elaborate hierarchical directory structure must be established, difficulties in compilation are commonly encountered, and reconfiguring the WRF grids often causes inconsistent values in the input files. In addition, a "landuse shift" error has recently been discovered in the WRF-SI nesting algorithm. On many occasions, especially when preprocessing gridded NAM model output files from the pre-WRF era, it produces initial/boundary datasets that cause a vexing slowdown problem in the middle of a WRF simulation on RENCI's dante cluster. Much effort was invested in diagnosing and trying

to remedy this problem through in-depth discussions with the WRF architects at NCAR, but no solution has yet been found.

### **3.7.3 Operational Workflow**

Operational WRF workflow run scripts (51 unix bash shell scripts) were obtained from Dr. Brian Etherton at UNC-Asheville and modified to make them more portable. Since the scripts were based on an old version of WRF, corrections to the nesting logic were required, and their reliability/robustness was improved by dividing the WRF-SI degridding process into multiple, lower memory demanding tasks. An option was added to allow the NAM model data to be downloaded from the National Climatic Data Center's NOAA Operational Model Archive Distribution System (NOMADS) data servers. Finally, the scripts were streamlined by removing unnecessary grid and model physics configuration and graphical output options, then deployed on RENCI's dante cluster. UNC-CEP scientists worked continuously with RENCI IT personnel during the course of the project to update and debug the WRF operational run scripts.

### **3.7.4 Scientific Visualization**

UNC-CEP scientists also introduced RENCI's visualization group to Unidata's Integrated Data Viewer (IDV) for visualizing both ADCIRC and WRF model output, then advised them how to generate scientifically consistent and meaningful graphical output products, which were saved as IDV bundles. RENCI visualization engineers automated the graphics generation process by utilizing IDV's XML scripting capabilities (Murray et al., 2003) and the images were streamed to the WRF page on RENCI's disaster research web site (in portable network graphics (PNG) format).

### **3.7.5 Additional Tasks in Progress**

Once the WRF-ARW model was up-and-running operationally at RENCI, two new tasks were undertaken that were beyond the original scope of this project and were not included in the statement of work: (1) interfacing WRF with the hydrology/river/runoff models at RENCI, and (2) creating a new data assimilation capability to ingest local NC weather observations into WRF.

Numerous discussions were held at RENCI to develop a strategy for integrating the numerical models and setting up a hydro-testbed over the Coweeta region in the western NC mountains, a region prone to flash floods, landslides and debris "runouts". UNC-CEP scientists provided a C language program to the NCFS hydrology group for computing relative humidity from a hybrid water-ice vapor pressure version of Teten's formula validated against the Smithsonian tables, then advised RENCI IT personnel how to compute photosynthetically active radiation (PAR) over visible wavelengths from WRF model output for input to the LDAS/RHESSYS models.

A high-resolution 1.333 km inner nested grid domain was developed for WRF and simulations were run for the Hurricane Frances/Ivan flooding events of September 2004. Unfortunately, the aforementioned WRF slowdown problem occurred at this stage, so the simulations could not proceed beyond 21 hours in length. Nevertheless, the weather conditions prior to and including

the Peeks Creek landslide in Macon County were successfully simulated so there was enough wind, precipitation, soil moisture and runoff information in the WRF output (Fig. 56) to develop and test the linkages between the meteorological and hydrological models.

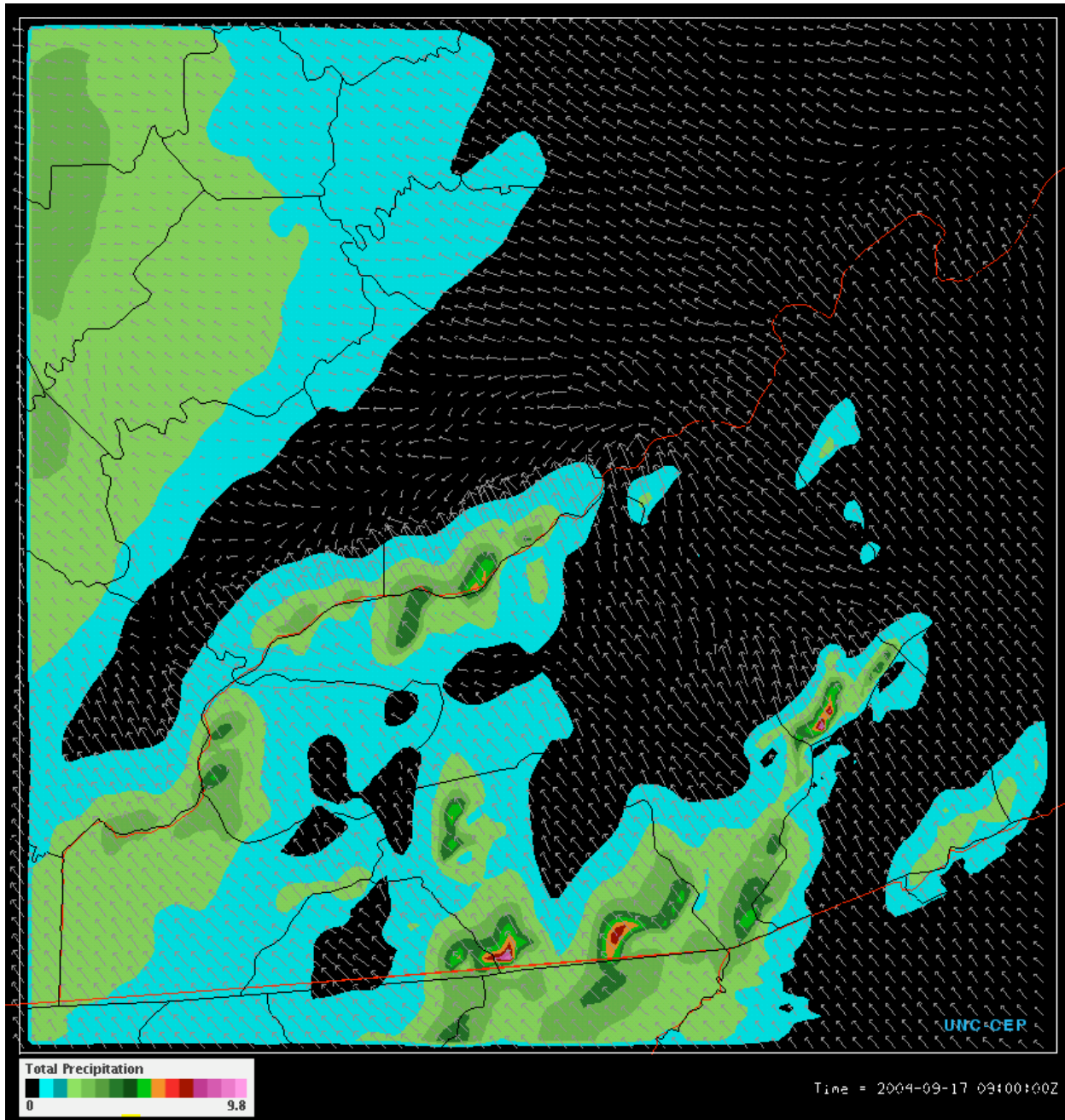


**FIG. 56.** Winds (grey vectors) and accumulated precipitation contours (inches), as simulated by the WRF model run at a horizontal resolution of 1.333 km, during the passage of Hurricane Ivan through the NC mountains. Copious amounts of rainfall were produced by strong upslope flow that wrapped around the hurricane, which triggered the Peeks Creek landslide in Macon County. Flow splitting and channeling through the valleys (gap winds) are also evident in the simulation.

In order to build a data assimilation capability for WRF, UNC-CEP scientists first obtained special permission from NOAA's Forecast Systems Laboratory (FSL, now the Earth System Research Laboratory's Global Systems Division) to set up a Meteorological Assimilation Data Ingest System (MADIS) real-time weather data feed, consisting of surface (metar, sao, marine, mesonet), rawinsonde, satellite and profiler data, for RENCI with anonymous ftp and LDM delivery capabilities. Unix shell scripts were written to download the MADIS weather data and to "scrape", decode and correct ECONet mesonet observations from the State Climate Office of North Carolina's NC CONOS web site. The MADIS data decoders were then set up to extract weather information from the compressed NetCDF files.

Since the decision was made to implement the ARPS Data Assimilation System (ADAS) in the NCFS because of its unique Doppler radar data assimilation/nudging capabilities, UNC-CEP scientists began working directly with the developers of the software at OU-CAPS to adapt the ADAS data decoders to ingest the MADIS and ECONet observations. ADAS is a complex system, consisting of a multitude of software components, five of which were required for this project:

- (1) **WRFSTATIC** is used to localize the WRF grid domains and process the static surface characteristics databases,
- (2) **ARPSTERN** creates terrain for the model grid domains,
- (3) **EXT2ARPS** processes the gridded NAM model files to create the background first-guess fields,
- (4) **ADAS** conducts an objective analysis using the Bratseth method to blend the weather observations and with the NAM background fields, and
- (5) **ARPS2WRF** reads the intermediate data files and generates initial/boundary conditions for WRF.

It was an enormous task to set up the workflow for ADAS, displayed in Fig. 57. Some of the namelist.input files are incredibly long (more than 3,000 lines in length) and expert knowledge is required to match up the ARPS model options with those corresponding to the WRF model. In addition, a separate workflow must be set up for each of the three WRF grids.

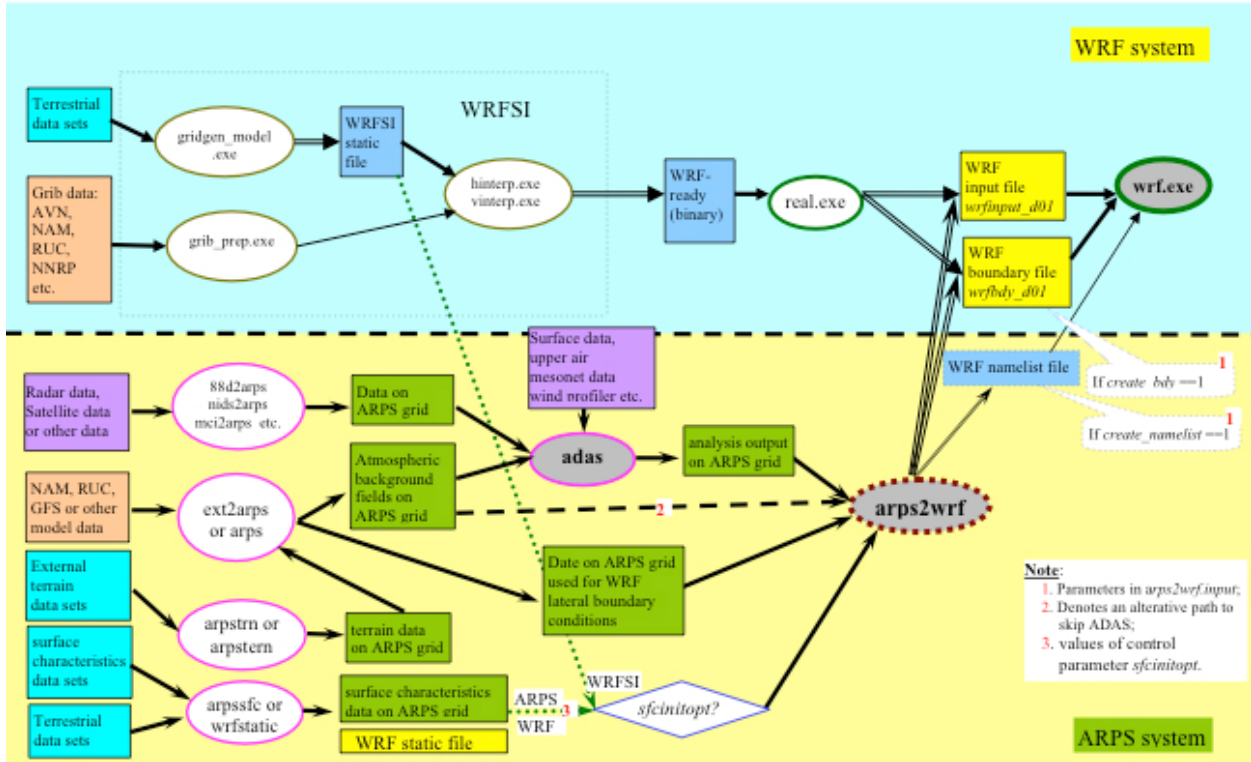


**FIG. 57.** Comparison of the WRF-SI data preprocessor workflow (light blue background) and the ADAS workflow (yellow background). The added complexity of the ADAS system is compensated by its capability to assimilate more types of weather observations, such as WSR-88D Doppler winds and reflectivity. Figure courtesy of the Center for the Analysis and Prediction of Storms (CAPS) at the University of Oklahoma.

An ADAS analysis was performed on the WRF 4 km grid domain for October 22, 2006 at 12 UTC, just after a strong cold frontal passage, utilizing the MADIS surface (metar, sao, marine) and upper-air (rawinsonde, profiler) observations. The surface potential temperature field after assimilation is displayed in Fig. 58 and the difference between the analysis and the NAM first-guess field is shown in Fig. 59. The impact of the assimilation is most pronounced in the mountains of North Carolina and in an area along the NC-VA border. Note that, at the time the assimilation was performed, the ADAS decoder for the local NC ECONet observations had not yet been written, so the differences are primarily due to performing the analysis at triple the resolution of the NAM model and ingesting laggard observations that weren't available at NCEP prior to the initialization of the NAM forecast run.

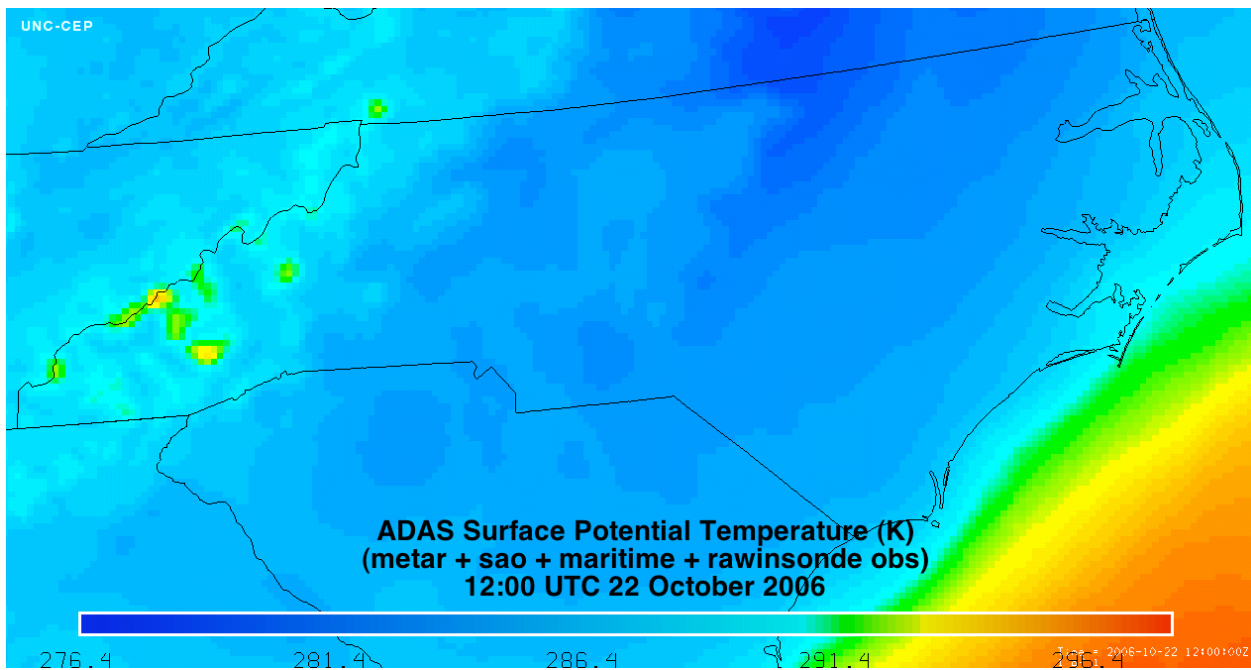


**FIG. 58.** ADAS analysis of surface potential temperature (K) valid at 12 UTC October 22, 2006.

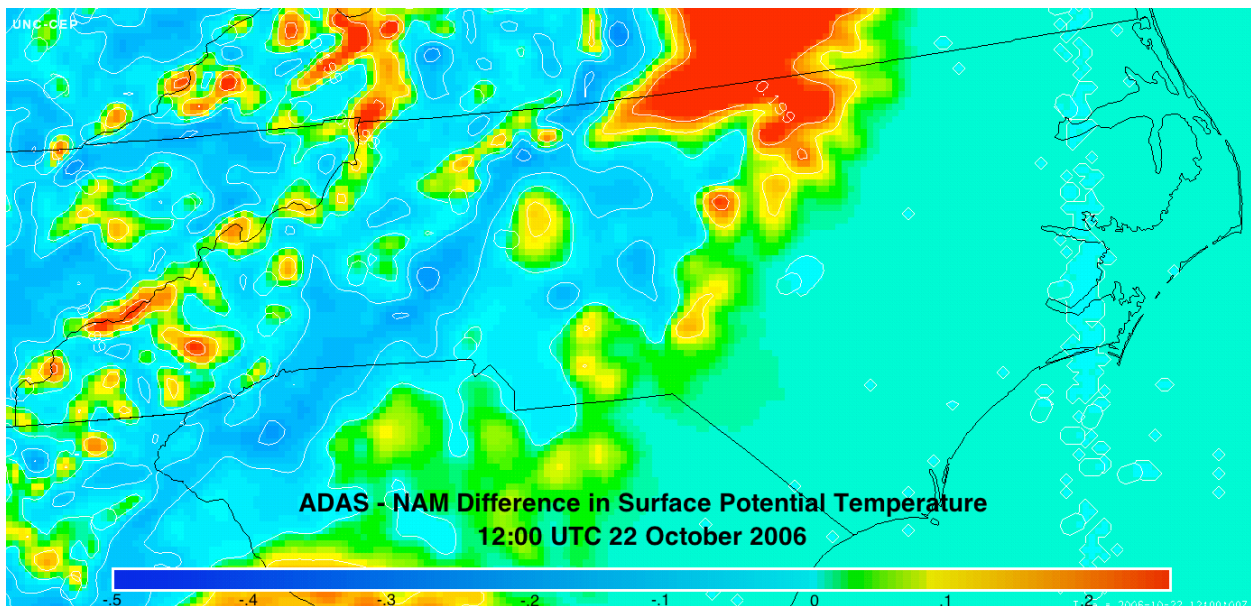


**FIG. 59.** Difference between the ADAS analysis displayed in Fig. 58 and the NAM model first-guess background field.

The implementation of ADAS into the NCFS workflow offers promise that local NC weather observations, such as those provided by RENCI's recently purchased microwave radar, could be ingested to improve the quality of the initial fields for WRF simulations. However, a significant amount of work still needs to be done to transform this research tool into an operational assimilation system.

## 4. Summary

Working in collaboration with the Renaissance Computing Institute (RENCI), scientists at UNC designed and built a new real-time storm surge prediction system for the state of North Carolina, consisting of the ADCIRC coastal ocean model and the WRF numerical weather prediction model. A “rapid response” assessment of hurricane threat is accomplished by driving the storm surge model with winds from a synthetic asymmetric gradient wind vortex generated from the National Hurricane Center (NHC) forecast advisories the moment they are inserted into the real-time weather data stream. Preliminary comparisons of the model results against actual sea surface elevations measured by NOAA tide gauges along the NC coast indicate that this new system produces remarkably realistic predictions of storm surge. In addition, the real-time WRF weather forecasts provide estimates of surface temperature, winds, soil moisture, accumulated precipitation and runoff at unprecedented horizontal resolution over North Carolina. These digital output products can be used in hydrometeorological model coupling algorithms for the prediction of dynamic streamflow, flash floods and inundation depth.

However, even though these numerical models are now running operationally, the NCFS should still be considered an experimental prototype. Further scientific enhancements, such as improving the wind forcing, extending the embedded high-resolution portion of the ADCIRC model grid more inland/southward to encompass the entire NC coastline and incorporating topographic data from the NC Floodplain Mapping Program’s LIDAR database, and verification/calibration of the system’s performance are required before it can be used as a mission-critical tactical decision aid (TDA) by state and county emergency management agencies. With the continued implementation of improvements such as these and critical evaluation by the coastal research community, this new forecast system offers the promise of minimizing the loss of life and structural damage that occurs in North Carolina during natural disasters.

*Acknowledgements.* This work was funded by the State of North Carolina through UNC-RENCI contract number 2-52130. The authors wish to thank Dr. Rick Luettich, Crystal Fulcher and Jason Fleming at UNC’s Institute of Marine Sciences in Morehead City, NC for their expert guidance and support in configuring and running the ADCIRC storm surge model as part of the North Carolina Forecast System. The Hurricane Specialists at the National Hurricane Center provided detailed information about NHC’s forecast products, their generation, timing and accuracy. We also appreciate the thoughtful discussions with Brian Blanton in the Marine Science and Engineering division at SAIC regarding operational workflows and ADCIRC tidal spinup. Consultant John Atkinson of Ayres Associates in Fort Collins, Colorado contributed invaluable advice on the directional surface roughness algorithm and the calculation of the Manning coefficients. Finally, we wish to thank the personnel at RENCI for their assistance in setting up the operational system.

## REFERENCES

- Blain, C. and A. McManus, 1998: A real-time application of the ADCIRC-2DDI hydrodynamic model for JTFEX97 at Camp Pendleton, CA, *NRL/FR/7322-98-9684*, Naval Research Laboratory, Department of the Navy, August 31, 1998.
- Blain, C. and E. Rogers, 1998: Coastal tidal prediction using the ADCIRC\_2DDI hydrodynamic finite element model, *NRL/FR/7322-98-9682*, Naval Research Laboratory, Department of the Navy, December 18, 1998.
- Blain, C., J. Westerink and R. Luettich, 1994: Domain and grid sensitivity studies for hurricane storm surge predictions, *Computational Methods in Water Resources*, X, A. Peters et al., [eds], Heidelberg, July, 1994.
- Blain, C. and C. Edwards, 2002: Forecast capability for coastal embayments of the Mississippi Sound. *Marine Technology Science*, **3**, 1501-1508.
- Blake, E. J. Jarrell, E. Rappaport and C. Landsea, 2005: The deadliest, costliest, and most intense United States Tropical Cyclones From 1851 to 2005. NOAA Technical Memorandum NWS TPC-4, NOAA/NWS/ Tropical Prediction Center/National Hurricane Center, Miami, Florida.
- Doodson, A., 1922: The harmonic development of the tide-generating potential. *Proc. Roy. Soc. London, Ser. A*, **100**, 305-329.
- Dietsche, D., S. Hagen, and P. Bacopoulos, 2006: Storm surge simulations for Hurricane Hugo (1989): On the significance of inundation areas. *Journal of Waterways, Port, Coastal, and Ocean Engineering* (in press).
- Graber, H., V. Cardone, R. Jensen, D. Slinn, S. Hagen, A. Cox, M. Powell, and C. Grassl, 2006: Coastal forecasts and storm surge predictions for tropical cyclones: A timely partnership program. *Oceanography*, **19 (1)**, 130-141.
- Holland, G. J., 1980: An analytical model of the wind and pressure profiles in hurricanes. *Mon. Wea. Rev.*, **108**, 1212-1218.
- Kaplan, J. and M. DeMaria, 1995: A simple empirical model for predicting the decay of tropical cyclone winds after landfall. *J. Appl. Met.*, **34**, 2499.
- Luettich, R. Jr., J. Hudgins and C. Goodall, 1996: Initial results from a combined tide and storm surge forecast model of the U.S. East Coast, Gulf of Mexico and Caribbean Sea, *Proceedings, 15th Conference on Weather Analysis and Forecasting*, American Meteorological Society, Norfolk, VA., August 1996, 547-550.
- Lynch, D., K. Smith, B. Blanton, R. Luettich Jr., F. Werner, 2004: Forecasting the coastal ocean: resolution, tide and operational data in the South Atlantic Bight, *Journal of Atmospheric and Oceanic Technology*, **21(7)**, 1074-1085.
- Murray, D., J. McWhirter, S. Wier, S. Emmerson, 2003: The Integrated Data Viewer: a Web-enabled application for scientific analysis and visualization. *Preprints, 19<sup>th</sup> Intl. Conf. on IIPS for Meteorology, Oceanography and Hydrology*.
- Powell, M., S. Houston, L. Amat, and N. Morisseau-Leroy, 1998: The HRD real-time hurricane wind analysis system. *J. Wind Engineer. and Indust. Aerodyn.* **77 & 78**, 53-64.
- Powell, M. D., P. J. Vickery and T. A. Reinhold, 2003: Reduced drag coefficient for high wind speeds in tropical cyclones. *Nature*, **422**, 279-283.
- Powell, M., D. Bowman, D. Gilhousen, S. Murillo, N. Carrasco, and R. St. Fleur, 2004: Tropical cyclone winds at landfall: The ASOS-CMAN wind exposure documentation project.", *Bull. Amer. Met. Soc.*, **85**, 845-851.
- Queensland Government, 2001: Queensland climate change and community vulnerability to tropical cyclones: Ocean hazards assessment – Stage 1. J0004-PR0001C, The State of Queensland (Australia), Department of Natural Resources and Mines, Brisbane, QLD, 383 pp.
- Skamarock, W., J. Klemp, J. Dudhia,, D. Gill, D. Barker, W. Wang and J. Powers, 2005: A description of the Advanced Research WRF version 2. *NCAR technical note NCAR/TN468+STR*.

- Westerink, J., 1993: Tidal prediction in the Gulf of Mexico/Galveston Bay using model ADCIRC-2DDI, *Contractors Report to the US Army Engineer Waterways Experiment Station*, Vicksburg, MS, January 1993.
- Westerink, J., R. Luettich, Jr. and N. Scheffner, 1993: ADCIRC: an advanced three-dimensional circulation model for shelves coasts and estuaries, Report 3: Development of a tidal constituent data base for the Western North Atlantic and Gulf of Mexico, *Dredging Research Program Technical Report DRP-92-6*, U.S. Army Engineers Waterways Experiment Station, Vicksburg, MS, 154 pp.
- Westerink, J. R. Luettich, J. Feyen, J. Atkinson, C. Dawson, M. Powell, J. Dunion, H. Roberts, E. Kubatko, and H. Pourtaheri, 2006: A basin to channel scale unstructured grid hurricane storm surge model applied to Southern Louisiana. *Mon. Wea. Rev.* (submitted).
- Westerink, J., R. Luettich, A. Baptista, N. Scheffner and P. Farrar, 1992: Tide and storm surge predictions using finite element model, *ASCE Journal of Hydraulic Engineering*, **118** (10), 1373-1390.
- Williams, B., S. Meinhold, N. Routhail, J. Hummer, and A. Tagliaferri. 2005: Traffic analysis of North Carolina's I-40 Lane Reversal Plan - 2005 Update. *Presentation before the Transportation Research Board Emergency Evacuation Subcommittee*, January 10, 2005.
- WRAL News, 2006: Time needed to evacuate the coast, *Stormtracker – Your Official Hurricane Survival Guide*, Capitol Broadcasting Company, Raleigh, NC, p. 2.
- Xie, L., S. Bao, L. J. Petrafesa, K. Foley and M. Fuentes, 2006: A real-time hurricane surface wind forecasting model: formulation and verification. *Mon. Wea. Rev.*, **134**, 1355-1370.

## 6. List of Deliverables

### ADCIRC Storm Surge Model

1. Developed a synthetic asymmetric Holland gradient wind vortex algorithm (written in object-oriented Fortran) for forcing the ADCIRC storm surge model in operational forecasts of sea surface elevation at the NC coast during tropical storm landfall to aid in emergency management planning. This technique has significant mission-critical advantages, including:
  - a. Allows a forecast simulation to be launched as soon as an NHC advisory is issued, instead of waiting at least 1-6 hours for the NCEP NAM model winds to become available, plus an additional 1-2 hours for pre-processing the data.
  - b. Synthetic asymmetric vortex winds can be generated "on the fly" (no pre-processing required) and are directly coupled to the ocean model at each time step.
  - c. Synthetic asymmetric vortex winds are calculated exactly at each location of the ADCIRC model nodes for "perfect" analytical resolution and "true" intensity. In contrast, the NCEP winds used in SCOOP have a coarse horizontal resolution and must be interpolated to model nodes.
  - d. An ADCIRC simulation initialized with synthetic asymmetric vortex winds can provide a "quick-look, rapid-response" storm surge forecast that can serve as the first member of an ensemble of simulations.
  - e. In the "near field", when a hurricane approaches the shoreline and the storm's circulation dominates over the background synoptic flow, a synthetic asymmetric vortex provides a fairly realistic representation of the wind field.
2. Enhanced the original NCSU formulation of the asymmetric wind vortex with a more precise radius of maximum winds root-finding algorithm, horizontal variation in Coriolis force, a translational storm velocity, frictional inflow angles, a surface boundary layer wind adjustment algorithm, and 1-minute to 10-minute wind averaging operators to attain more realistic wind distributions.
3. Generated tidal components for the open-water lateral boundary conditions for the high resolution NC grid version of the ADCIRC model from the OSU Topex/Poseidon global model of ocean tides. Spun up and included tides in the ADCIRC model simulations to obtain more accurate forecasts of storm surge along the NC coastline.
4. Ran a series of benchmarks on 8, 16, 32, 64, 128, ..., 512 processors to provide performance measurements to RENCI management.
5. Compared and calibrated ADCIRC asymmetric vortex winds against the NOAA Hurricane Research Division's operational H\*Winds analyses. Adjusted storm shape parameter, horizontal

damping of translational velocity, PBL wind reduction and time-averaging factors to obtain more realistic simulations and forecasts. Also ran simulations forced with NHC "best track" data from past storms to compare and calibrate the asymmetric winds and storm surge.

- 6.** Compared ADCIRC storm surge amplitude and phase predictions with real sea surface elevation measurements from NOAA coastal tidal stations.
- 7.** Researched real-time data sources (available via LDM and NHC anonymous ftp) for initializing and running the ADCIRC storm surge model. Spoke with Hurricane Specialists at NHC to obtain detailed information about NHC's forecast products, their generation, timing and accuracy.
- 8.** Developed 'readnhc' NHC forecast advisory decoding program (written in Fortran) for extracting real time and forecast hurricane winds and radii information for constructing a synthetic asymmetric vortex to drive the ADCIRC model operationally.
- 9.** Devised and documented NCFS real time operational workflow strategy for tides + nowcast + forecast modes.
- 10.** Provided initial and revised versions of ADCIRC operational run scripts to RENCI IT personnel.
- 11.** Tested several high-resolution versions of the NC grid and directional surface roughness data in ADCIRC model simulations.
- 12.** Ran historical (Hurricanes Isabel and Ophelia) and real time (TS Beryl, Chris and Ernesto) storm surge simulations, provided RENCI management with graphical output.
- 13.** Provided RENCI's visualization group with a new capability (IDV) for visualizing ADCIRC and WRF model output, instructed them on how to use IDV, and coached them on how to generate scientifically consistent and meaningful graphical output products.
- 14.** Worked with RENCI's visualization group to produce 3-D merged ADCIRC + WRF animations for RENCI's Board of Directors meeting.

## **WRF-ARW Numerical Weather Prediction Model**

- 1.** Set up initial 12 and 4 km grid domains and the WRF-SI data preprocessor for the new North Carolina Forecast System (NCFS) version of the WRF-ARW numerical weather prediction model.
- 2.** Ran NCFS simulation of Tropical Storm Ernesto to produce graphics of winds, precipitation and cloud water vapor for RENCI's Board of Directors meeting.
- 3.** Modified WRF registry to reduce the number of output variables and the size of the output files WRF generates.
- 4.** Developed Fortran program to compute an optimum, stretched hyperbolic tangential vertical coordinate distribution for WRF, reduced number of levels from 66 to 45.
- 5.** Modified and ported operational WRF workflow run scripts (51 bash shell scripts) from UNC-Asheville to the RENCI dante cluster. Improved scripts to increase their portability/robustness and allow NAM model data to be downloaded from NCDC NOMADS data servers.
- 6.** Worked continuously with RENCI IT personnel to improve and debug the WRF operational run scripts.
- 7.** Implemented new NC Air Quality grid in WRF to broaden community interest in, and the applicability of, RENCI output products.
- 8.** Created new ultra high resolution 1.333 km inner nested grid domain over the western NC mountains for hydrological/landslide simulations. Generated prototype WRF simulations over 3 nested grid domains for hydrology group at RENCI.
- 9.** Provided a C language program to the NCFS hydrology group for computing relative humidity from a hybrid water-ice vapor pressure version of Teten's formula validated against the Smithsonian tables.
- 10.** Advised RENCI IT personnel how to compute PAR (photosynthetically active radiation) over visible wavelengths from WRF output for input to the LDAS/RHESSYS models.
- 11.** Provided scientific input on the purchase of a new microwave radar by RENCI.
- 12.** Compiled new native Infiniband version of WRF to improve runtime performance. Modified operational run scripts to spawn Infiniband version of WRF simulations on dante cluster.
- 13.** Adjusted WRF cloud microphysics, short wave radiation, turbulence and planetary boundary layer schemes to further improve fidelity and runtime performance.

- 14.** Obtained special permission from NOAA-FSL to set up real time weather data feed [surface (metar, sao, mesonet), rawinsonde, profiler] for RENCI with anonymous ftp and LDM delivery capabilities.
- 15.** Developed unix scripts to download real time NOAA-FSL weather data and NC CRONOS ECONet observations, set up and tested MADIS data decoders to extract weather variables.
- 16.** Collaborated with the authors of the ADAS software at OU-CAPS to adapt data decoders so real time local NC weather data could be ingested by ADAS and used to improve the quality of initial fields for WRF simulations.
- 17.** Worked with software architects at NCAR to diagnose and try to solve a vexing WRF slowdown problem on the RENCI dante cluster (issue unresolved).

## 7. List of Tables

**TABLE 1.** Estimates of the peak tourist population and the time required to evacuate the coast for a list of counties in North Carolina (WRAL News, 2006).

**TABLE 2.** A summary of the maximum/minimum sea surface height and surge above tides (m) for the NOAA tidal station at Wrightsville Beach, NC, the corresponding model recording station and for the domain shown in the previous figures, accompanied by the maximum winds for the various simulations performed: 12-hour forecast (FOR-12), 6-hour forecast (FOR-6), nowcast with NHC forecast advisory derived asymmetric winds (NOW-NHC), nowcast with asymmetric winds derived from the best track dataset, and H\*Winds analyses. Times are on Sept 1, 2006.

**TABLE 3.** NLCD landuse classes with assigned values for the Manning coefficient and surface roughness length.

**TABLE 4.** Summary of the cross correlations between the NOAA/NOS/CO-OPs observed minus predicted sea surface elevation and ADCIRC surge above model tides simulation results, at lag 0 and maximum correlation and the corresponding lag in hours at Wrightsville Beach, NC.

**TABLE 5.** Summary of the RMS error between the NOAA/NOS/CO-OPs observed minus predicted sea surface elevation and ADCIRC surge above model tides simulation results.

**TABLE 6.** Vertical levels used in the operational version of the WRF-ARW numerical weather prediction model. A hyperbolic tangentially stretched distribution was specified to retain resolution in the planetary boundary layer.

## 8. List of Figures

**FIG. 1.** Model grid domain used in the NCFS version of the ADCIRC coastal ocean storm surge prediction model.

**FIG. 2a.** High-resolution grid and topography used in the NCFS version of the ADCIRC coastal ocean storm surge prediction model.

**FIG. 2b.** ADCIRC elevation recording stations used in the NCFS.

**FIG. 3.** Wind speeds produced by the synthetic asymmetric Holland gradient wind vortex algorithm for Hurricane Ophelia, valid at 22:30 UTC on September 14, 2005. The white circle indicates the approximate radius of maximum winds that would have been computed using a purely symmetric Holland wind formulation.

**FIG. 4.** Radial wind profiles from the asymmetric wind vortex in Fig. 3 along the NE-SW and NW-SE transects without (solid) and with (dashed) boundary layer adjustment using the Powell et al., (2003) wind reduction factor. Note how the wind adjustment increases the hurricane shape parameter B, which broadens the eye of the storm and enhances the tangential velocity gradient.

**FIG. 5.** Effect of including the radially dependent frictional inflow angle formulation in the asymmetric gradient wind vortex model. Note how the frictionally enhanced wind vectors (white) turn toward the center of the storm in a cross-isobaric manner.

**FIG. 6.** Numerical discontinuity in the wind speed at  $\theta = 0, 360$  degrees due to the use of a 4<sup>th</sup>-order polynomial curve fit to obtain a relationship between the radius of maximum winds and the azimuth angle. This artifact, caused by the accumulation of error at the endpoints of the curve, was eliminated by switching to a cubic splines under tension curve fit. An added benefit of the new

approach was an enhancement in the asymmetry of the vortex, making its shape more consistent with the observed/forecast wind radii reported by the National Hurricane Center.

**FIG. 7a.** H\*Wind analysis for Hurricane Ophelia, valid at 22:30 UTC on September 14, 2005.

**FIG. 7b.** Asymmetric gradient wind vortex for Hurricane Ophelia, valid at 22:30 UTC on September 14, 2005. The quality of the parametric rendition is quite remarkable, given that the asymmetric vortex was constructed from very little observed meteorological data. The greatest difference between the two wind representations is due to the use of an exponential inland wind speed decay algorithm in the H\*Wind product.

**FIG. 8.** A three dimensional perspective of the wind speeds generated using the asymmetric Holland gradient wind model for Hurricane Ophelia at 22:30 UTC on September 14, 2005. The view is from the northwest, looking offshore as the storm approached the NC coast.

**FIG. 9.** Schematic depiction of the NCFS operational workflow set up at RENCI for the 2006 hurricane season, showing its three different modes of operation.

**FIG. 10.** Ernesto's track from Florida to North Carolina.

**FIG. 11.** The NOAA/NOS/CO-Ops sea surface elevation record for the station at Wrightsville Beach.

**FIG. 12.** Official National Hurricane Center “best track” (red) of Tropical Storm Ernesto superimposed with the operational 12-hour (green) and 6-hour (brown) forecast tracks. Note the abrupt shift eastward in the predicted landfall location over 12 hours.

**FIG. 13.** The 10-minute averaged synthetic winds (kts) generated from the NHC’s 12-hour forecast advisory valid at 3Z on September 1, 2006.

**FIG. 14.** Predicted sea surface elevation (m) and currents (m/s) from a 12-hour forecast of TS Ernesto, valid at 3Z on September 1, 2006.

**FIG. 15.** Predicted storm surge (m) above tides from a 12-hour forecast of TS Ernesto, valid at 3Z on September 1, 2006.

**FIG. 16.** The 10-minute averaged synthetic winds (kts) generated from the NHC’s 6-hour forecast advisory valid at 3Z on September 1, 2006.

**FIG. 17.** Predicted sea surface elevation (m) and currents (m/s) from a 6-hour forecast of TS Ernesto, valid at 3Z on September 1, 2006.

**FIG. 18.** Predicted storm surge (m) above tides from a 6-hour forecast of TS Ernesto, valid at 3Z on September 1, 2006.

**FIG. 19.** Nowcast 10-minute averaged synthetic winds (kts) generated from the NHC’s forecast advisory valid at 3Z on September 1, 2006.

**FIG. 20.** Nowcast sea surface elevation (m) and currents (m/s) produced by TS Ernesto, valid at 3Z on September 1, 2006.

**FIG. 21.** Nowcast storm surge (m) above tides produced by TS Ernesto, valid at 3Z on September 1, 2006.

**FIG. 22.** Evolution of the sea surface elevations (m) predicted from a 12-hour ADCIRC forecast (green), 6-hour forecast (brown) and nowcast (red) simulations of TS Ernesto vs. NOAA/NOS/CO-OP observations (blue dots).

**FIG. 23.** The 10-minute averaged synthetic winds (kts) generated from the best track data at 3Z on September 1, 2006.

**FIG. 24.** Sea surface elevation (m) and currents (m/s) forced with best track winds from TS Ernesto, valid at 3Z on September 1, 2006.

**FIG. 25.** Simulated storm surge (m) above tides forced with best track winds from TS Ernesto, valid at 3Z on September 1, 2006.

**FIG. 26.** ADCIRC winds (kts) generated by H\*Winds analysis for 03Z September 1, 2006.

**FIG. 27.** Sea surface elevation (m) and currents (m/s) from ADCIRC simulation forced with H\*Winds for TS Ernesto, valid at 3Z on September 1, 2006

**FIG. 28.** Simulated storm surge (m) above tides forced with H\*Winds for TS Ernesto, valid at 3Z on September 1, 2006.

**FIG. 29.** ADCIRC model sea surface elevations (m) vs. NOAA/NOS/CO-OP observations (m) at Wrightsville Beach, NC from simulation day 88 (August 28, 2006 at 0Z) until simulation day 92.375 (September 1, 2006 at 9Z). (a) ADCIRC model tides (m) vs. NOAA predicted tides (m), (b) NOAA tidal station observations (m) vs. ADCIRC model elevations (m) produced by simulations driven with best track data, NHC advisories, and H\*Winds. (c) NOAA observed minus predicted surface elevation (m) and ADCIRC surge above tides (m) using different wind forcing: best track, NHC advisories, and H\*Winds analyses.

**FIG. 30.** Elevation values (red indicates positive, blue indicates negative) from **(a)** LIDAR, and **(b)** current ADCIRC model grid.

**FIG. 30c.** Difference between the LIDAR elevation (Fig. 30a) and ADCIRC model terrain (Fig. 30b) values (red indicates positive, blue indicates negative).

**FIG. 31.** 2001 NLCD 30-meter resolution landuse data for Beaufort County, North Carolina.

**FIG. 32.** Surface roughness length (m) computed from the 2001 NLCD 30-meter resolution landuse data for Beaufort County, North Carolina using the GIS/Java data processing techniques described in the text.

**FIG. 33.** Cell surface roughness length (m) assigned to ADCIRC model nodes in the high-resolution portion of the grid in eastern North Carolina.

**FIG. 34.** Cape Lookout, North Carolina.

**FIG. 35.** Categories of landuse assigned to ADCIRC model grid nodes over Cape Lookout. Node #70717, located in the center of the figure, is circled.

**FIG. 36.** Cell surface roughness length (m) assigned to ADCIRC model grid nodes in the Cape Lookout area.

**FIG. 37.** Polar coordinate “rose” plot of the surface roughness as a function of wind direction at ADCIRC model node #70717.

**FIG. 38.** Anisotropic surface roughness field for the 12 wind directions specified in 30° increments, starting from the north and proceeding clockwise.

**FIG. 39.** Cell Manning coefficient values assigned to ADCIRC model nodes in the NC high-resolution grid.

**FIG. 40.** Average Manning coefficient computed in 5 x 5 cell windows (150 m x 150 m in size) for the high-resolution NC grid.

**FIG. 41.** The (a) cell Manning coefficient and (b) average Manning coefficient over Cape Lookout, NC.

**FIG. 42.** Hurricane Ophelia's track from September 6-17, 2005. Data from the NHC advisories for this period were used to drive the ADCIRC storm surge model.

**FIG. 43a.** 10-minute averaged winds (kts) from the ADCIRC model at 22:30 UTC on September 14, 2005 without surface roughness (no Sr).

**FIG. 43b.** 10-minute averaged winds (kts) from the ADCIRC model at 22:30 UTC on September 14, 2005 with surface roughness (Sr).

**FIG. 44a.** Sea surface elevation (m) and surface currents (m/s) from the ADCIRC model at 22:30 UTC on September 14, 2005 using NHC advisory derived winds - cold start without nodal attributes (no Mn, no Sr).

**FIG. 44b.** Sea surface elevation (m) and surface currents (m/s) from the ADCIRC model at 22:30 UTC on September 14, 2005 using NHC advisory derived winds - hot start without nodal attributes (no Mn, no Sr).

**FIG. 45a.** Surge above tides (m) from the ADCIRC model at 22:30 UTC on September 14, 2005 using NHC advisory derived winds - cold start without nodal attributes.

**FIG. 45b.** Surge above tides (m) from the ADCIRC model at 22:30 UTC on September 14, 2005 using NHC advisory derived winds - hot start without nodal attributes.

**FIG. 46a.** Sea surface elevation (m) and surface currents (m/s) from the ADCIRC model at 22:30 UTC on September 14, 2005 using NHC advisory derived winds with Manning coefficient (Mn) and surface roughness (Sr).

**FIG. 46b.** As in Fig. 46a, but sea surface height difference field (m) with - without Manning coefficient (Mn) and surface roughness (Sr).

**FIG. 46c.** As in Fig. 46a, but surge above tides (m) with Manning coefficient (Mn) and surface roughness (Sr).

**FIG. 46d.** As in Fig. 46a, but surge above tides (m) with surface roughness (Sr) only.

**FIG. 47a.** Sea surface elevation (m) and surface currents (m/s) and with Manning coefficient (Mn) and surface roughness (Sr) from the ADCIRC model at 22:30 UTC on September 14, 2005 using best track derived winds.

**FIG. 47b.** Surge above tides (m) with Manning coefficient (Mn) and surface roughness (Sr) from the ADCIRC model at 22:30 UTC on September 14, 2005 using best track derived winds.

**FIG. 48.** Predicted, observed and observed minus predicted sea surface elevation (m) at Wrightsville Beach during Hurricane Ophelia from NOAA/NOS/CO-OP data.

**FIG. 49.** Sea surface height residuals (m) at Wrightsville Beach, NC, Sunset Beach, NC and Springmaid Pier, NC during Hurricane Ophelia from ADCIRC model simulations with different initialization modes, different nodal attributes and different wind forcing.

**FIG. 50.** Cross correlations between observed and model sea surface height residuals at Wrightsville Beach, NC for cold start (no Mn, no Sr), hot start (no Mn, no Sr) , hot start (Mn, Sr) forced with NHC advisory derived winds and Best Track (Mn, Sr) wind data.

**FIG. 51.** ADCIRC parallel performance (time in minutes) on the UNC Topsail cluster for different numbers of processors.

**FIG. 52.** WRF-ARW nested simulation of Hurricane Katrina just prior to landfall, valid at 11 UTC August 28, 2005. Winds (white vectors) and surface pressure (color-filled contours) are from the 12 km outer grid, while the cloud water vapor (green isosurface) is from the 4 km inner nest.

**FIG. 53.** Results from real-time operational predictions of the clouds (blue isosurface of water vapor) and surface winds (grey vectors) produced by the WRF numerical weather prediction model, and storm surge (color-filled contours) produced by the ADCIRC coastal ocean model as Tropical Storm Ernesto made landfall along the North Carolina coast on September 1, 2006.

**FIG. 54.** The NC Department of Air Quality grid implemented in the NCFS operational version of WRF, consisting of three (12, 4, and 1.333 km resolution) two-way nested telescoping grids.

**FIG. 55.** Comparison of the inner 1.333 km nested grid, deployed over the western mountains of NC to support hydrology modeling, with its 12 km “grandparent” grid. Note the superior level of detail in the predicted surface temperature (°F) over mountainous terrain.

**FIG. 56.** Winds (grey vectors) and accumulated precipitation contours (inches), as simulated by the WRF model run at a horizontal resolution of 1.333 km, during the passage of Hurricane Ivan through the NC mountains. Copious amounts of rainfall were produced by strong upslope flow that wrapped around the hurricane, which triggered the Peeks Creek landslide in Macon County. Flow splitting and channeling through the valleys (gap winds) are also evident in the simulation.

**FIG. 57.** Comparison of the WRF-SI data preprocessor workflow (light blue background) and the ADAS workflow (yellow background). The added complexity of the ADAS system is compensated by its capability to assimilate more types of weather observations, such as WSR-88D Doppler winds and reflectivity. Figure courtesy of the Center for the Analysis and Prediction of Storms (CAPS) at the University of Oklahoma.

**FIG. 58.** ADAS analysis of surface potential temperature (K) valid at 12 UTC October 22, 2006.

**FIG. 59.** Difference between the ADAS analysis displayed in Fig. 58 and the NAM model first-guess background field.